NASA TECHNICAL NOTE

NASA TN D-5634

c. 1

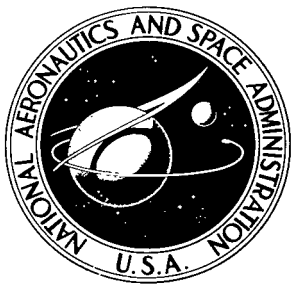

NASA TN D-5634

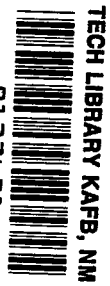

DISCONTINUOUS FLOWS AND FREE STREAMLINE SOLUTIONS FOR AXISYMMETRIC BODIES AT ZERO AND SMALL ANGLES OF ATTACK

by Heinz G. Struck

George C. Marshall Space Flight Center
Marshall, Ala.

NATIONAL AERONAUTICS AND SPACE ADMINISTRATION • WASHINGTON, D. C. • FEBRUARY 1970

1. REPORT NO. NASA TN D-5634	2. GOVERNMENT ACCESSION NO.
3. RECIPIENT'S CATALOG NO.	
4. TITLE AND SUBTITLE DISCONTINUOUS FLOWS AND FREE STREAMLINE SOLUTIONS FOR AXISYMMETRIC BODIES AT ZERO AND SMALL ANGLES OF ATTACK	5. REPORT DATE February 1970 6. PERFORMING ORGANIZATION CODE
7. AUTHOR(S) Heinz G. Struck	8. PERFORMING ORGANIZATION REPORT # M160
9. PERFORMING ORGANIZATION NAME AND ADDRESS NASA - George C. Marshall Space Flight Center Marshall Space Flight Center, Alabama 35812 Aero-Astrodynamics Laboratory	10. WORK UNIT NO. 933-50-07-00-62 11. CONTRACT OR GRANT NO.
12. SPONSORING AGENCY NAME AND ADDRESS National Aeronautics and Space Administration Washington, D.C. 20546	13. TYPE OF REPORT & PERIOD COVERED Technical Note 14. SPONSORING AGENCY CODE
15. SUPPLEMENTARY NOTES	

16. ABSTRACT

Except for a few numerical results, nothing has been published, comparable in magnitude to the two-dimensional case, concerning free streamline solutions of the axisymmetric problem. Since the method of using conformal transformations is not available in axisymmetric and three-dimensional flows, it is necessary to adopt approximate methods for the free streamline analysis.

In this study an integral equation procedure has been applied to calculate the free streamline flow behind axisymmetric bodies at zero and small angles of attack. The method uses a modified condition for irrotational flow and iterates until the proper streamline location is found. Some of the results obtained by this procedure will be discussed in this report.

17. KEY WORDS	18. DISTRIBUTION STATEMENT Unclassified - Unlimited

19. SECURITY CLASSIF. (of this report) UNCLASSIFIED	20. SECURITY CLASSIF. (of this page) UNCLASSIFIED	21. NO. OF PAGES 144	22. PRICE* $3.00

*For sale by the Clearinghouse for Federal Scientific and Technical Information
Springfield, Virginia 22151

LIST OF TABLES

LIST OF ILLUSTRATIONS

DEFINITION OF SYMBOLS

Symbol	Definition
C_D	drag coefficient
C_L	lift coefficient
C_M	moment coefficient
C_T	tangential force coefficient
C_{M_N}	moment coefficient due to normal force
C_{M_T}	moment coefficient due to tangential force
C_N	normal force coefficient
C_P	pressure coefficient
C_{P_B}	cavitation coefficient, base pressure coefficient
C	constant part of the perturbation potential at the separation point
$f(s,\sigma)$	series approximation of the Kernel function at the singular point
g_n	nondimensional normal component of the undisturbed velocity component (g_n/U_∞)
P; P_B; P_∞	static pressures
q_n	nondimensional strength of the source rings (q_n/U_∞)
U_∞	velocity of the undisturbed flow field
V_N	nondimensional normal velocity component $(V_N U_\infty)$
V_T	nondimensional tangential velocity component (V_T/U_∞)
n	index, designating the particular case, n = 0, axisymmetric, and n = 1 normal flow
x,r,ω; ξ,ρ,ω'	cylindrical coordinates, made dimensionless by a typical length, usually the maximum radius of the body (x/R, r/R; ξ/R, ρ/R)

DEFINITION OF SYMBOLS (Continued)

Symbol	Definition
x, ρ^*, φ	spherical coordinates for the half-body. Made dimensionless with the maximum radius $R_\infty = 1$ of the half-body at infinity.
x_o	nondimensional distance of the point source from the stagnation point of the half-body (x_o/R_∞)
Δx	distance of the neutral point of the body from the reference point ($\Delta x/R$)
R	radius of body; reference length
R^*	radius of stream tube (R^*/R)
L	length of cavitation bubble (L/R)
D_c	maximum diameter of cavitation bubble (D_c/R)
s, σ	nondimensional arc length (s/R, σ/R)
s_B	separation point (s_B/R)
s_E	upper limit of integration for a closed wake (Riabouchinsky model) (s_E/R), or truncated wake
s_A	length of a typical section of the body (s_A/R)
$C_n(s,\alpha)$	local normal force coefficient
$E(k^2)$; $K(k^2)$ $F_n(k^2)$; $G_n(k^2)$	complete elliptical integrals of second and first kind, respectively, and of higher order
k^2	elliptical modulus
$z_1(s)$	nondimensional shift function, or centerline of the wake of a body at an angle of attack ($z_1(s)/R$)
α; $\alpha(s)$	fixed angle of attack of the rigid forebody and variable angle of attack along the wake semi-apex angle of a cone
β	semi-apex angle of a cone

DEFINITION OF SYMBOLS (Continued)

Symbol	Definition
$\delta(s)$	camber of wake centerline, measures displacement angle of wake
θ	angle between contour tangent and body axis
ϕ; φ	nondimensional potential function ($\phi/(U_\infty R)$; $\varphi/(U_\infty R)$).
Γ_1	body contourline from stagnation to separation point
Γ_2	contour of the free streamline
Γ_3	contour of the wake cylinder of the dissipation model
σ_m	nondimensional reference area
$\kappa(s)$	nondimensional curvature ($R/R_c(s)$)
$R_c(s)$	radius of curvature
ρ	density of the flowing medium
$\mu(s,\alpha)$	nondimensional source strength of the lifting body ($\mu(s,\alpha)/U_\infty$)
ϕ_s	separation angle of the sphere measured from the stagnation point

SUMMARY

Supercavitating flows about axisymmetric bodies at zero and small angles of attack are of wide practical importance. These flows are not so amenable to theoretical treatment as the plane flows, because the conformal mapping technique is not available in axisymmetric and three-dimensional flows. Approximate methods must therefore be adopted for the free streamline analysis.

In this study an integral equation has been applied to calculate the free streamline flow behind axisymmetric bodies at zero and small angles of attack. The problem could be reduced to the solution of the mixed boundary value problem of potential theory with the additional condition that a specified velocity shall be attained along the free streamline.

I. INTRODUCTION

The flow field about a body of revolution is usually determined by placing singularities along the axis of symmetry. Rankine [1] was thus able to calculate families of bodies by distributing point sources of variable strengths on the axis. This method was later improved by Taylor [2] and Fuhrmann [3]. Many years later, Weinstein [4] applied surface singularities to determine the flow fields about obstacles such as rings, disks, and cylinders. Further contributions to the indirect problem, in which the source strength is given and the corresponding body shape is sought, were made by Van Tuyl [5] and Sadowsky and Sternberg [6].

The direct problem, where the contour of the body is given and the corresponding strength of the sources is to be determined, was first solved by von Kármán [7] with an axial distribution of singularities for the zero and finite angle-of-attack case. Lotz [8] probably published the first method using surface singularities; however, before that, Trefftz [9] had used annular sources to calculate the contraction coefficient of the vena contracta. Later, Riegels [10] extended the method of reference 8 and applied it to bodies of revolution that

deviate slightly from rotational symmetry. All of these methods dealt with Dirichlet flows that do not permit the calculation of any drag force.

The Helmholtz flow concept, since it enabled the aerodynamicist to calculate a drag coefficient, meant an improvement. Over the years, a tremendous amount of literature on the two-dimensional Helmholtz-flow has accumulated. The first approximate solution of the axisymmetric problem was published by Bauer [11], who applied an axial distribution of sources to determine the drag of a sphere. However, this method is not well suited, since the flow field is everywhere continuous except on the axis. Therefore, the proper discontinuities cannot be duplicated at the separation point of the flow.

Consequently, Armstrong and Dunham [12] applied a surface distribution and devised an iterative scheme to determine the proper location of the free streamline. However, results calculated with this method were never published. The first numerical results for a disk placed normally to the stream were given by Garabedian [13].

In this report, the method of Riegels [10] is extended to the Helmholtz-flow concept. The surface of the forebody and the free streamline are replaced by surface singularities. The location of the free streamline must be assumed for the first iteration. The final proper location must be obtained by an iteration that satisfies certain specified boundary conditions. The problem contains at least one parameter for a forebody with fixed separation, problème du sillage, the base pressure C_{P_B} right behind the separation point, which is assumed to be constant along the remainder of the streamline. However, if the flow separates from a smooth body, for example, a sphere or ellipsoid, the problem will have one additional parameter, the separation point S_B, problème de la proue. In cavitational flow, the base pressure is approximately equal to the vapor pressure of the liquid, and the pressure is constant throughout the cavity. For wake flow, the base pressure must be obtained from experimental data, and the assumption that the pressure is constant along the wake is questionable. Boundary layer theory can be applied to determine the separation point.

A new linearized model is developed for the lifting body. The assumption of the Helmholtz-flow is also valid for this model. The pressure within the separated cavity remains constant, and additional pressures due to the normal flow are equalized across the circumference of the cavity, thus causing the local normal force along the cavity to vanish. The cavity is therefore shifted to an asymmetrical location to satisfy the no-lift condition.

II. THE DIFFERENT CAVITY OR WAKE MODELS

Several free streamline models discussed in this chapter will be compared with the original Helmholtz-Kirchhoff classical model. The four models are all characterized by the fact that the tangential velocity V_T along the free streamline is greater than the approach velocity U_∞.

For the Helmholtz-Kirchhoff model, or infinite cavity model, the base pressure C_{P_B} is zero, and consequently the calculated drag is less than the drag observed in experiments. To correct this deficiency, higher velocities must be permitted on the free streamline. Then, however, the streamlines curve back to the axis of symmetry, and certain cavity closure devices must be introduced. Thus, in model 2, the image or Riabouchinsky model, the free streamline reattaches to an artificial image of the forebody introduced at the end of the cavity. Only the drag of the first body is determined. The ultimate wake thickness is zero. In the third model, the reentrant jet model, the wake or cavity ends in a free stagnation point from which a reentrant jet projects forward toward the body base and vanishes there. This is an unreal feature, though it has some similarity to the often forward-thrown spray observed in cavities at low pressure. As in the Riabouchinsky model, there is a stagnation point at the end of the cavity, and the ultimate wake thickness is slightly negative on account of the fluid removed in the reentrant jet. One model, sometimes called the dissipation model or parallel streamline model, probably describes the wake flow better than the cavity flow. Here, the downstream wake thickness is not zero. The pressure is initially constant along the streamline, springing from the disk edges until they reach their maximum wake diameter. From here on, the direction of the velocity vector remains constant; its magnitude, however, decreases until $V_T(s)$ is equal to U_∞, the velocity of the undisturbed flow. This model was used for most of the calculated zero-angle-of-attack cases of this report. However, it was used exclusively for the lifting cases.

One can devise another model with exactly the wake width that is required to produce the drag force of the forebody. Here the far wake consists, again, of a parallel stream tube of radius $\sqrt{C_D}/2$. At some location downstream of the base of the body, the free streamlines intersect the stream tube forming thus a free stagnation point; therefore, the constant pressure condition cannot be satisfied over the rearward part of the free streamline, and other assumptions have to be made there.

The literature abounds with other models which are more or less of practical usefulness. Originally all models were devised for the plane case; however, one can apply them to the axisymmetric case without difficulty.

III. DISCUSSION OF THE THEORY

The Potential and the Velocities of an Axisymmetric Body

The perturbation potential function of an axisymmetric body covered with surface singularities of strength $q(s,\omega) = \cos(n\omega)q_n(s)$ is given by the surface integral of the source strength times the reciprocal distance between the fixed (x,r,ω) and the running point (ξ,ρ,ω'):

$$\varphi_n(s,\omega,\alpha) = -\frac{1}{4\pi}\int_0^{s_E}\int_0^{2\pi} q_n(\sigma,\alpha)\,\frac{\rho\cos(n\omega')\,d\omega'\,d\sigma}{[(x-\xi)^2+r^2+\rho^2-2r\rho\cos(\omega-\omega')]^{1/2}}\,. \tag{1.1}$$

For the case n = 0, the body is covered with source rings of constant circumferential strength, representing the zero angle of attack case, and for n = 1, the source strength varies with the cosine of the meridian angle ω. This case represents the body placed with its axis normal to the stream.

In general, the strength of the source rings and the surface of the body is defined as

$$q_n(s,\omega,\alpha) = \cos(n\omega)\; q(s,\alpha).$$

To integrate the potential function around the body, we rearrange equation (1.1) and write

$$\varphi_n(s,\omega,\alpha) = -\frac{1}{4\pi}\int_0^{s_E} q_n(\sigma,\alpha)\,\frac{\rho}{\sqrt{(x-\xi)^2+(r+\rho)^2}}\int_0^{2\pi}\frac{\cos(n\omega')}{\sqrt{1-k^2(1+\cos(\omega'-\omega))/2}}\,d\omega'\,d\sigma, \tag{1.2}$$

where k^2 is the elliptic modulus

$$k^2 = \frac{4r\rho}{(x-\xi)^2+(r+\rho)^2}\,.$$

With the substitution

$$\omega' - \omega = 2\chi; \quad d\omega' = 2d\chi, \tag{1.3}$$

we express the second integral in (1.2) as

$$I_{\varphi_n} = \int_0^{2\pi} \frac{\cos(n\omega')\, d\omega'}{\sqrt{1-k^2(1+\cos[\omega'-\omega])/2}} = 2\int_0^{\pi} \frac{\cos[n(2\chi+\omega)]}{\sqrt{1-k^2\cos^2\chi}}\, d\chi. \tag{1.4}$$

To reduce the elliptic integral to Legendre's form, we use the substitution

$$\cos\chi = \sin\varphi, \quad \chi = \arccos(\sin\varphi) = \frac{\pi}{2} - \varphi. \tag{1.5}$$

Reversing the limits $-\pi/2$ and $\pi/2$ yields finally, for (1.4),

$$I_{\varphi_n} = 2\left\{\cos(n\omega)\; 2\int_0^{\pi/2} \frac{\cos\{2n(\pi/2-\varphi)\}}{\sqrt{1-k^2\sin^2\varphi}}\, d\varphi \right.$$

$$\left. - \sin(n\omega)\int_{-\pi/2}^{\pi/2} \frac{\sin[2n(\pi/2-\varphi)]}{\sqrt{1-k^2\sin^2\varphi}}\, d\varphi \right\}.$$

With the relations

$$\cos[2n(\tfrac{\pi}{2} - \varphi)] = (-1)^n \cos(2n\varphi)$$

and (1.6)

$$\sin[2n(\tfrac{\pi}{2} - \varphi)] = -(-1)^n \sin(2n\varphi),$$

one can define two integrals. The first one is

$$F_n(k^2) = (-1)^n \int_0^{\pi/2} \frac{\cos(2n\varphi)}{\sqrt{1-k^2\sin^2\varphi}}\, d\varphi.$$

The second integral

$$-(-1)^n \int_{-\pi/2}^{\pi/2} \frac{\sin(2n\varphi)}{\sqrt{1-k^2\sin^2\varphi}}\, d\varphi = 0$$

vanishes for all n. The perturbation potential can finally be written as

$$\varphi_n(s,\omega,\alpha) = -\frac{\cos(n\omega)}{2\pi} \int_0^{s_E} q_n(\sigma,\alpha) \frac{2\rho\, F_n(k^2)\, d\sigma}{\sqrt{(x-\xi)^2 + (r+\rho)^2}}. \qquad (1.7)$$

Partial differentiation of the perturbation potential (1.1) with respect to x yields the perturbation velocity in the x-direction.

$$\frac{\partial\varphi_n}{\partial x} = \frac{1}{4\pi} \int_0^{s_E} q_n(\sigma,\alpha) \frac{\rho(x-\xi)}{[(x-\xi)^2 + (r+\rho)^2]^{3/2}} \int_0^{2\pi} \frac{\cos(n\omega')\, d\omega'}{[1-k^2(1+\cos(\omega'-\omega))/2]^{3/2}}. \qquad (1.8)$$

With the aid of the substitutions (1.3) and (1.5), we can write for the second integral on the right-hand side of (1.8)

$$I_{\varphi_x} = \int_0^{2\pi} \frac{\cos(n\omega')\, d\omega'}{[1-k^2(1+\cos(\omega'-\omega))/2]^{3/2}} = 2\cos(n\omega)(-1)^n \int_0^{\pi/2} \frac{\cos(2n\varphi)}{[1-k^2\sin^2\varphi]^{3/2}}\, d\varphi$$

(equation continued on next page)

$$+ \sin(n\omega)(-1)^n \int_{-\pi/2}^{\pi/2} \frac{\sin(2n\varphi)\, d\varphi}{[1-k^2 \sin^2\varphi]^{3/2}} .$$

We define now the first integral on the right-hand side as

$$G_n(k^2) = (-1)^n \int_{o}^{\pi/2} \frac{\cos(2n\varphi)\, d\varphi}{[1-k^2 \sin^2\varphi]^{3/2}} . \tag{1.9}$$

The second integral on the right-hand side

$$(-1)^n \int_{-\pi/2}^{\pi/2} \frac{\sin(2n\varphi)}{[1-k^2 \sin^2\varphi]^{3/2}}\, d\varphi = 0 \tag{1.10}$$

vanishes for all n.

The perturbation velocity component in the x-direction is now

$$\frac{\partial \varphi_n}{\partial x} = \frac{1}{2\pi} \int_{o}^{s_E} \frac{q_n(s,\alpha)\; 2\rho(x-\xi)\; G_n(k^2)}{[(x-\xi)^2 + (r+\rho)^2]^{3/2}}\, d\sigma .$$

Partial differentiation of equation (1.1) with respect to the radius r yields the perturbation velocity component in this direction.

$$\frac{\partial \varphi_n}{\partial r} = \frac{1}{4\pi} \int_{o}^{s_E} q_n(\sigma,\alpha) \cdot \frac{\rho}{[(x-\xi)^2 + (r+\rho)^2]^{3/2}}$$

$$\cdot \int_{o}^{2\pi} \frac{r\cos(n\omega') - \rho\cos(\omega'-\omega)\cos(n\omega')}{[1 - k^2(1 + \cos(\omega'-\omega))/2]^{3/2}}\, d\omega'\, d\sigma .$$

The second integral on the right-hand side, together with substitution (1.3), yields

$$I_{\varphi_r} = 2r \int_0^{\pi} \frac{\cos\ (2n\chi + n\omega)}{[1-k^2\ \cos^2\chi]^{3/2}}\ d\chi - 2\rho \int_0^{\pi} \frac{\cos\ (2\chi)\ \cos\ (2n\chi + n\omega)}{[1 - k^2\ \cos^2\chi]^{3/2}}\ d\chi. \quad (1.11)$$

The numerator of the second integral can be written as

$$\cos\ (2\chi)\ \cos\ (2n\chi + n\omega) = \cos\ (n\omega)\ [\cos\ \{2(n-1)\chi\} + \cos\ \{2(n + 1)\chi\}]$$

$$- \sin\ (n\omega)\ [\sin\ \{2(n + 1)\chi\} + \sin\ \{2(n-1)\chi\}]. \quad (1.12)$$

With the definition (1.9) and the substitution (1.5), the first integral on the right-hand side of (1.11) becomes

$$2\ \cos\ (n\omega)\ G_n(k^2) = \int_0^{\pi} \frac{\cos\ \{2n\chi + n\omega\}}{[1-k^2\ \cos^2\chi]^{3/2}}\ d\chi,$$

and the second integral is

$$\int_0^{\pi} \frac{\cos\ (2n\chi + n\omega)}{(1-k^2\ \cos^2\varphi)^{3/2}} \cos\ (2\chi)\ d\chi = \frac{\cos\ (n\omega)}{2} \int_0^{\pi} \frac{\cos[2(n-1)\chi]+\cos[2(n+1)\chi]}{(1 + k^2\ \cos^2\chi)^{3/2}}\ d\chi$$

$$- \frac{\sin\ (n\omega)}{2} \int_0^{\pi} \frac{\sin[2(n+1)\chi]+\sin[2(n-1)\chi]}{[1+k^2\cos^2\chi]^{3/2}}\ d\chi.$$

$$= \frac{2\ \cos(n\omega)}{2} \int_0^{\pi/2} \frac{(-1)^{n-1}\cos[2(n-1)\varphi]+(-1)^{n+1}\cos[2(n+1)\varphi]}{[1-k^2\ \sin^2\varphi]^{3/2}}\ d\varphi = \text{(continued on next page)}$$

$$= 2 \cos(n\omega) \frac{G_{n-1}(k^2) + G_{n+1}(k^2)}{2} .$$

The integral with the factor sin $(n\omega)$ vanishes for all n according to definition (1.10). The perturbation velocity component finally becomes

$$\frac{\partial \varphi_n}{\partial r} = \frac{1}{2\pi} \int_0^{s_E} q(\sigma,\alpha) \frac{2\rho \cos(n\omega)}{[(x-\xi)^2 + (r+\rho)^2]^{3/2}} \left\{ rG_n(k^2) - \frac{\rho}{2} [G_{n-1}(k^2)+G_{n+1}(k^2)] \right\} d\sigma.$$

The perturbation velocity component in circumferential direction ω is obtained by partial differentiation with respect to ω and multiplication with the factor 1/r:

$$\frac{1}{r} \frac{\partial \varphi_n}{\partial \omega} = \frac{-1}{4\pi} \int_0^{s_E} q_n(\sigma,\alpha) \frac{\rho^2}{[x-\xi)^2+(r+\rho)^2]^{3/2}} \int_0^{2\pi} \frac{\cos(n\omega') \sin(\omega'-\omega)}{[1-k^2(1+\cos(\omega'-\omega))/2]^{3/2}} d\omega' d\sigma. \tag{1.13}$$

We apply (1.3) to the second integral in (1.13) and write

$$I_{\varphi_\omega} = \int_0^{2\pi} \frac{\cos(n\omega') \sin(\omega'-\omega) d\omega'}{[1-k^2(1+\cos(\omega'-\omega))/2]^{3/2}} = 2 \int_0^{\pi} \frac{\cos(2\pi\chi+n\omega) \sin 2\chi}{[1-k^2 \cos^2\chi]^{3/2}} d\chi. \tag{1.14}$$

Using substitution (1.15) in equation (1.14) produces

$$\frac{-2 \sin(n\omega)}{2} \int_0^{\pi/2} (-1)^{n-1} \frac{\cos(2[n-1]\varphi) - (-1)^{n+1} \cos(2(n+1)\varphi)}{(1 - k^2 \sin^2\varphi)^{3/2}} d\varphi$$

$$= \sin(n\omega) [G_{n-1}(k^2) - G_{n+1}(k^2)].$$

The integral with the factor cos (nω) vanishes according to (1.10) and finally the w-perturbation velocity component becomes

$$\frac{\partial\varphi_n}{r\partial\omega} = \frac{1}{2\pi}\int_0^{s_E} q(\sigma,\alpha)\,\frac{\rho^2 \sin(n\omega)}{[(x-\xi)^2 + (r+\rho)^2]^{3/2}}\left(\frac{G_{n-1}(k^2) - G_{n+1}(k^2)}{2}\right).$$

For zero angle of attack with n = 0, we obtain from definition (1.9) the relation $G_{-1}(k^2) = G_{+1}(k^2)$. Therefore, $\partial\varphi_n/r\partial\omega$ equals zero for this case. The complete elliptic integrals $F_n(k^2)$ and $G_n(k^2)$ will be developed in appendix A.

The derived perturbation velocities u, v, and w are the velocities for fixed points (x,r,ω) which do not coincide with the surface on which the sources are placed. The general solution of the problem, however, requires that we know the normal or tangential velocities on the boundaries of the outer flow field. Part of the boundary is provided by the surface of the body. A closer investigation of the normal component of the velocity on the body surface reveals a discontinuity [14]. The jump in the velocity across the surface is exactly equal to the source strength, $+q(s,\alpha)/2$ to the outer flow field, and $-q(s,\alpha)/2$ to the inner flow field. The tangential velocity component, on the other hand, is continuous. In this respect, we have to account for this discontinuity by adding the proper component to the various perturbation velocities on the body surface.

We obtain for the axisymmetric flow, n = 0,

$$u_o(s) = -\frac{q_o(s)r'(s)}{2} + \frac{1}{2\pi}\int_0^{s_E} q_o(\sigma)\frac{2\rho(x-\xi)\,G_o(k^2)}{[(x-\xi)^2 + (r+\rho)^2]^{3/2}}\,d\sigma, \qquad (1.15)$$

and

$$v_o(s) = \frac{q_o(s)x'(s)}{2} + \frac{1}{2\pi}\int_0^{s_E} q_o(\sigma)\,\frac{2\rho[rG_o(k^2) - \rho G_1(k^2)]}{[(x-\xi)^2 + (r+\rho)^2]^{3/2}}\,d\sigma. \qquad (1.16)$$

The perturbation velocity components for the angle of attack case (n = 1) are

$$\frac{u_1(s,\alpha)}{\alpha \cos \omega} = -\frac{q_1(s,\alpha)r'}{2} + \frac{1}{2\pi}\int_0^{s_E} q_1(\sigma,\alpha) \frac{2\rho(x-\xi)\, G_1(k^2)}{[(x-\xi)^2 + (r+\rho)^2]^{3/2}}\, d\sigma, \tag{1.17}$$

$$\frac{v_1(s,\alpha)}{\alpha \cos \omega} = \frac{q_1(s,\alpha)x'}{2} + \frac{1}{2\pi}\int_0^{s_E} q_1(\sigma,\alpha) \frac{2\rho[rG_1(k^2) - \frac{\rho}{2}(G_0(k^2) + G_2(k^2))]}{[(x-\xi)^2 + (r+\rho)^2]^{3/2}}\, d\sigma \tag{1.18}$$

and

$$\frac{w_1(s,\alpha)}{\alpha(\cos \omega)} = \frac{1}{2\pi}\int_0^{s_E} q_1(\sigma,\alpha) \frac{2\rho^2[G_0(k^2) - G_2(k^2)]/2}{[(x-\xi)^2 + (r+\rho)^2]^{3/2}}\, . \tag{1.19}$$

The notations $r'(s)$ and $x'(s)$ are differentiations with respect to the arc length s. For $k^2 = 1$, the elliptic integrals have a pole with a logarithmic discontinuity. Therefore, the finite part of the integrals of equations (1.15) through (1.19) have to be taken.

The total potential of the body is obtained by superimposing the perturbation potential on the potential of the undisturbed flow field.

$$\phi_n(s,\omega,\alpha) = x(s) \cos \alpha + r(s) \sin \alpha \cos \omega + \varphi_n(s,\omega,\alpha). \tag{1.20}$$

From the boundary condition

$$\frac{\partial \phi_n(s,\omega,\alpha)}{\partial \bar{\nu}} \equiv V_N = 0, \tag{1.21}$$

we obtain the source strength on the surface of the body. We differentiate (1.20) with respect to the normal $\bar{\nu}$

$$\frac{\partial \phi_n(s,\omega,\alpha)}{\partial \bar{\nu}} = \frac{\partial x(s)}{\partial \bar{\nu}} \cos \alpha + \frac{\partial r(s)}{\partial \bar{\nu}} \sin \alpha \cos \omega + \frac{\partial \varphi_n(s,\omega,\alpha)}{\partial \bar{\nu}} .$$

With the equations of appendix C, we can write now

$$V_N = 0 = -r'(s) \cos \alpha + x'(s) \sin \alpha \cos \omega - u_n(s,\alpha)\, r'(s) + v_n(s,\alpha)\, x'(s) \tag{1.22}$$

where $u_n(s,\alpha)$ and $v_n(s,\alpha)$ are the perturbation velocities of equations (1.15) to (1.18). The first two terms on the right-hand side of the equation are the velocities of the undisturbed flow field.

Let us consider first the axially symmetric flow field with n = 0, $\alpha = 0$. The normal component of the parallel flow is independent of the meridian angle ω:

$$g_o(s,\alpha) = r'(s) \cos \alpha \approx r'(s). \tag{1.23}$$

The normal component sin α of the parallel flow is proportional to cos ω:

$$g_1(s,\alpha,\omega) = -\sin \alpha \cos \omega\, x'(s) \approx -x'(s)\, \alpha \cos \omega. \tag{1.24}$$

In the future, we will mostly use the linearized form of the boundary conditions. Only once in a while we will refer to the exact expressions.

We obtain the integral equation for determining the source strength on the surface of the body by replacing in (1.22) the terms $u_n(s,\alpha)$ and $v_n(s,\alpha)$ by their respective expressions (1.15) through (1.18):

$$q_n(s,\alpha) = 2g_n(s,\alpha) + \frac{1}{\pi} \int_o^{s_E} q_n(\sigma,\alpha)\, K_q(s,\sigma)\, d\sigma, \tag{1.25}$$

where the Kernel function depends only on the geometry of the body

$$K_q(s,\sigma) = \frac{-2\rho}{[(x-\xi)^2+(r+\rho)^2]^{3/2}} \left\{ [rx'-(x-\xi)r'] \, G_n(k^2) \right.$$

$$\left. - \frac{\rho x'}{2} \left(G_{n-1}(k^2) + G_{n+1}(k^2)\right) \right\} . \qquad (1.26)$$

The source strength $q_n(s,\alpha)$ is the only unknown of the integral equation (1.25); all other functions are known. The elliptic integrals of (1.26) have a pole at $k^2 = 1$. The singularity, however, has logarithmic character, and the quadratic integrability for solving (1.25) exists. Special procedures must be applied to solve the integral equation numerically. Equation (1.25), a linear integral equation of the second kind, shows the dependency of the source strength q on the angle of attack α and the shape of the contour of the body. If we set n = 0, we are considering the axisymmetric flow field, and we replace $q_n(s,\alpha)$ by the linearized form of (1.23). The source strength is then not dependent on α. However, for the angle of attack case with n = 1, we use (1.24) and we notice that $q_1(s,\alpha) = \alpha q_1(s)$.

Asymptotic Development of the Velocity Components

The integrands of the integral expression for the velocity components are now developed into a power series of small $\epsilon = \sigma - s$:

$$\rho = r + r'\epsilon + r''\epsilon^2/2 + \ldots$$

$$\xi = x + x'\epsilon + x''\epsilon^2/2 + \ldots ,$$

where primed values represent derivatives with respect to the arc length s. To solve the integrals numerically, the following procedure is used which shall be demonstrated as an example with the u-component. We repeat equation (1.15) for n = 0:

$$u_o(s) = -\frac{q_o(s)r'}{2} + \frac{1}{2\pi} \int_o^{s_E} q_o(\sigma) \, \frac{2\rho}{[(x-\xi)^2 + (r+\rho)^2]^{3/2}} \, (x-\xi) \, G_o(k^2) \, d\sigma .$$

The integrand has a singularity at $x = \xi$. However, the value of the integral is finite if the principal value of the integral is taken. To avoid the singularity, the series approximation of the integrand containing the constant term free of ϵ is subtracted from the integrand. Then the expression under the integral sign is zero at the singular point $s = \sigma$, and the integral can be treated numerically. By designating the approximating series as $f(s,\sigma)$ one obtains, for the u_o-component:

$$u_o(s) = -\frac{q_o(s)r'}{2} + \frac{1}{2\pi}\int_o^{s_E} [q_o(\sigma)\, K(s,\sigma) - f(s,\sigma)]\, d\sigma + \frac{1}{2\pi}\int_o^{s_E} f(s,\sigma)\, d\sigma. \tag{2.1}$$

The first integral on the right-hand side is now free of any singularity, and can be solved numerically. The second integral contains the singularity and it can be treated analytically. The principal value of the integral must be used. This is the general procedure which is applied to all integrals as long as they are singular.

Continuing now with the general development, one obtains, after some algebra, the series $f(s,\sigma)$ for the potential φ

$$-f_\varphi(s,\sigma) = -q_n(s,\alpha)\left[\ln\frac{8r}{|s-\sigma|} - 2n\right] + \ldots .$$

The integration of this function yields

$$-\frac{1}{2\pi}\int_o^{s_E} f_\varphi(s,\sigma)\, d\sigma = -\frac{q_n(s,\alpha)}{2\pi}\left[s_E \ln\frac{8r}{|s-\sigma|} + s \ln\left|1 - \frac{s_E}{s}\right| + (1-2n)s_E\right] + \ldots,$$

where $n = 0, 1$, respectively.

For the velocity components, the respective functions are

$$f_u(s,\sigma) = -q_n(s,\alpha)\left[\frac{x'}{\sigma - s} + \frac{x'r'+rx''}{2r}\right] - q_n'(s,\alpha)x' + \ldots$$

$$f_v(s,\sigma) = -q_n(s,\alpha)\left[\frac{r'}{\sigma-s} - \frac{1}{2r}\left(\ln\frac{8r}{|s-\sigma|} - (1+2n)\right) + \frac{r'^2 + rr''}{2r}\right] - q_n'(s,\alpha)r'$$

$$f_w(s,\sigma) = \frac{n}{r}\, q_n(s,\alpha)\left[\ln\frac{8r}{|s-\sigma|} - 2\right] + \ldots ,$$

and integration again yields

$$\frac{1}{2\pi}\int_0^{s_E} f_u(s,\sigma)\, d\sigma = -\frac{q_n(s,\alpha)}{2\pi}\left[x'\ln\left|1 - \frac{s_E}{s}\right| + \frac{x'r' + rx''}{2r}\, s_E\right]$$

$$- \frac{q_n'(s,\alpha)}{2\pi}\, x's_E + \ldots$$

$$\frac{1}{2\pi}\int_0^{s_E} f_v(s,\sigma)\, d\sigma = -\frac{q_n(s,\alpha)}{2\pi}\left[r'\ln\left|1 - \frac{s_E}{s}\right| + \frac{r'^2 + rr''}{2r}\, s_E\right.$$

$$\left. - \frac{1}{2r}\left(s_E \ln\frac{8r}{|s - s_E|} + s\ln\left|1 - \frac{s_E}{s}\right| - 2n\, s_E\right)\right] - q_n'(s,\alpha)r's_E/2\pi + \ldots$$

$$\frac{1}{2\pi}\int_0^{s_E} f_w(s,\sigma)\, d\sigma = n\,\frac{q_n(s,\alpha)}{2\pi r}\left[s_E \ln\frac{8r}{|s - s_E|} + s\ln\left|1 - \frac{s_E}{s}\right| - s_E\right] + \ldots .$$

The function $f(s,\sigma)$ and the respective integral for determining the strength of the source distribution (1.25) are

$$f_q(s,\sigma) = q_n(s,\alpha)\left[x'\left(\ln\frac{8r}{|s-\sigma|} - (1+2n)\right) - r\kappa\right]/2r + \ldots$$

$$\frac{1}{\pi}\int_0^{s_E} f_q(s,\sigma)\,d\sigma = \frac{q_n(s,\alpha)}{2\pi r}\left[x'\left(s_E \ln\frac{8r}{|s-s_E|} + s\ln\left|1-\frac{s_E}{s}\right| - 2n\,s_E\right)\right.$$

$$\left. - rK\,s_E\right] + \ldots\,,$$

where K is the curvature of the contour or the free streamline

$$K = x'r'' - r'x''.$$

For acute cone apex angles, the above series expansion is not very well suited. For this case, a special expansion which is only applicable to small cone angles is given in appendix B.

With the above series expansion, we can finally write the complete perturbation potential for arbitrary meridian angles ω

$$\frac{\varphi_n(s,\omega,\alpha)}{\cos(n\omega)} = -\frac{1}{2\pi}\int_0^{s_E}\left\{q_n(\sigma,\alpha)\,\frac{2\rho\,F_n(k^2)}{\sqrt{(x-\xi)^2+(r+\rho)^2}} - q_n(s,\alpha)\left(\ln\frac{8r}{|s-\sigma|} - 2n\right)\right\}d\sigma$$

$$- \frac{q_n(s,\alpha)}{2\pi}\left[s_E\ln\frac{8r}{|s-s_E|} + s\ln\left|1-\frac{s_E}{s}\right| + (1-2n)\,s_E\right]. \qquad (2.2)$$

The velocity components become

$$\frac{u_n(s,\omega,\alpha)}{\cos(n\omega)} = -\frac{q_n(s,\alpha)r'}{2} + \frac{1}{2\pi}\int_0^{s_E}\left\{q_n(\sigma,\alpha)\,\frac{2\rho(x-\xi)\,G_n(k^2)}{[(x-\xi)^2+(r+\rho)^2]^{3/2}}\right.$$

$$\left. + q_n(s,\alpha)\left[\frac{x'}{\sigma-s} + \frac{x'r'+rx''}{2r}\right] + q'(s,\alpha)x'\right\}d\sigma$$

$$- \frac{q_n(s,\alpha)}{2\pi}\left[x'\ln\left|1-\frac{s_E}{s}\right| + \frac{x'r'+rx''}{2r}\,s_E\right] - \frac{q_n'(s,\alpha)}{2\pi}\,x's_E, \qquad (2.3)$$

$$\frac{v_n(s,\omega,\alpha)}{\cos(n\omega)} = \frac{q_n(s,\alpha)}{2}\,x' + \frac{1}{2\pi}\int_0^{s_E}\Bigg\{q_n(\sigma,\alpha)\,\frac{2\rho}{[(x-\xi)^2+(r+\rho)^2]^{3/2}}\Bigg(rG_n(k^2)$$

$$-\frac{\rho}{2}\,[G_{n-1}(k^2)+G_{n+1}(k^2)]\Bigg)+q_n(s,\alpha)\left[\frac{r'}{\sigma-s}-\frac{1}{2r}\left(\ln\frac{8r}{|\sigma-s|}-(1+2n)\right)\right.$$

$$\left.+\frac{r'^2+rr''}{2r}\right]+q_n'(s,\alpha)r'\Bigg\}\,d\sigma-\frac{q_n(s,\alpha)}{2\pi}\left[r'\ln\left|1-\frac{s_E}{s}\right|+\frac{r'^2+rr''}{2r}\,s_E\right.$$

$$\left.-\frac{1}{2r}\left(s_E\ln\frac{8r}{|s-s_E|}+s\ln\left|1-\frac{s_E}{s}\right|-2n\,s_E\right)\right]-\frac{q_n'(s,\alpha)}{2\pi}\,s_Er' \tag{2.4}$$

and

$$\frac{w(s,\omega,\alpha)}{\sin(n\omega)} = \frac{1}{2\pi}\int_0^{s_E}\Bigg\{q_n(\sigma,\alpha)\,\frac{2\rho}{[(x-\xi)^2+(r+\rho)^2]^{3/2}}\,\frac{\rho}{2}\,(G_{n-1}(k^2)-G_{n+1}(k^2))$$

$$-\frac{n}{r}\,q_n(s,\alpha)\left(\ln\frac{8r}{|\sigma-s|}-2\right)\Bigg\}\,d\sigma+n\,\frac{q_n(s,\alpha)}{2\pi r}\left[s_E\ln\frac{8r}{|s-\sigma|}\right.$$

$$\left.+s\ln\left|1-\frac{s_E}{s}\right|-s_E\right]. \tag{2.5}$$

The integral equation (1.25) becomes now

$$\frac{2g_n(s,\omega,\alpha)}{\cos(n\omega)} = q_n(s,\alpha)+\frac{1}{\pi}\int_0^{s_E}\Bigg\{q_n(\sigma,\alpha)\,\frac{2\rho}{[(x-\xi)^2+(r+\rho)^2]^{3/2}}\left[(rx'-r'(x-\xi))G_n(k^2)\right.$$

(equation continued on next page)

$$- \frac{\rho x'}{2} \left(G_{n-1}(k^2) + G_{n+1}(k^2)\right)\Big] - \frac{q_n(s,\alpha)}{2r}\left[x'\left(\ln\frac{8r}{|s-\sigma|} - (1+2n)\right)\right.$$

$$\left. - r\kappa\right]\Big\} d\sigma + \frac{q_n(s,\alpha)}{2\pi r}\left[x'\left(s_E \ln\frac{8r}{|s-s_E|} + s \ln\left|1 - \frac{s_E}{s}\right| - 2n\, s_E\right)\right.$$

$$\left. - \kappa r\, s_E\right] . \qquad (2.6)$$

In this report, we very often refer to the normal and tangential velocities of the body surface, which are quoted here for n = 0 and n = 1 separately. According to the equations (C.1) and (C.2) of appendix C, we obtain for the normal velocity of the body in axial flow

$$V_N(s) = -r' + \frac{q_o(s)}{2} + \frac{1}{2\pi}\int_o^{s_E}\left\{2\rho q_o(\sigma)\,\frac{(rx'-r'(x-\xi))G_o(k^2)-x'\rho G_1(k^2)}{[(x-\xi)^2+(r+\rho)^2]^{3/2}}\right.$$

$$\left. - \frac{q_o(s)}{2r}\left(x' \ln\frac{8r}{|\sigma-s|} - x' - r\kappa\right)\right\} d\sigma$$

$$+ \frac{q_o(s)}{2\pi}\left[\frac{x'}{2r}\left(s_E \ln\frac{8r}{|s-s_E|} + s \ln\left|1 - \frac{s_E}{s}\right|\right) - \frac{\kappa s_E}{2}\right] . \qquad (2.7)$$

The tangential velocity for this case is given as

$$V_T(s) = x' + \frac{1}{2\pi}\int_o^{s_E}\left\{2\rho q_o(\sigma)\,\frac{(x'(x-\xi)+rr')G_o(k^2)-\rho r' G_1(k^2)}{[(x-\xi)^2+(r+\rho)^2]^{3/2}}\right.$$

$$\left. + q_o(s)\left[\frac{1}{\sigma-s} + \frac{r'}{2r}\left(2 - \ln\frac{8r}{|s-\sigma|}\right)\right] - q_o'(s)\right\} d\sigma - \frac{q_o(s)}{2\pi}\left\{\left(1 -\right.\right.$$

$$\left.\left. - \frac{r's}{2r}\right)\ln\left|1 - \frac{s_E}{s}\right| + \frac{r's_E}{2r}\left(1 - \ln\frac{8r}{|s-s_E|}\right)\right\} - \frac{q_o'(s)s_E}{2\pi} . \qquad (2.8)$$

The corresponding velocities for the body at an angle of attack α are, according to (C.17) and C.18) for the meridian angle $\omega = 0$,

$$V_{N1}(s,\alpha) = \alpha x' + \frac{q_1(s,\alpha)}{2} + \frac{1}{2\pi}\int_0^{s_E} \cdot\left\{\frac{2\rho q_1(\sigma,\alpha)\left[(rx'-r'(x-\xi))G_1(k^2) - x'\rho(G_0(k^2)+G_2(k^2))/2\right]}{\left[(x-\xi)^2 + (r+\rho)^2\right]^{3/2}}\right.$$

$$\left. - \frac{q_1(s,\alpha)}{2r}\left(x' \ln\frac{8r}{|\sigma-s|} - 3x' - rK\right)\right\} d\sigma$$

$$+ \frac{q_1(s,\alpha)}{2\pi}\left[\frac{x'}{2r}\left(s_E \ln\frac{8r}{|s-s_E|} + s \ln\left|1 - \frac{s_E}{s}\right| - 2s_E\right) - \frac{Ks_E}{2}\right] \qquad (2.9)$$

and

$$V_{T1}(s,\alpha) = \alpha r' + \frac{1}{2\pi}\int_0^{s_E}\left\{2\rho q_1(\sigma,\alpha)\frac{(x'(x-\xi)+rr')G_1(k^2) - \rho r'(G_0(k^2)+G_2(k^2))/2}{\left[(x-\xi)^2 + (r+\xi)^2\right]^{3/2}}\right.$$

$$\left. + q_1(s,\alpha)\left[\frac{1}{\sigma-s} + \frac{r'}{2r}\left(4 - \ln\frac{8r}{|\sigma-s|}\right)\right] + q_1'(s,\alpha)\right\} d\sigma$$

$$- \frac{q_1(s,\alpha)}{2\pi}\left\{\left(1 - \frac{r's}{2r}\right)\ln\left|1 - \frac{s_E}{s}\right| + \frac{r's_E}{2r}\left(3 - \ln\frac{8r}{|s-s_E|}\right)\right\}$$

$$- \frac{q_1'(s,\alpha)s_E}{2\pi}\,. \qquad (2.10)$$

The Solution of the Integral Equation

We replace the integral equation (2.6) by a system of N-linear equations and solve this system for the N-unknown q_ν. From now on, we reserve the index ν for the fixed point s on the contour and the free streamline (which is here considered a fixed surface, too) and the index μ for the running point σ. For the numerical integration scheme, we use the quadrature procedure of Gauss, where the value of the function at certain prescribed abscissas s_μ is multiplied with a certain weight A_μ. We call $A_\mu = \Delta L_m a_\mu$ the modified weight. It is obtained by multiplying the original weight a_μ, which is normalized to 1, with the sectional length ΔL_m as shown in figure 1. The total length of the body is therefore given as

$$s_E = \sum_{\mu=1}^{N} A_\mu = \sum_{m=1}^{M} \Delta L_m \sum_{\mu=1}^{P} a_\mu,$$

where the number of body sections is designated by M and P is the number of points in one segment. This number does not change. It is the same for all segments. The total number of points is therefore given by $N = M \cdot P$.

After replacing in equation (2.6) the integral sign with the summation sign and collecting all terms multiplied with q_ν, we now obtain

$$\frac{2(g_n)_\nu}{\cos(n\omega)} = (q_n)_\nu \left[1 + \frac{1}{2r_\nu\pi}\left\{x'_\nu\left(\ln\frac{8r_\nu}{|s_\nu - s_E|} + s_\nu \ln\left|1 - \frac{s_E}{s_\nu}\right| - 2ns_E\right)\right.\right.$$

$$\left.\left. -\kappa_\nu r_\nu s_E - \sum_{\mu=1}^{N}{}' \left[x'\left(\ln\frac{8r_\nu}{|s_\nu - s_\mu|} - (1+2n)\right) - r_\nu\kappa_\nu\right] A_\mu\right\}\right]$$

$$- \frac{1}{\pi}\sum_{\mu=1}^{N}{}' (q_n)_\mu 2r_\mu \frac{(r_\nu x'_\nu - r'_\nu(x_\nu - x_\mu))G_n(k^2_{\nu\mu}) - r_\mu x'_\nu (G_{n-1}(k^2_{\nu\mu}) + G_{n+1}(k^2_{\nu\mu}))/2}{[x_\nu - x_\mu)^2 + (r_\nu + r_\mu)^2]^{3/2}} A_\mu. \qquad (3.1)$$

The primed summation sign means that the term $\mu = \nu$ is omitted in the summation process, since $f_{\nu,\mu}$ was originally defined as the series expansion of the Kernel function $K_{\nu,\mu}$ at the singular point. The inclusion of the constant term in this expansion insures that the two terms under the summation signs cancel each other at the point $\mu = \nu$.

In equation (3.1) the source strength q_ν is the unknown. The left-hand side of the equation is known and is substituted by either equations (1.23) or (1.24) depending on n = 0 or n = 1. In matrix notation we write the N-linear equation as

$$\begin{bmatrix} a_{11} & a_{12} & .. & a_{1N} \\ a_{21} & a_{22} & .. & a_{2N} \\ . & . & .. & . \\ a_{N1} & a_{N2} & .. & a_{NN} \end{bmatrix} \begin{bmatrix} q_{n1} \\ q_{n2} \\ . \\ q_{nN} \end{bmatrix} = \begin{bmatrix} 2(g_n)_1 \\ 2(g_n)_2 \\ . \\ 2(g_n)_N \end{bmatrix}. \tag{3.2}$$

The elements of the main-diagonal are given by the expression

$$a_{\nu\nu} = 1 + \frac{1}{2\pi r_\nu}\left[x'_\nu\left(s_E \ln\frac{8r_\nu}{|s_\nu - s_E|} + s_\nu \ln\left|1 - \frac{s_E}{s}\right| - 2ns_E\right) - \kappa_\nu r_\nu s_F\right]$$

$$- \frac{1}{2\pi r_\nu}\sum_{\mu=1}^{N}{}' \left[x'_\nu\left(\ln\frac{8r_\nu}{|s_\mu - s_\nu|} - (1+2n)\right) - \kappa_\nu v_\nu\right] A_\mu$$

and the elements of the neighboring diagonals are

$$a_{\nu\mu} = 2r_\mu \frac{(r_\nu x'_\nu - r'_\nu(x_\nu - x_\mu))G_n(k^2_{\nu\mu}) - r_\mu x'_\nu (G_{n-1}(k^2_{\nu\mu}) + G_{n+1}(k^2_{\nu\mu}))/2}{\pi[(x_\nu - x_\mu)^2 + (r_\nu + r_\mu)^2]^{3/2}} A_\mu.$$

The matrix is usually conditioned satisfactorily [15]. The elements of the principal diagonal $a_{\nu\nu}$ are larger by one magnitude than the elements $a_{\nu\mu}$ of the neighboring diagonals. The solution function q_ν is usually very smooth. For one particular example of calculation, the value of the determinant was det A = 53.4. The conditioning number of the system had a value of $K_H = 2.7 \times 10^{-14}$. The number of points used to calculate the flow field was N = 64. The determinant, as well as the conditioning number, depends on N. With decreasing N, the conditioning of the system usually improves, provided the determinant is different from zero.

After having solved the system of equations for the source strength q_ν, one obtains the velocity components by a simple quadrature:

$$\frac{(u_n)_\nu}{\cos(n\omega)} = -\frac{(q_n)_\nu}{2} r'_\nu + \frac{1}{2\pi} \sum_{\mu=1}^{N}{}' \left[(q_n)_\mu \frac{2r_\nu (x_\nu - x_\mu) G_n(k^2_{\nu\mu})}{[(x_\nu - x_\mu)^2 + (r_\nu + r_\mu)^2]^{3/2}} \right.$$

$$\left. + (q_n)_\nu \left\{ \frac{x'_\nu}{s_\mu - s_\nu} + \frac{x'_\nu r'_\nu + r_\nu x''_\nu}{2r_\nu} \right\} + (q'_n)_\nu x'_\nu \right] A_\mu$$

$$- \frac{(q_n)_\nu}{2\pi} \left[x'_\nu \ln \left| 1 - \frac{s_E}{s_\nu} \right| + \frac{x'_\nu r'_\nu + r_\nu x''_\nu}{2r_\nu} s_E \right] - \frac{(q'_n)_\nu}{2\pi} x'_\nu s_E, \qquad (3.3)$$

$$\frac{(v_n)_\nu}{\cos(n\omega)} = \frac{(q_n)_\nu}{2} x'_\nu + \frac{1}{2\pi} \sum_{\mu=1}^{N}{}' \left\{ (q_n)_\mu \frac{2r_\mu [r_\nu G_n(k^2_{\nu\mu}) - r_\mu (G_{n-1}(k^2_{\nu\mu}) + G_{n+1}(k^2_{\nu\mu}))/2]}{[(x_\nu - x_\mu)^2 + (r_\nu + r_\mu)^2]^{3/2}} \right.$$

$$+ (q_n)_\nu \left[\frac{r'_\nu}{s_\mu - s_\nu} - \frac{1}{2r_\nu} \left(\ln \frac{8r_\nu}{|s_\mu - s_\nu|} - (1+2n) \right) + \frac{r'^2_\nu + r_\nu r''_\nu}{2r_\nu} \right]$$

$$\left. + \frac{(q'_n)_\nu}{2\pi} r'_\nu \right\} A_\mu - \frac{(q_n)_\nu}{2\pi} \left\{ r'_\nu \ln \left| 1 - \frac{s_E}{s_\nu} \right| + \frac{r'^2_\nu + r_\nu r''_\nu}{2r_\nu} s_E \right.$$

$$\left. - \frac{1}{2r_\nu} \left(s_E \ln \frac{8r_\nu}{|s_\nu - s_E|} + s_\nu \ln \left| 1 - \frac{s_E}{s_\nu} \right| - 2n s_E \right) \right\} - \frac{(q'_n)_\nu}{2\pi} r'_\nu s_E, \qquad (3.4)$$

and

$$\frac{(w_n)_\nu}{\sin(n\omega)} = \frac{1}{2\pi} \sum_{\mu=1}^{N}{}' \left\{ (q_n)_\mu \frac{r_\mu^2 (G_{n-1}(k_{\nu\mu}^2) - G_{n+1}(k_{\nu\mu}^2))}{[(x_\nu - x_\mu)^2 + (r_\nu + r_\mu)^2]^{3/2}} \right.$$

$$\left. - \frac{n}{r_\nu} (q_n)_\nu \left[\ln \frac{8r_\nu}{|s_\mu - s_\nu|} - 2 \right] \right\} A_\mu \qquad (3.5)$$

$$+ n \frac{(q_n)_\nu}{2\pi r_\nu} \left[s_E \ln \frac{8r_\nu}{|s_\nu - s_E|} + s_\nu \ln \left| 1 - \frac{s_E}{s_\nu} \right| - s_E \right].$$

This is the usual procedure to solve the flow field about a body of revolution with a fixed contour. So far, the wake or cavitation bubble has not been mentioned specifically. However, for the solution of the wake problem, which will be discussed in the following chapter, a solution q_ν of (3.2) is necessary and will be used to calculate the perturbation potential and the tangential velocity.

The Axisymmetric Cavity

Following Helmholtz's suggestion, the free streamline discontinuity surface is taken as an idealization of the separation surface which divides the main flow from the wake or cavity which follows separation. The thickness of the sheet is taken vanishingly small, and the flow on one side is assumed to have no effect on the other except through the pressure. For cavitating flows with ratios of cavity density vanishingly small, the flow in the cavity is assumed as quiescent, and it is therefore a constant pressure region.

The problem to find solutions to the discontinuous flow about bodies of revolution with a smooth contour has two parameters. These are the separation point s_B and the cavity pressure coefficient C_{PB}. In order to explain the general method of solution in principle, we calculate the flow about a body where the flow separates abruptly at the corner of the base. The problem then has only one parameter which is the cavity pressure coefficient C_{PB} or the equivalent tangential velocity V_{TB}.

These prescribed parameters are constant along the free streamline Γ_2 in accordance with the assumption that the flow in the cavity is quiescent. For small velocities in the cavity, C_{PB} and V_{TB} are functions of the arc length s. For the discussion of the general theory, we assume a constant V_{TB} and we adopt the infinite cavity concept, which is the Helmholtz model ($V_{TB} = 1$). Special changes of the general method of solution if other models are applied will be described at the end of this chapter.

In particular, we assume the flow to be (1) inviscid, (2) gravityless, and (3) steady. Figure 1a represents the upper half-plane of a body of revolution and the corresponding cavity. According to our assumptions, the body possesses a sharp corner at s_B where the flow separates abruptly. Otherwise, the contour Γ_2 of the body is smooth except at the stagnation point. The cavity is separated from the outer flow field by the free streamline Γ_2. On the given contour Γ_1, the absolute value of the velocity vector $|\vec{V}_T(s)|$ is unknown; its direction, however, is known with condition (1.21). Downstream of s_B the absolute value of the tangential velocity vector $|\vec{V}_{TB}|$ is specified on Γ_2; its direction, however, is unknown. With the specified velocity V_{TB} on Γ_2, the velocity potential is also known on Γ_2 except for a constant. The position of Γ_2 is therefore not known and we have to choose it arbitrarily on some reasonable basis (see Fig. 1b). We designate this line Γ_2^*.

It is our goal to determine the position of Γ_2. For the solution of the problem, we formulate that:

(a) The boundary condition $V_N(s) = 0$ has to be satisfied on Γ_1.

(b) On the arbitrary line Γ_2^*, the velocity and therefore also the potential except for a constant is known.

(c) If Γ_2^* is not identical with the free streamline Γ_2, the normal velocity ($V_N(s) \neq 0$) does not vanish on Γ_2^* and therefore Γ_2^* is not a streamline.

(d) From the magnitude of $V_N(s)$ on Γ_2^*, we can deduce the shift of the line Γ_2^*. The solution of the problem is therefore obtained by iteration.

(e) Since the position of the free streamline is not known, we have to conduct all numerical calculations on the arbitrary line Γ_2^*.

Besides the velocity V_{TB}, we mentioned also the potential $\phi_{oB}(s)$ in (b). Later on, we will employ this potential function rather than the velocity V_{TB}. The reason for this choice will be given later in this report.

(1) The Solution of the Problem by Specifying the Potential Function

As a next step, we establish the set of integral equations with which we determine the source strength $q_o(s)$. On the contour Γ_1, we satisfy $V_N(s) = 0$ and obtain therefore

$$q_o(s) = 2r'(s) + \frac{1}{\pi} \int_o^{s_E} q_o(\sigma)\, K_q(s,\sigma)\, d\sigma, \tag{4.1}$$

where the Kernel function $K_q(s,\sigma)$ is given for $n = 0$ by equation (1.26). For points within the region Γ_2^*, we obtain the integral equation

$$\phi_{\sigma B}(s) - x^*(s) = -\frac{1}{2\pi} \int_o^{s_E} q_o(\sigma)\, K_\varphi(s,\sigma)\, d\sigma \tag{4.2}$$

with the Kernel function

$$K_\varphi(s,\sigma) = \frac{2\rho F_o(k^2)}{\sqrt{(x^*-\xi)^2+(r^*+\rho)^2}}.$$

With known potential $\phi_{oB}(s)$, equation (4.2) is an integral equation of the first kind. In both equations (4.1) and (4.2), the source strength $q_o(s)$ is the only unknown function. The Kernel functions $K_q(s,\sigma)$ and $K_\varphi(s,\sigma)$ depend only on the geometry of the body contour Γ_1 and the arbitrary line Γ_2^*. The integration limits are the stagnation point ($s = 0$) and the point where the wake is truncated. About the choice of the point s_E and the influence of the truncated part of the "infinite" cavity or wake, some explanation will be given at a later time.

On the left-hand side of equation (4.2), we recognize the total potential of the free streamline Γ_2 which is defined as

$$\phi_{oB}(s) = \phi_{oB}(s_B) + \int_{s_B}^{s} V_{TB}\, ds, \tag{4.3}$$

where only the value of the integral is known. The value of the potential at the separation point s_B is a constant and unknown.

$$\phi_{oB}(s_B) = C.$$

The two terms on the left side of equation (4.2) would represent the perturbation potential of the body with the exact free streamline Γ_2 if $x^*(s)$ would have been the abscissa of Γ_2. Since, however, $x^*(s)$ belongs to the arbitrary line Γ_2^*, the term $(\phi_{oB}(s) - x^*(s))$ is only approximately $\varphi_{oB}(s)$, except at the separation point where $x^*(s) = x(s)$. For a convergent procedure, however, where $\Gamma_2 = \Gamma_2^*$, the left-hand side becomes, after a sufficient number of iterations, identical with $\varphi_{oB}(s)$. We define there

$$\varphi_{oB}(s) = \phi_{oB}(s) - x^*(s) = \overline{\varphi_o(s)} + C. \tag{4.4}$$

The barred expression

$$\overline{\varphi_o(s)} = \int_{s_B}^{s} V_{TB}\, ds - x^*(s) \tag{4.5}$$

represents all known functions. The subscript B refers here to quantities compatible with the specified pressure coefficient C_{PB}.

The perturbation potential $\varphi_{oB}(s)$ can also be represented by the function $\varphi_o^*(s)$ plus some corrective term which will approach 0 as $\Gamma_2^* \to \Gamma_2$. We obtain $\varphi_o^*(s)$ by solving the system (3.2) for $q_o^*(s)$ and insertion of this function into equation (2.2), where we set n = 0, for the axisymmetric flow case. Since the system (3.2) was obtained with the

boundary condition $V_N(s) = 0$ along Γ_1 and Γ_2^*, the line Γ_2^* is temporarily a streamline. All functions obtained with $q_o^*(s)$ of the system (3.2) will in the future be marked by asterisks, in order to distinguish them from those obtained with the solution $q_o(s)$ of the system of integral equations (4.1) and (4.2). We add and subtract in equation (4.3) the terms

$$\phi_o^*(s_B) \quad \text{and} \quad \int_{s_B}^{s} V_T^*(s)\, ds$$

and obtain

$$\phi_{oB}(s) = \left[\phi_{oB}(s_B) - \phi_o^*(s_B)\right] + \left[\phi_o^*(s_B) - \int_{s_B}^{s} V_T^*(s)\, ds\right] + \int_{s_B}^{s} (V_{TB} - V_T^*(s))\, ds.$$

Due to the definition (1.20) of $\phi_o^*(s)$, the terms

$$\phi_o^*(s_B) + \int_{s_B}^{s} V_T^*(s)\, ds = \phi_o^*(s) = x^*(s) + \varphi_o^*(s)$$

can be collected, and we obtain instead of equation (4.4) now

$$\varphi_{oB}(s) = \phi_o^*(s) - x^*(s) + \int_{s_B}^{s} (V_{TB} - V_T^*(s))\, ds + C = \overline{\varphi_o(s)} + C, \quad (4.6)$$

where the constant is given as

$$C = [\phi_{oB}(s_B) - \phi^*_{oB}(s_B)]. \tag{4.7}$$

The barred function in equation (4.4) can be expressed with $\varphi^*_o(s) = \phi^*_o(s) - x^*(s)$ as

$$\overline{\varphi_o(s)} = \varphi^*_o(s) + \int_{s_B}^{s} (V_{TB} - V^*_T(s))\, ds. \tag{4.8}$$

All terms on the right-hand side are known quantities. We insert equation (4.6) into the integral equation (4.2). Since $\varphi_{oB}(s)$ is not necessarily identical with $\varphi^*_o(s)$, the normal velocities on Γ^*_2 are not zero ($V_N(s) \neq 0$), and Γ^*_2 is not a streamline any more. Our goal is to shift Γ^*_2 in such a fashion that (a) the condition of zero normal velocity along Γ^*_2 is satisfied ($\Gamma^*_2 \rightarrow \Gamma_2$) and (b) the specified perturbation potential $\varphi_{oB}(s)$ is attained along Γ^*_2.

The representation of the exact perturbation potential as a correction of the approximate $\varphi^*_o(s)$ has certain advantages for the numerical calculation. The advantages will be discussed at the end of this chaper in more detail.

The problem still has one unknown quantity: the constant C, as given by equation (4.7). We must therefore later establish an equation for calculating C; only then the problem is completely determined. The constant C is for the time being arbitrarily assumed to be unity. However, since the geometric functions of Γ^*_2 are introduced into the Kernel functions of the integral equations (4.1) and (4.2) the exact free streamline Γ^*_2 can only be obtained by an iteration procedure.

The system of integral equations (4.1) and (4.2) will now be satisfied in N points along the contour Γ_1 and the line Γ^*_2. For this purpose, we replace the integral sign by a summation sign and apply the Gaussian quadrature. For simplicity, we drop the asterisks for the geometric functions of the line Γ^*_2, but we keep in mind that x(s), r(s), and their higher derivatives belong to the assumed line Γ^*_2. Occasionally, we will return to the use of asterisks if it seems necessary to the understanding of the problem.

For the points $1 \leq \nu \leq i$ on the contour Γ_2, we obtain the equation

$$r'_\nu = \frac{(q_o)_\nu}{2}\left[1 - \frac{1}{2\pi r_\nu}\sum_{\mu=1}^{N}{}'\left\{x'_\nu\left(\ln\frac{8r_\nu}{|s_\mu - s_\nu|} - 1\right) - r_\nu\kappa_\nu\right\}A_\mu\right.$$

$$\left. + \frac{1}{2\pi r_\nu}\left\{x'_\nu\left(s_E \ln\frac{8r_\nu}{|s_\nu - s_E|} + s_\nu \ln\left|1 - \frac{s_E}{s_\nu}\right| - r_\nu\kappa_\nu s_E\right\}\right]\right.$$

$$+ \frac{1}{2\pi}\sum_{\mu=1}^{N}{}'\frac{2(q_o)_\mu r_\mu[(r_\nu x'_\nu - r'_\nu(x_\nu - x_\mu))G_o(k^2_{\nu\mu}) - r_\mu x'_\nu G_1(k^2_{\nu\mu})]}{[(x_\nu - x_\mu)^2 + (r_\nu + r_\mu)^2]^{3/2}}A_\mu. \qquad (4.9)$$

The point i is the last point on the body contour Γ_1 immediately upstream of the separation point s_B. The numbering system of the points ν is explained in Figure 1.

For the points $j \leq \nu < N$ on the line Γ_2^*, we obtain the equation:

$$\overline{(\varphi_o)}_\nu + 1 = \frac{(q_o)_\nu}{2\pi}\left[\sum_{\mu=1}^{N}{}'\ln\frac{8r_\nu}{|s_\mu - s_\nu|}A_\mu - \left\{s_E \ln\frac{8r_\nu}{|s_\nu - s_E|}\right.\right.$$

$$\left.\left. + s_\nu \ln\left|1 - \frac{s_E}{s_\nu}\right| + s_E\right\}\right] - \frac{1}{2\pi}\sum_{\mu=1}^{N}{}'(q_o)_\mu \frac{2r_\mu F_o(k_{\nu\mu})A_\mu}{[(x_\nu - x_\mu)^2 + (r_\nu + r_\mu)^2]^{1/2}}, \qquad (4.10)$$

where j is the point on Γ_2^* immediately downstream of the separation point s_B.

Equations (4.9) and (4.10) replace now equations (4.1) and (4.2), and form a system of N linear algebraic equations whose solution is the source strength $q_o(s)$ along Γ_1 and Γ_2^*. The equations are in matrix form:

$$\begin{bmatrix} a_{11} & a_{12} & \cdots & a_{1N} \\ \cdot & \cdot & \cdots & \cdot \\ a_{i1} & a_{i2} & \cdots & a_{iN} \\ - & - & - & - \\ a_{j1} & a_{j2} & \cdots & a_{jN} \\ \cdot & \cdot & \cdots & \cdot \\ a_{N1} & a_{N2} & \cdots & a_{NN} \end{bmatrix} \begin{bmatrix} \overline{q_{o1}} + \Delta q_{o1} \\ \cdot \\ \overline{q_{oi}} + \Delta q_{oi} \\ - \\ \overline{q_{oj}} + \Delta q_{oj} \\ \cdot \\ \overline{q_{oN}} + \Delta q_{oN} \end{bmatrix} = \begin{bmatrix} 2r_1 + 0 \\ \cdot \\ 2r_i + 0 \\ - \\ \overline{\varphi_{oj}} + 1 \\ \cdot \\ \overline{\varphi_{oN}} + 1 \end{bmatrix}. \tag{4.11}$$

The coefficients of the matrix are calculated by the expressions:

$$a_{\nu\nu} = \left[1 + \frac{1}{2\pi r_\nu}\left\{x'_\nu\left(\ln\frac{8r_\nu}{|s_\nu - s_E|} + s_\nu \ln\left|1 - \frac{s_E}{s_\nu}\right|\right) - r_\nu K_\nu s_E - \sum_{\mu=1}^{N}{}' \left[x'_\nu\left(\ln\frac{8r_\nu}{|s_\mu - s_\nu|} - 1\right) - r_\nu K_\nu\right] A_\mu\right\}\right]$$

for the region $1 \leqq \nu \leqq i$,

$$a_{\nu\mu} = \frac{r_\mu}{\pi/2}\frac{(r_\nu x'_\nu - r'_\nu(x_\nu - x_\mu))G_0(k^2_{\nu\mu}) - r_\mu r'_\nu G_1(k^2_{\nu\mu})}{[(x_\nu - x_\mu)^2 + (r_\nu + r_\mu)^2]^{3/2}} A_\mu$$

for the region $1 \leqq \nu \leqq i$ and $\nu \neq \mu$,

$$a_{\nu\nu} = \frac{1}{2\pi}\left[\sum_{\mu=1}^{N}{}' \ln\frac{8r_\nu}{|s_\mu - s_\nu|} A_\mu - \left(s_E \ln\frac{8r_\nu}{|s_\nu - s_E|} + s_\nu \ln\left|1 - \frac{s_E}{s_\nu}\right| + s_E\right)\right]$$

for the region $j \leqq \nu \leqq N$ and

$$a_{\nu\mu} = -\frac{A_\mu}{\pi} \frac{r_\mu F_o(k^2_{\nu\mu})}{[(x_\nu - x_\mu)^2 + (r_\nu + r_\mu)^2]^{1/2}}$$

for the region $j \leq \nu \leq N$ and $\nu \neq \mu$.

An estimation of the magnitude of the elements of the matrix shows that the elements increase in size toward the main diagonal. Also, the sign of the elements is the same on either side of the main diagonal. The elements $a_{\nu\mu}$ on Γ_1 and Γ_2^* are essentially represented by $\ln(8r_\nu|s_\nu - s_\mu|)$. We remember that the integrals possess a logarithmic singularity. The elements of the main diagonal are determined by the finite part of the singular integral. In calculated examples, the main diagonal elements were greater than the neighboring $a_{\nu\mu}$ by at least a magnitude.

The right sides of the system of equations are formed now. According to equations (4.1), (4.2) and (4.4), we obtain

$$b_\nu = 2r'_\nu \quad \text{for the region } 1 \leq \nu \leq i$$

and

$$b_\nu = \overline{\varphi_{o\nu}} \quad \text{for the region } j \leq \nu \leq N.$$

The solution of the system with these right sides yields $\overline{q_{o\nu}}$. The solution $q_o(s)$ usually jumps at the separation point. However, if $q_o(s)$ is also the solution of the system (3.2), then the source strength $q_o(s)$ behaves like $r'(s)$ at this point; $r'(s)$ has in s_B a corner for the abrupt and a contact point of first order for the smooth separation.

If the source strength $\overline{q_{o\nu}}$ is inserted into the equation for the tangential velocity, V_{T_ν} on Γ_2^* is not necessarily equal to V_{TB}. We have to add an additional source strength $\Delta q_{o\nu}$, which is multiplied with a constant C to obtain V_{TB} on Γ_2^*. We do not know yet the constant C of the perturbation potential; therefore, we set in (4.11) C = 1 along the line Γ_2^*, and on the body contour Γ_1, the constant is C = 0, since the normal velocities shall still vanish there.

The right sides of the system (4.11) are now, with the same elements $a_{\nu\mu}$ given as

$$b_\nu = 0 \quad \text{for the region } 1 \leq \nu \leq i$$

and

$$b_\nu = 1 \quad \text{for the region } j \leqq \nu \leqq N.$$

We solve this system for the additional source strength $\Delta q_{o\nu}$. This source strength refers to the constant C = 1 and always possesses a jump at s_B, since the right sides have a jump there.

For an arbitrary constant C, we obtain the complete solution of the system of equations (4.11), therefore, as

$$q_{o\nu} = \overline{q_{o\nu}} + C\Delta q_{o\nu}. \tag{4.12}$$

Before we discuss the determination of the constant C, we want to list the quadratures for the tangential and normal velocities. Gauss quadrature procedure is applied to equations (2.7) and (2.8), and we obtain two expressions which contain the derivative of the source strength $q'_{o\nu} = (dq_o(s)/ds)$ and which can be combined:

$$(q'_o)_\nu \left\{ \sum_{\mu=1}^{N}{}' A_\mu - s_E \right\} = -(q'_o)_\nu A_\nu. \tag{4.13}$$

The tangential velocity is thus given as

$$V_{T\nu} = x'_\nu - \frac{(q'_o)_\nu}{2\pi} A_\nu + \frac{(q_o)_\nu}{2\pi} \left[\sum_{\mu=1}^{N}{}' \left\{ \frac{1}{s_\mu - s_\nu} + \frac{r'_\nu}{2r_\nu} \left(2 - \ln \frac{8r_\nu}{|s_\mu - s_\nu|} \right) \right\} A_\mu \right.$$

$$\left. - \left\{ \left(1 - \frac{s_\nu r'_\nu}{2r_\nu} \right) \ln \left| 1 - \frac{s_E}{s_\nu} \right| + \frac{r'_\nu s_E}{2r_\nu} \left(1 - \ln \frac{8r_\nu}{|s_\nu - s_E|} \right) \right\} \right]$$

$$+ \frac{1}{2\pi} \sum_{\mu=1}^{N}{}' 2(q_o)_\mu r_\mu \frac{(x'_\nu [x_\nu - x_\mu] + r_\nu r'_\nu) G_o(k^2_{\nu\mu}) - r_\mu r'_\nu (G_1(k^2_{\nu\mu})}{[(x_\nu - x_\mu)^2 + (x_\nu + x_\mu)^2]^{3/2}} A_\mu. \tag{4.14}$$

The normal velocity is given with equation (2.7) as

$$V_{N\nu} = -r'_\nu + \frac{(q_o)_\nu}{2}\left[1 - \frac{1}{2\pi r_\nu}\sum_{\mu=1}^{N}{}'\left\{x'_\nu\left(\ln\frac{8r_\nu}{|s_\mu - s_\nu|} - 1\right) - r_\nu K_\nu\right\}A_\mu\right.$$

$$\left. + \frac{1}{2\pi r_\nu}\left\{x'_\nu\left(s_E \ln\frac{8r_\nu}{|s_\nu - s_E|} + s_\nu \ln\left|1 - \frac{s_E}{s_\nu}\right|\right) - r_\nu K_\nu s_E\right\}\right]$$

$$+ \frac{1}{2\pi}\sum_{\mu=1}^{N}{}' 2r_\mu (q_o)_\mu \frac{(r_\nu r'_\nu - r'_\nu(x_\nu - x_\mu))G_o(k^2_{\nu\mu}) - r_\mu r'_\nu G_1(k^2_{\nu\mu})}{[(x_\nu - x_\mu)^2 + (r_\nu + r_\mu)^2]^{3/2}} A_\mu . \tag{4.15}$$

We now turn to the determination of the constant C of equations (4.4) or (4.12).

We prescribe on Γ_2^* in $\nu = j$ the tangential velocity to be equal to the given V_{TB} one. Since we have already corrected the perturbation potential of Γ_2^* to that of the exact free streamline and obtained the corresponding $q_o(s)$, we expect the tangential velocity along the entire length Γ_2^* to be equal to V_{TB}.

The complete solution (4.12) is inserted into equation (4.14), and we solve for the constant C.

$$C = \frac{V_{TB} - x'_j - \frac{\overline{(q_o)_j}}{2\pi}F_1 + \frac{\overline{(q'_o)_j}}{2\pi}A_j - \frac{1}{2\pi}\sum_{\mu=1}^{N}{}' \overline{(q_o)_\mu} K_{V_T}(\mu, j) A_\mu}{\frac{(\Delta q_o)_j}{2\pi}F_1 - \frac{(\Delta q'_o)_j}{2\pi}A_j + \frac{1}{2\pi}\sum_{\mu=1}^{N}{}' (\Delta q_o)_\mu K_{V_T}(\mu, j) A_\mu} , \tag{4.16}$$

where the function F_1 is given as

$$F_1 = \sum_{\mu=1}^{N}{}' \left\{ \frac{1}{s_\mu - s_\nu} + \frac{r'_j}{2r_j}\left(2 - \ln\frac{8r_j}{|s_\mu - s_\nu|}\right)\right\} A_\mu$$

$$- \left\{\left(1 - \frac{s_j r'_j}{2r_j}\right)\ln\left|1 - \frac{s_E}{s_\nu}\right| + \frac{r'_j s_E}{2r_j}\left(1 - \ln\frac{8r_j}{|s_j - s_E|}\right)\right\}$$

and the Kernel $K_{V_T}(\mu,j)$ is

$$K_{V_T}(\mu,j) = \frac{2r_\mu\{(x'_j(x_j - x_\mu) + r_j r'_j)G_0(k^2_{\mu j})_j - r_\mu r'_j G_1(k^2_{\mu j})\}}{[(x_\mu - x_j)^2 + (r_\mu + r_j)^2]^{3/2}} .$$

The differentiation of the source strength will be discussed later on in greater detail. The function Δq_o changes rapidly on Γ_2^* in the neighborhood of s_B. It is therefore difficult to obtain the derivative $(\Delta q'_o)_j$ sufficiently accurate. We encounter these difficulties always, during the first integration steps where C is relatively large. In this case, we use C as obtained by (4.16) as the zeroth approximation for determining C by the regula falsi with equation (4.14).

After the constant C has been determined, we insert (4.12) into equation (4.15) and calculate the normal velocity component $V_N(s)$ on Γ_2^* and improve the coordinates of the new line Γ_2^{**}.

From the velocity diagram of figure 1b, we obtain for small angular differences, the radial component of $V_T(s)$ as:

$$r'^{**}(s)V_T(s) = r'^{*}(s)V_T(s) + x'^{*}(s)V_N(s) - r'^{*}(s)V_N^2(s)/(2V_T(s)) \tag{4.17}$$

and the axial component

$$x'^{**}(s)V_T(s) = x'^{*}(s)V_T(s) + r'^{*}(s)V_N(s) - x'^{*}(s)V_N^2(s)/(2V_T(s)). \tag{4.18}$$

Multiplication of equation (4.17) with $x'^{*}(s)$ and (4.18) with $r'^{*}(s)$ and subtracting the latter from the first yields

$$\frac{V_N(s)}{V_T(s)} = x'^{*}(s)\, r'^{**}(s) - r'^{*}x'^{**}(s).$$

We solve the equations for x'^{**} and r'^{**} and obtain the derivatives of the new line Γ_2^{**}, which will be much closer to the exact streamline Γ_2 if the procedure converges.

$$x'^{**}(s) = x'^{*}(s)\sqrt{1 - (V_N(s)/V_T(s))^2} - r'^{*}(s)\, V_N(s)/V_T(s) \tag{4.19}$$

and

$$r'^{**}(s) = r'^{*}(s)\sqrt{1 - (V_N(s)/V_T(s))^2} + x'^{*}(s)\, V_N(s)/V_T(s). \tag{4.20}$$

The second derivatives $x''^{**}(s)$ and $r''^{**}(s)$ are obtained by a numerical differentiation of the corresponding slopes. In the vicinity of the separation point s_B, the slopes of Γ_2 and Γ_2^{**}, respectively, are to be considered separately in order to find the proper shape there. Integrating the derivatives $r'^{**}(s)$ and $x'^{**}(s)$ yields the new coordinates of the improved line Γ_2^{**}

$$r^{**}(s) = r(s_B+\epsilon) + \int_{s_B+\epsilon}^{s} r'^{**}(s)\, ds$$

and

$$x^{**}(s) = x(s_B+\epsilon) + \int_{s_B+\epsilon}^{s} x'^{**}(s)\, ds.$$

The determination of the coordinates in the region $s_B \leqq s \leqq s_B + \epsilon$ will be discussed later.

Two possibilities of representing the perturbation potential $\varphi_{o_B}(s)$ were given at the beginning of this chapter. The reason why the perturbation potential (4.6) was chosen shall now be given:

The matrix of system (4.11) is in general not very well conditioned [15]. For one specific case, which was the flow around the disk with $C_{PB} = 0$ and N = 64 points on Γ_1 and Γ_2^*, the determinant had the value of det A = 5.4 x 10^{-33}, and the conditioning number was $K_H = 2.8 \times 10^{-52}$. If the right sides of the system were determined by equation (4.4) and Γ_2^* in the region $j \leqq \nu \leqq N$ (case A), then the function $\overline{(q_o)}_\nu$, as well as $(\Delta q_o)_\nu$, had a discontinuity of approximately equal magnitude at the separation points s_B. The constant C was approximately 1. Both functions had small oscillations in the vicinity of s_B on Γ_2^* which did not disappear after the combination of both functions, according to (4.12). The amplitude of the oscillations was relatively small; therefore, the procedure still converged. However, the difference in the tangential velocities (V_{TB} - $V_T(s)$) did not fall below a tolerance of .01. These oscillations did not appreciably disappear when a larger number of significant digits were employed.

However, if equation (4.6) determines the right side of the system (4.11) (case B), the jump in the function $\overline{(q_o)}_\nu$ at s_B disappeared with equation (4.8). We remember that originally the perturbation function $(\varphi_o^*)_\nu$ was obtained with a continuous source strength $(q_o^*)_\nu$ of the system (3.2); and $(q_o^*)_\nu$ is continuous if r'(s) is continuous on Γ_1 and Γ_2^*. In the second solution $(\Delta q_o)_\nu$ of the system, the oscillations remain, since the jump in the right side remains the same. However, the oscillations disappear now with the constant C. The tangential velocity difference (V_{TB} - $V_T(s)$) could be made smaller than .001 for this case.

Where accuracy is not the leading factor, approach (A) is the shortest to obtain a solution. Here, the additional solution of the system (3.2) is not called for, since $\varphi_o^*(s)$ and $V_T^*(s)$ do not appear in the evaluation of the perturbation potential.

(2) The Direct Solution of the Problem by Specifying V_{TB} on Γ_2^*

Instead of using the specified potential along Γ_2^*, one understandably would prefer to use the tangential velocity V_{TB} directly.. With this approach, one would eliminate the determination of the constant C, and the procedure would be shortened considerably. However, one has to overcome other obstacles.

In lieu of the integral equation (4.2) or (4.10), we write now equation (4.14) with $(V_T)_\nu = (V_{TB})_\nu$ for the region Γ_2^*:

$$(V_{TB})_\nu - x'_\nu = -\frac{(q'_o)_\nu}{2\pi} A_\nu + \frac{(q_o)_\nu}{2\pi}\left[\sum_{\mu=1}^{N}{}' \left\{\frac{1}{s_\mu - s_\nu} + \frac{r'_\nu}{2r_\nu}\left(2 - \ln\frac{8r_\nu}{|s_\mu - s_\nu|}\right)\right\} A_\mu\right.$$

$$\left. - \left\{\left(1 - \frac{s_\nu r'_\nu}{2r_\nu}\right)\ln\left|1 - \frac{s_E}{s_\nu}\right| + \frac{r'_\nu s_E}{2r_\nu}\left(1 - \ln\frac{8r_\nu}{|s_\nu - s_E|}\right)\right\}\right]$$

$$+ \frac{1}{2\pi}\sum_{\mu=1}^{N}{}' 2(q_o)_\mu r_\mu \frac{[x'_\nu(x_\nu - x_\mu) + r_\nu r'_\nu]G_o(k^2_{\mu\nu}) - r_\mu r'_\nu G_1(k^2_{\nu\mu})}{[(x_\nu - x_\mu)^2 + (r_\nu + r_\mu)^2]^{3/2}} A_\mu .$$

This expression represents formally an integro-differential equation for the unknown quantities $(q_o)_\nu$ and $(q'_o)_\nu$. The geometric functions x_ν, r_ν, and their derivatives are temporarily provided by the line Γ_2^*. We express the derivative of the source strength $(q'_o)_\nu$ by the differentiated Lagrange interpolation formula.

$$(q'_o)_\nu = L'_{\nu-1}(q_o)_{\nu-1} + L'_\nu(q_o)_\nu + L'_{\nu+1}(q_o)_{\nu+1}.$$

The coefficients of the interpolation formula $L_i(s)$ are polynomials of degree n, which contain only s_i.

The elements of the matrix (4.11) for points of the region ($j \leqq \nu \leqq N$) on Γ_2^* are given now by

$$a_{\nu\nu} = -L'_\nu \frac{A_\nu}{2\pi} + \frac{1}{2\pi}\left[\sum_{\mu=1}^{N}{}' \left\{\frac{1}{s_\mu - s_\nu} + \frac{r'_\nu}{2r_\nu}\left(2 - \ln\frac{8r_\nu}{|s_\mu - s_\nu|}\right)\right\} A_\mu\right.$$

$$\left. - \left\{\left(1 - \frac{s_\nu r'_\nu}{2r_\nu}\right)\ln\left|1 - \frac{s_E}{s_\nu}\right| + \frac{r'_\nu s_E}{2r_\nu}\left(1 - \ln\frac{8r_\nu}{|s_\nu - s_E|}\right)\right\}\right] .$$

For the points $\nu \neq \mu$ and $\mu \neq \nu \mp 1$, the elements are given by

$$a_{\nu\mu} = \frac{A_\mu r_\mu}{\pi} \cdot \frac{[x'_\nu(x_\nu - x_\mu) + r_\nu r'_\nu]G_o(k^2_{\nu\mu}) - r_\mu r'_\nu G_1(k_{\nu\mu})}{[(x_\nu - x_\mu)^2 + (r_\nu + r_\mu)^2]^{3/2}} .$$

For the diagonals immediately neighboring the principal diagonal, we write, with the above expression,

$$a^{+}_{\nu(\nu\mp1)} = L'_{\nu\mp1} + a_{\nu(\nu\mp1)} .$$

If the points $\nu = j$ and $\nu = N$ are approached, the abscissas s_ν of Lagrange's interpolation formula have to be shifted downstream, or upstream by a point, respectively. In the neighborhood of the separation point s_B, the differentiated interpolation polynomial represents only a rough approximation to $\overline{(q'_o)}_\nu$, since $(q'_o)_\nu$ is singular there for the abrupt separation.

The integrand of the integral expression for the tangential velocity component was developed into a series with small $\epsilon = (s - s_B)$. The dominating term was $1/(s_\mu - s_\nu)$. The elements $a_{\nu\mu}$ therefore change sign when passing across the main diagonal. The absolute value of the elements on both sides of the principal diagonal is large. In all calculated cases, the value of the elements $|a_{\nu(\nu\pm1)}|$ was larger than the value of the element of the main diagonal, which was given by the finite part and the central differentiated coefficient of Lagrange's interpolation polynomial. A matrix of this kind is usually not very well conditioned. The resulting solution $q_o(s)$ was oscillating severely; therefore it was not fit to be used for determining the normal velocity $V_N(s)$ with equation (4.15). The procedure diverged. The amplitude of the oscillation varied with the number of points along Γ^*_2. Other methods to solve the system (4.11) were not employed. This method of solution was dropped and, instead of V_{TB}, the potential $\phi_{o_B}(s)$ was specified along Γ^*_2.

(3) The Free Streamline in the Neighborhood of the Separation Point

The special behavior of the free streamline Γ_2 at the separation point is now investigated in more detail. In analogy to the plane cavity flow, one can calculate families of convex and concave free

streamline flows, which have the separation point s_B and the cavity pressure coefficient c_{PB} as parameters. One can also apply the behavior of the plane free streamline at the separation point to the rotational symmetric one, especially since the two first terms of the Laplace equation $\phi_{xx} + \phi_{rr} + \phi_r/r = 0$ at and in the vicinity of a singularity are overwhelmingly large compared to the third term of the left side. In this respect the solutions of the Laplace equations for both flows are similar. This argument is definitely true for the abrupt separation. For this case the free streamline Γ_2 the infinite curvature at s_B and the tangential velocity has an infinite gradient on Γ_1 at s_B.

Smooth bodies with continuous curvature, furthermore, contain points on their surface in which smooth separation occurs. For these points s_B the curvature κ of the free streamline Γ_2 is finite and equal to the curvature of the body at s_B. The tangential velocity is smooth and continuous at s_B when passing from Γ_1 to Γ_2. The discussion of these flows will be taken up again at a later time when special calculated cases are presented.

The free streamline is approximated by a suitable polynomial at the separation point s_B. We assume, in accordance with the above argument, that the two-dimensional free streamline has the same behavior as the rotational one at s_B. Let us, therefore, for illustration, consider and discuss the Helmholtz flow around a plate of width b = 2. From reference 16, we obtain the coordinates of the free streamline Γ_2 as a function of the parameter t.

$$x = \frac{b}{4+\pi}\left[t\sqrt{t^2-1} - \ln\left|t+\sqrt{t^2-1}\right|\right]; \quad r = \frac{2b}{4+\pi}(t-1) + \frac{b}{2}. \tag{4.21}$$

The parameter t attains values between t = 1 and t = ∞. For t = 1, we obtain the separation point s_B of the plate. To change the equations (4.21) to the arc length s, we differentiate x and r with respect to t, form the expression ds/dt and integrate over t. The arc length is, consequently,

$$s = s_B + \frac{b}{4+\pi}(t^2-1).$$

The coordinates finally become, with the abbreviation $\epsilon = s - s_B$,

$$r(s) = 1 + \frac{2b}{4+\pi}\left(\sqrt{\epsilon\frac{4+\pi}{b} + 1} - 1\right)$$

and

$$x(s) = \frac{b}{4+\pi}\left[\sqrt{\epsilon\frac{4+\pi}{b}+1}\ \sqrt{\epsilon\frac{4+\pi}{b}} - \ln\left|\sqrt{\epsilon\frac{4+\pi}{b}+1}+\sqrt{\epsilon\frac{4+\pi}{b}}\right|\right].$$

The first derivatives of the coordinates are

$$x'(s) = \sqrt{\epsilon\frac{4+\pi}{b}}\Bigg/\sqrt{\epsilon\frac{4+\pi}{b}-1}\ ;\quad r'(s) = 1\Bigg/\sqrt{\epsilon\frac{4+\pi}{b}-1}, \tag{4.22}$$

and finally the second ones

$$x''(s) = \frac{b}{4+\pi}\Bigg/\left(2\sqrt{\epsilon}\left[\epsilon+\frac{b}{4+\pi}\right]^{3/2}\right);\quad r''(s) = -\sqrt{\frac{b}{4+\pi}}\Bigg/\left(2\left[\epsilon+\frac{b}{4+\pi}\right]^{3/2}\right). \tag{4.23}$$

These combine to yield the curvature

$$\kappa(s) = -\frac{x''(s)}{x'(s)} = -\sqrt{\frac{b}{4+\pi}}\Bigg/\left(2\sqrt{\epsilon}\left[\epsilon+\frac{b}{4+\pi}\right]\right).$$

Looking at the second derivative, we observe that the singularity is caused by $x''(s)$. The expression $r''(s)$, however, approaches with $\epsilon \to 0$ a finite value.

$$\lim_{\epsilon\to 0} r''(s) = -\frac{4+\pi}{2b} = -1.7854.$$

For the rotational case, we choose a similar polynomial which, however, includes a wider variety of cases, the abrupt as well as the smooth separation. After having inspected a large number of cases, we decided that the expression

$$r'(s) = \frac{r'_o \mp x'_o\sqrt{\epsilon a_1}}{\sqrt{1+\epsilon a_1}} + r''_o\epsilon + b_1\epsilon^{3/2}\ \ldots \tag{4.24}$$

was the best fit to the free streamline Γ_2 in the vicinity of the separation point s_B. The terms r'_o, x'_o and their higher derivatives are the slopes, etc., of the body contour Γ_1 at s_B, $x'_o = x'(s_B)$.

According to the relation $x'(s)^2 = 1 - r'(s)^2$, we obtain, after some algebra,

$$x'(s) = \frac{x'_o \pm r'_o\sqrt{\epsilon a_1}}{\sqrt{1+\epsilon a_1}} \left\{1 - \left[\frac{2(r''_o\epsilon + b_1\epsilon^{3/2})(r'_o \mp x'_o\sqrt{\epsilon a_1})\sqrt{1+\epsilon a_1}}{(x'_o \pm r'_o\sqrt{\epsilon a_1})^2} - \frac{(r''_o\epsilon + b_1\epsilon^{3/2})(1+\epsilon a_1)}{(x'_o \pm r'_o\sqrt{\epsilon a_1})^2}\right]\right\}^{1/2} . \tag{4.25}$$

The second derivatives are

$$r''(s) = \frac{\mp x'_o\sqrt{a_1}}{2\sqrt{\epsilon}\sqrt{1+\epsilon a_1}} - \frac{a_1(r'_o \mp x'_o\sqrt{\epsilon a_1})}{2(1+\epsilon a_1)^{3/2}} + r''_o + \frac{3}{2}b_1\epsilon^{1/2} \ldots , \tag{4.26}$$

and, with $r'r'' + x'x'' = 0$, we obtain

$$x''(s) = -\frac{r'(s)r''(s)}{x'(s)} = -\left[\frac{\mp x'_o\sqrt{a_1}}{2\sqrt{\epsilon}}\frac{(r'_o \mp x'_o\sqrt{\epsilon a_1})}{(1+\epsilon a_1)} \mp \frac{x'_o r''\sqrt{\epsilon a_1}}{2\sqrt{1+\epsilon a_1}} - \frac{a_1(r'_o \mp x'_o\sqrt{\epsilon a_1}}{(1+\epsilon a_1)^2} + \right]\left(\frac{\sqrt{1+\epsilon a_1}}{(x'_o \pm r'_o\sqrt{\epsilon a_1})} + \ldots\right) .$$

The second derivatives show again which of the expressions contribute to the singularity. In the case of a flow separating from the disk, with $x'_o = 0$ and $r'_o = 1$, $x''(s)$ causes the singularity, and $r''(s)$ approaches a finite value $(a_1 r'_o/2 + r''_o)$. If we set $a_1 = (4+\pi)/b$, we obtain the exact expressions for the plane case (equation (4.23)). On the other hand, if $x'_o = 1$ and $r'_o = 0$, $r''(s)$ will cause the singularity. This case, for

instance, represents the flow about a sphere with the point of separation at $s_B = \pi/2$.

We choose the sign according to

$$r'(s) - (r'_o + r''_o\epsilon + b_1\epsilon^{3/2}) \lesseqgtr 0.$$

We obtain this relation from equation (4.24) with the denominator of the first term neglected. At the point of smooth separation, the square root $\sqrt{\epsilon a_1}$ changes the sign and $r'(s)$ has for this case the series development:

$$r'_o + r''_o\epsilon + b_1\epsilon^{3/2} + \ldots .$$

Integration of equation (4.24) yields the radius of the free streamline Γ_2. We integrate between the limits s_B and s, or $\epsilon = 0$ and ϵ, and obtain

$$r(s) = r_o + \frac{2r'_o}{a_1}\left(\sqrt{1+\epsilon a_1}-1\right) \mp \frac{x'_o}{a_1}\left(\sqrt{\epsilon a_1}\sqrt{1+\epsilon a_1} - \ln\left|\sqrt{\epsilon a_1} + \sqrt{1+\epsilon a_1}\right|\right)$$

$$+ r''_o\frac{\epsilon^2}{2} + \frac{2b_1}{5}\epsilon^{5/2} + \qquad (4.27)$$

and

$$x(s) = x_o + \frac{2x'_o}{a_1}\left(\sqrt{1+\epsilon a_1} - 1\right) \pm \frac{r'_o}{a_1}\left(\sqrt{\epsilon a_1}\sqrt{1+\epsilon a_1} - \ln\left|\sqrt{\epsilon a_1} + \sqrt{1+\epsilon a_1}\right|\right)$$

$$- \frac{1}{2}\int\left(2\,\frac{(r'_o \mp x'_o\sqrt{\epsilon a_1})}{(x'_o \pm r'_o\sqrt{\epsilon a_1})} + \frac{(r''_o+b_1\epsilon^{1/2})\epsilon\sqrt{1+\epsilon a_1}}{(x'_o \pm r'_o\sqrt{\epsilon a_1})} + \ldots\right)(r''_o+b_1\epsilon^{1/2})\epsilon d\epsilon$$

$$+ \ldots . \qquad (4.28)$$

For the determination of the two constants a_1 and b_1, we employ the points $\nu = j,k$, the two points immediately downstream of the separation point. With the abbreviation $A = r'_j - \epsilon_j^{3/2} r'_k/\epsilon_k^{3/2} - r''_o \epsilon_j (1-(\epsilon_j/\epsilon_k)^{1/2})$,

$$a_1 = \left(\frac{A - r'_o \left(\frac{1}{\sqrt{1+\epsilon_j a_1}} - (\epsilon_j/\epsilon_k)^{3/2} \frac{1}{\sqrt{1+\epsilon_k a_1}} \right)}{x'_o \left(\frac{\sqrt{\epsilon_j}}{\sqrt{1+\epsilon_j a_1}} - (\epsilon_j/\epsilon_k)^{3/2} \frac{\sqrt{\epsilon_k}}{\sqrt{1+\epsilon_k a_1}} \right)} \right)^2 .$$

Since a_1 appears also on the right side, we solve the expression for a_1 with the regula falsi. The constant b_1 is now given as

$$b_1 = \frac{1}{\epsilon_k^{3/2}} \left(r'_k - \frac{r'_o \mp x'_o \sqrt{\epsilon_k a_1}}{\sqrt{1+\epsilon_k a_1}} - r''_o \epsilon_k \right) .$$

The curvature of the free streamline can now approximately be written as

$$\kappa(s) = \frac{r''(s)}{x'(s)} = \frac{\mp x'_o \sqrt{\epsilon a_1}}{2\sqrt{\epsilon}\,(x'_o \pm r'_o \sqrt{\epsilon a_1})} - \frac{a_1 (r'_o \mp x'_o \sqrt{\epsilon a_1})}{2(1+\epsilon a_1)(x'_o \pm r'_o \sqrt{\epsilon a_1})}$$

$$+ \frac{(r''_o - 3b_1 \epsilon^{1/2}/2)\sqrt{1+\epsilon a_1}}{(x'_o \pm r'_o \sqrt{\epsilon a_1})} - \ldots . \qquad (4.29)$$

If the flow separates smoothly from a curved obstacle, the constant a_1 disappears and the singular term drops out of the expression.

$$\lim_{\substack{\epsilon \to 0 \\ a_1 \to 0}} \kappa(s) = \frac{r''_o}{x'_o} .$$

This is the curvature of the contour Γ_1 at the separation point.

For this case the derivative of the radius with respect to the arc length is, with one additional term,

$$r'(s) = r'_o + r''_o\epsilon + b_1\epsilon^{3/2} + r'''_o\,\epsilon^2/2.$$

The second derivative is continuous since the singular term vanished. The third derivative, however,

$$r'''(s) - \frac{3}{4}\frac{b_1}{\sqrt{\epsilon}} + r'''_o ,$$

can be singular, depending upon b_1 becoming zero or not. The derivative of the x-coordinate becomes now

$$x'(s) = x'_o - \frac{r'_o r''_o}{x'_o}\epsilon + \frac{r''_o\epsilon^2}{2x'_o} + \frac{b_1 r'_o}{x'_o}\epsilon^{3/2} + \frac{b_1 r''_o\epsilon^{5/2}}{x'_o} + \frac{b_1^2\epsilon^2}{2x'_o} + \cdots ,$$

where $-x''_o = r''_o r'_o/x'_o$ and $\kappa_o = r''_o/x'_o$. To determine the constant b_1, we employ the point $\nu = k$, downstream of the separation point and retain only the term with b_1:

$$b_1 = [r'_k - (r'_o + r''_o\epsilon_k)]/\epsilon_k^{3/2}.$$

The radius of the free streamline becomes now for the smooth separation

$$r(s) = r_o + r'_o\epsilon + r''_o\frac{\epsilon^2}{2} + \frac{2}{5}b_1\epsilon^{5/2},$$

and the x-coordinate is

$$x(s) = x_o + x'_o\epsilon - \frac{r'_o r''_o}{2x'_o}\epsilon^2 - \frac{2b_1 r'_o}{5x'_o}\epsilon^{5/2} - \frac{r''_o\epsilon^3}{6x'_o} - \ldots .$$

The function (4.24) is chosen more or less intuitively; only for the Helmholtz flow around a disk has (4.24) a justification to represent the free streamline in the vicinity of the separation point. However, equation (4.24) was fitted to a great number of calculated cases, all of which the curve fit was very good and represented the geometric functions of Γ_2 in the immediate neighborhood excellently for the abrupt as well as for the smooth separation.

For the determination of certain velocity components, for instance, the tangential velocity, the series expansion of the Kernel function needs the derivative of the source strength, dq'(s)/ds. In general, the source strength varies with the derivative of the contour as indicated by equation (4.1). The derivative of the source strength behaves, consequently, like r"(s). We assume, therefore,

$$q(s) = q_o + C_1\sqrt{\epsilon} + q'_o\epsilon + C_2\epsilon^{3/2}.$$

The points $\nu = j,k$ downstream of s_B are again used to determine the two constants C_1 and C_2. We designate the value of the source strength at s_B as q_o. We obtain this value by a simple extrapolation of the source strength at points upstream of s_B. It is

$$C_1 = \frac{\epsilon_k\epsilon_j}{(\epsilon_j - \epsilon_k)}\left[\frac{q_k - (q_o+q'_o\epsilon_k)}{\epsilon_k^{3/2}} - \frac{q_j - (q_o+q'_o\epsilon_j)}{\epsilon_j^{3/2}}\right]$$

and

$$C_2 = \frac{q_j - (q_o+q'_o\epsilon_j)}{\epsilon^{3/2}} - \frac{C_1}{\epsilon_j} .$$

The derivative of the source strength with respect to the arc length is finally

$$q'(s) = \frac{C_1}{2\sqrt{\epsilon}} + q'_o + C_2 \frac{3}{2}\sqrt{\epsilon} + \ldots .$$

Again, the constant C_1 disappears if the separation of the free streamline is smooth.

(4) Certain Changes of the General Procedure for the Application of Other Models

In the general discussion of the theory, we did not mention the changes for other than the Helmholtz model. As we already mentioned, this model has infinite streamlines Γ_2. The integration, however, is terminated in s_E. This point must be placed sufficiently downstream of s_B in order to render the errors small. A special error investigation approach is given in appendix D which determines, when applied, whether the termination point s_E should be placed still further downstream.

Levinson [17] determined the asymptotic form of the free streamline. With the assumption of suitable regularity conditions, he showed that the free streamline had the asymptotic form of

$$r = \frac{C^* \sqrt{x}}{(\ln x)^{1/2}} \left[1 - \frac{1}{8} \frac{\ln(\ln x)}{\ln x} + 0 \ (1/\ln x) \right] .$$

The constant C^* is a form factor and can be linked to the drag of the body by the relation

$$D = \frac{\pi}{8} \rho C^{*4} U_\infty .$$

Sufficiently downstream of s_B, the slope of the free streamline is small and we can assume, according to the slender body theory, that the source strength is proportional to the slope of the contour

$$q_o(x) \approx \frac{dr}{dx} \approx \frac{C^*}{2\sqrt{x}} \frac{1}{(\ln x)^{1/4}} \left[1 - \frac{1}{2} (1/\ln x)^{1/2} + \ldots\right].$$

We observe that the source strength decreases in proportion to $C^*/\sqrt{x}$. The asymptotic form for $q_o(x)$ was fitted to $q_o(x)$ of table 2, and an excellent agreement was obtained.

According to equation (D.18) of appendix D, the induced normal velocity at s_B of that part of the infinite wake which is neglected is proportional to the source strength at s_E, to the inverse of x_E, and to the inverse of the exponent (k+1), which is a measure for the decay of the source strength q with increasing s. Since in the Helmholtz model the source strength attenuates only moderately with x, the end point s_E or x_E has to be taken rather large in order to keep $\Delta V_N(s_B)$ small.

The Riabouchinsky model requires rather extensive changes in the method of solution. The symmetry of the model is reflected in the symmetry of the matrix elements: $a_{\nu\mu} - a_{(m-\nu)(m-\mu)}$, where $m = N + 1$. Due to the model symmetry the calculation effort is reduced to half. The right side of the system of equations is an odd function $(b_\nu = -b_{(m-\nu)})$ with respect to s_R for $2r'_\nu$ and $\overline{(\varphi_o)}_\nu$, it is an even function $(b_\nu = b_{(m-\nu)})$ for the constant C. From this behavior of the system, we can deduce that $\overline{(q_o)}_\nu$ is an odd function and $(\Delta q_o)_\nu$ is an even function with respect to s_R. We have now the possibility to combine certain elements of the matrix. For the numerical solution, we use only the N/2 points on the forward position of the body and streamline up to the point of symmetry s_R.

We write the matrix as

$$\begin{bmatrix} A_{1\,1} & A_{1\,2} & \cdots & A_{1N/2} \\ \cdot & \cdot & \cdots & \cdot \\ A_{i\,1} & A_{i\,2} & \cdots & A_{iN/2} \\ - & - & - & - \\ A_{j\,1} & A_{j\,2} & \cdots & A_{jN/2} \\ \cdot & \cdot & \cdots & \\ A_{N/2\,1} & A_{N/2\,2} & \cdots & A_{N/2\,N/2} \end{bmatrix} \begin{bmatrix} \overline{q_{o1}} + \Delta q_{o1} \\ \cdot \\ \overline{q_{oi}} + \Delta q_{oi} \\ - \\ \overline{q_{oj}} + \Delta q_{oj} \\ \cdot \\ \overline{q_{oN/2}} + \Delta q_{oN/2} \end{bmatrix} = \begin{bmatrix} 2r_1 + 0 \\ \cdot \\ 2r_i + 0 \\ - \\ \overline{\varphi_{oj}} + 1 \\ \cdot \\ \overline{\varphi_{oN/2}} + 1 \end{bmatrix}. \quad (4.30)$$

The elements are now formed by the difference or sum of two $a_{\nu\mu}$'s. For the region $1 \leq \nu \leq i$, the elements are formed by the expressions

$$A_{\nu\nu} = a_{\nu\nu} \mp a_{\nu(m-\nu)} = \left[1 + \frac{1}{2\pi r_\nu}\left\{x'_\nu\left(\ln\frac{8r_\nu}{|s_\nu - s_E|} + s_\nu \ln\left|1 - \frac{s_E}{s_\nu}\right|\right)\right.\right.$$

$$\left.\left. - r_\nu K_\nu s_E - \sum_{\mu=1}^{N}{}' \left[x'_\nu\left(\ln\frac{8r_\nu}{|s_\mu - s_\nu|} - 1\right) - r_\nu K_\nu\right] A_\mu\right\}\right]$$

$$\mp \frac{r_{m-\nu}}{\pi/2} \frac{[r_\nu x'_\nu - r'_\nu(x_\nu - x_{m-\nu})]G_o(k^2_{\nu(m-\nu)}) - r_{m-\nu} x'_\nu G_1(k^2_{\nu(m-\nu)})}{[(x_\nu - x_{m-\nu})^2 + (r_\nu + r_{m-\nu})^2]^{3/2}} A_{(m-\nu)}$$

and

$$A_{\nu\mu} = a_{\nu\mu} \mp a_{\nu(m-\mu)} = \frac{2}{\pi}\left[\frac{(r_\nu x'_\nu - r'_\nu(x_\nu - x_\mu))G_o(k^2_{\nu\mu}) - r_\mu r'_\nu G_1(k^2_{\nu\mu})}{[(x_\nu - x_\mu)^2 + (r_\nu + r_\mu)^2]^{3/2}} r_\mu A_\mu\right.$$

$$\left. \mp \frac{[r_\nu x'_\nu - r'_\nu(x_\nu - x_{m-\mu})]G_o(k^2_{\nu(m-\mu)}) - r_{(m-\mu)} x'_\nu G_1(k^2_{\nu(m-\mu)})}{[(x_\nu - x_{(m-\mu)})^2 + (r_\nu + r_{(m-\mu)})^2]^{3/2}} r_{m-\nu} A_{m-\nu}\right].$$

For points on the free streamline ($j \leq \nu \leq N/2$), we obtain

$$A_{\nu\nu} = a_{\nu\nu} \mp a_{\nu(m-\nu)} = \frac{1}{\pi}\left\{\frac{1}{2}\left[\sum_{\mu=1}^{N}{}' \ln\frac{8r_\nu}{|s_\mu - s_\nu|} A_\mu - \left(s_E \ln\frac{8r_\nu}{|s_\nu - s_E|}\right.\right.\right.$$

$$\left.\left.\left. + s_\nu \ln\left|1 - \frac{s_E}{s_\nu}\right| + s_E\right)\right] \pm \frac{r_{(m-\nu)} F_o(k^2_{\nu(m-\nu)}) A_{m-\nu}}{[(x_\nu - x_{m-\nu})^2 + (r_\nu + r_{m-\nu})^2]^{3/2}}\right.$$

and

$$A_{\nu\mu} = a_{\nu\mu} \mp a_{\nu(m-\mu)} = -\frac{1}{\pi}\left\{\frac{A_\mu r_\mu F_o(k^2_{\nu\mu})}{\sqrt{(x_\nu - x_\mu)^2 + (r_\nu + r_\mu)^2}}\right.$$

$$\left. \mp \frac{A_{(m-\mu)} r_{(m-\mu)} F_o(k^2_{\nu(m-\mu)})}{\sqrt{(x_\nu - x_{m-\mu})^2 + (r_\nu + r_{(m-\mu)})^2}}\right\}.$$

If we solve the system for the function $\overline{(q_o)_\nu}$, we apply the upper sign. The lower sign is used, however, when $(\Delta q_o)_\nu$ is the solution to the system.

The procedure to solve the system (4.30) is the same as it is with the Helmholtz model. The position of the plane of symmetry is found with the condition $r'(s) = 0$ on Γ_2^*. We call this point s_R.

The solution of the system (3.2) provides us with the perturbation potential $(\varphi_o^*)_\nu$ and the tangential velocity $(V_T^*)_\nu$ on the contour Γ_1 and Γ_2^*. As a next step, we determine with (4.8) the expression $\overline{(\varphi_o)_\nu}$. The perturbation potential of the symmetric body-cavity configuration is an odd function with respect to s_R. However, it can only be an odd function if the integral expression in (4.8) disappears. In general, this will not be the case; therefore, we have to subtract from the function $\overline{(\varphi_o)_\nu}$ the value of this function at s_R in order to make $\overline{(\varphi_o)_\nu}$ an odd function

$$\overline{\varphi_o(s)} = \varphi_o^*(s) + \int_{s_B}^{s} (V_{TB} - V_T^*(s))\, ds - \overline{\varphi_o(s_R)}.$$

In the past we could freely change the constant C. For the solution of this system, we again set $C = 1$. With equation (4.16), we determine the constant C. If the constant C does not vanish, the general solution $(q_o)_\nu$ is not an odd function with respect to s_R, since it still contains the even contribution $C(\Delta q_o)_\nu$. The normal velocity $(V_N)_\nu$ is calculated along the entire length of Γ_2^*, and with it and equations (4.17) and (4.18) an improved line Γ_2^{**} is determined. Again we apply the condition $r'(s) = 0$, and a new point of symmetry s_R is obtained. The cycle can thus start anew.

Few changes are required for the dissipation model. For cavity pressures $C_{PB} < 0$, the absolute value of the curvature has a minimum downstream of s_B; thereafter it increases again. The curvature increase of the free streamline in the theoretical flow will not be realized in the physical flow because of turbulent dissipation. The tangential velocity V_{TB} along the free streamline is constant only for a short distance behind the base of the body. After that it decreases in order to obtain the freestream value at infinity; $V_T = 1$. Therefore, the free streamline of the dissipation model is replaced by a straight line Γ_3. The contact between Γ_2^* and Γ_3 is of first order. Γ_3 represents the trace of a stream tube of constant diameter. The point of contact is s_D, where $r'(s) = 0$. The contact point s_D is to be determined for each iteration step. It represents also the end and starting points of two characteristic sections of the body. Therefore, the fixed points in these two sections separated by s_D must be determined for each step

The stream tube Γ_3 is considered to be a solid surface. Consequently, the boundary condition (1.21) must be satisfied on Γ_3. The integral equation (4.1) or (4.9) which is to be used for the region Γ_1 and which satisfies (1.21) is now also applied to the region Γ_3. Thus, the linear algebraic equation has the following matrix form:

$$\begin{bmatrix} a_{11} & a_{12} & \cdots & a_{1N} \\ \cdot & \cdot & \cdots & \cdot \\ a_{i1} & a_{i2} & \cdots & a_{iN} \\ - & - & - & - \\ a_{j1} & a_{j2} & \cdots & a_{jN} \\ \cdot & \cdot & \cdots & \cdot \\ a_{k1} & a_{k2} & \cdots & a_{kN} \\ - & - & - & - \\ a_{l1} & a_{l2} & \cdots & a_{lN} \\ \cdot & \cdot & \cdots & \cdot \\ a_{N1} & a_{N2} & \cdots & a_{NN} \end{bmatrix} \begin{bmatrix} \overline{q_{o1}} + \Delta q_{o1} \\ \cdot \\ \overline{q_{oi}} + \Delta q_{oi} \\ - \\ \overline{q_{oj}} + \Delta q_{oj} \\ \cdot \\ \overline{q_{ok}} + \Delta q_{ok} \\ - \\ \overline{q_{ol}} + \Delta q_{ol} \\ \cdot \\ \overline{q_{oN}} + \Delta q_{oN} \end{bmatrix} = \begin{bmatrix} 2r_1' + 0 \\ \cdot \\ 2r_i' + 0 \\ - \\ \overline{\varphi_{oj}} + 1 \\ \cdot \\ \overline{\varphi_{ok}} + 1 \\ - \\ 0 + 0 \\ \cdot \\ 0 + 0 \end{bmatrix} . \qquad (4.31)$$

The elements of the matrix (4.31) for the regions $1 \leqq \nu < i$ and $j \leqq \nu \leqq k$ are exactly the same as those of the system (4.11) for the regions $1 \leqq \nu \leqq i$ and $j \leqq \nu \leqq N$. The elements of the additional region Γ_3 ($\ell \leqq 0 \leqq N$) of (4.31) are given by the relation

$$a_{\nu\nu} = \left[1 + \frac{1}{2\pi r_\nu}\left\{x'_\nu\left(\ln\frac{8r_\nu}{|s_\nu - s_E|} + s_\nu \ln\left|1 - \frac{s_E}{s_\nu}\right|\right) - r_\nu K_\nu s_E\right.\right.$$

$$\left.\left. - \sum_{\mu=1}^{N}{}' \left[x'_\mu\left(\ln\frac{8r_\nu}{|s_\mu - s_\nu|} - 1\right) - r_\nu K_\nu\right] A_\mu\right\}\right]$$

and

$$a_{\nu\mu} = \frac{r_\mu}{\pi/2}\,\frac{(r_\nu x'_\nu - r'_\nu[x_\nu - x_\mu])G_0(k^2_{\nu\mu}) - r_\mu x'_\nu G_1(k^2_{\nu\mu})}{[(x_\nu - x_\mu)^2 + (r_\nu + r_\mu)^2]^{3/2}}\,A_\mu .$$

The right-hand sides of (4.31) for the same region are

$$b_\nu = 2r'_\nu = 0$$

if we solve for $\overline{(q_0)}_\nu$, and

$$b_\nu = C = 0$$

if we solve the system (4.31) for $(\Delta q_0)_\nu$. The source strength $q_0(s)$ is continuous at the point of contact s_D; its derivative, however, is discontinuous and we have to treat $q_0(s)$ in the neighborhood of s_D separately. The integral of (4.8) is evaluated only between $s_B \leqq s \leqq s_D$, since $\overline{(\varphi_0)}_\nu$ is used only along Γ_2^*.

The position of s_D is a function of the cavitation coefficient C_{PB}. With decreasing C_{PB}, the point of contact approaches the separation point s_B. For the numerical calculation, we terminate the stream tube Γ_3 a certain distance s_E downstream of the separation point. According to the error estimation given in the appendix, it is sufficient

to let Γ_3 extend approximately 10 radii downstream, since $q_o(s_E)$ attenuates rather quickly on Γ_3 and the exponent k is rather large.

For the investigation of the rearward separation point from a sphere, the free streamline Γ_2 has to be altered in the vicinity of the x-axis. We understand by the rearward separation points those points s_B for which the free streamline forms a cusp or intersects the x-axis. For these cases, the curvature of the free streamline is positive, and therefore concave to the outer flow field. Due to the vicinity of the x-axis, the nature of the series expansion ($1/r \gg 1$), and the inadequate treatment of the rearward stagnation point, small errors in $q_o(s)$ appear in that region. The normal velocities computed with these $q_o(s)$ tended to make Γ_2^* convex; whereas, the real solution should remain concave in order to form a cusp. Therefore, Γ_2^* was replaced in the region of the rearward stagnation point. Whenever the curvature of the free streamline became lower than a certain value κ_o, the curvature $\kappa(s)$ was replaced from this point on with an exponential function

$$\kappa(s) = \kappa_o \exp(-a(s-s_L)).$$

The factor a was determined thus: that the next derivative of the curvature $\kappa'(s_L)$ was continuous. The curvature $\kappa_o = \kappa(s_L)$ can be determined with an expression derived from (C.16) by requiring that the tangential velocity at s_L be equal to the specified velocity V_{TB}.

We write

$$V_T\kappa = \partial V_T/\partial \bar{\nu} = (1-V_T)/\Delta h$$

with an unspecified Δh. Next, we form the ratio $\kappa_o/\kappa^*(s_L)$ and set $\Delta h^*/\Delta h = 1$. Thus, we obtain an approximate equation to determine κ_o

$$\kappa_o = \kappa^*(s_L)\,\frac{V_T^*(s_L)(1 - V_{TB})}{V_{TB}(1 - V_T^*(s_L))}\ ; \qquad V_{TB};\ V_T(s_L) \neq 1$$

where $\kappa^*(s_L)$ is the curvature of Γ_2^* at s_L. On the remainder of the line, which we will designate Γ_3 in accordance with the dissipation model, the pressure cannot be specified any more. Therefore, the rearward stagnation point location is in error, and also the curvature at that point is wrong. Another method to find the cusped cavity is mentioned in a later chapter.

The system of equations for determining the source strength is the same as given by (4.31) with the exceptions of the right side for region $\ell \leq \nu \leq N$, which becomes now

$$b_\nu = 2r'_\nu$$

if we solve the system for $\overline{(q_o)}_\nu$, and

$$b_\nu = C = 0$$

if we solve for $(\Delta q_o)_\nu$. Since the derivative of the curvature is continuous in s_L, the derivative of the source strength $dq_o(s)/ds$ is continuous and smooth in the neighborhood of that point. Therefore, no special treatment of the region adjoining s_L is given.

For a certain (s_B; C_{PB}) combination with $C_{PB} > 0$ and $C_D < 0$, the free streamline Γ_2 does not intersect the axis of symmetry. The curvature of the free streamline is still positive and concave; however, it has a minimum downstream of s_B and after that, it increases rather rapidly. The function $r'(s)$, originally negative, changes its sign in the vicinity of the curvature minimum and Γ_2 diverges. Whenever this happens, we determine the point of contact between Γ_2 and Γ_3 with the condition $r'(s) = 0$ and apply the concept of the dissipation model. With C_{PB} decreasing and C_D approaching zero, the stream cylinder Γ_3 will diminish until finally $C_D = 0$ and Γ_2 is forming a cusped cavity. Thus, an extrapolation of the above-mentioned dissipation model will lead to the cusped cavity.

In the general discussion, it is implied that the parameter s_B, the separation point, is given and it is kept constant during the iteration. However, if one wants to determine the point of smooth separation from round bodies, one must apply an iterative procedure. For a number of tentatively chosen separation points, one conducts the complete iteration procedure as described and determines the constant $|\sqrt{a_1}|$ of equation (4.24). If two points s_B are encountered between which the expression $\pm\sqrt{a_1}$ changes sign, one can easily determine the point for which a_1 vanishes or becomes sufficiently small. This is the point of smooth separation s_B (smooth). By plotting the curvature of Γ_2 versus $(s-s_B)$ logarithmically, one can decide if s_B can be improved. At the same time, one can check (4.29) for its validity.

The Cavity of the Lifting Body

The cavity of a body placed at an angle α toward the flow will shift to an asymmetric position. The body experiences a lift proportional to the angle of attack α. The circumferential velocity $w_1(s,\alpha)$ on the body surface will also exist on the wake or cavity surface, thus creating locally over- or under-pressures which in turn will reshape the cavity and will destroy the rotational symmetry. The local pressures will shift the wake surface to such a position that the condition of pressure continuity across the wake surface is satisfied. We assume, again, negligible velocities within the wake. Consequently, a necessary conclusion is the vanishing of the local normal force along the wake or cavity.

$$C_n(s,\alpha) = 0. \tag{5.1}$$

Our main concern in this report is not so much the proper conditions of the flow along and around the wake stream surface and its exact position in space, but the influence of the wake on the lift distribution of the forebody. An exact treatment of the wake especially of the distant wake is not necessary since velocity and thus pressure perturbations attenuate rather quickly. We employ therefore a simplified model. Its schematic is given in Figure 1c. Since we treat again only bodies with rotational symmetry, we must assume that the flow separates along a circumferential line which lies entirely in one plane normal to the body axis. This exemption excludes round bodies with an interior separation line.

Condition (5.1) requires a certain tangential velocity. We can calculate it and call it V_{T_1B}. With this velocity we can define a potential $\phi_{1B}(s)$ which is known along Γ_2 except for a constant C.

To describe the general theory we employ again the Helmholtz model (or infinite streamline model). We assume for reason of simplicity that the wake pressure coefficient C_{PB} is independent of the angle of attack α. This is a reasonable assumption for small angles of attack. We therefore use the same C_{PB} of the axisymmetric flow case. For the cavity subjected to under-pressure we will use the dissipation model exclusively. Special changes of the general theory will be discussed at a later time.

(1) The Potential and the Velocity Components

We place now the forebody at an angle of attack α toward the parallel flow field. The wake will shift to a new equilibrium position where condition (5.1) is satisfied. The exact potential of this body will be developed now. Assumptions (1) through (3) of chapter 4 are also valid for this case.

The total potential of the body is in body-fixed coordinates, x^o, y^o, z^o, with the assumption that the x^o,z^o-plane contains the velocity vector U_∞ given as

$$\phi_1(x^o, y^o, z^o) = z^o \sin\alpha + \varphi_1(x^o, y^o, z^o). \tag{5.2}$$

The axial component of the undisturbed flow is $U_\infty \sin\alpha$, the normal component is $V_\infty = U_\infty \sin\alpha$. Only this component will be considered here. The first term on the right-hand side of (5.2) represents the potential of this field. The function $\varphi_1(x^o, y^o, z^o)$ is the perturbation potential of the body with bent cavity,

$$\varphi_1(x^o, y^o, z^o) = \frac{-1}{4\pi} \iint_S \frac{\mu(\xi^o,\eta^o,\zeta^o)\, dS}{\sqrt{(x^o-\xi^o)^2 + (y^o-\eta^o)^2 + (z^o-\zeta^o)^2}}, \tag{5.3}$$

where dS designates a surface element.

The potential (5.2) is for our purpose still too general. We therefore want to make it more accessible to calculation by using certain characteristics of the cavity at small angles of attack. Since we deal usually with the pressure distribution of the forebody an exact description of the wake is not necessary. The only "lift-producing" component along the wake is $U_\infty \sin(\alpha(s))$. This component will shift the cavity centerline, which can now be described by the function $z_1(s)$ of Figure 1c. Our goal is to find the position of the centerline of the cavity or wake which will be attained due to condition (5.1).

To formulate the problem, we make the following simplifying assumptions:

(a) The cavity cross section remains rotationally symmetric. Its diameter is fixed and obtained from the axisymmetric flow case.

(b) The planes normal to the body axis are shifted parallel to itself. The new trace of the bent axis in this plane is situated along a line $z_1(s)$.

(c) The local normal force vanishes along the wake or cavity. This requires a special function $z_1(s)$. The velocity V_{T_1B} is known as the cavity streamline; so in the total potential $\phi_{1B}(s)$ except for a constant.

(d) We neglect locally the condition of pressure continuity across the stream surface. The condition is satisfied only in the mean according to assumption (c).

(e) Only terms linear in α are considered, higher terms are neglected. The contour of the cavity or the wake is assumed to be small and negligible, $\delta(s) \ll 1.0$.

(f) Only those body forms shall be considered here which have the line of flow separation in one plane normal to to the body axis. This excludes bodies which permit an interior separation.

(g) Since the exact angle of attack distribution $\alpha(s)$ along the free streamline is not known a priori an approximate distribution $\alpha^*(s)$ must be assumed. The resulting cavity boundary is designated as Γ_2^*. All calculations are performed approximately with $\alpha^*(s)$.

(h) Normal velocities ($V_{N_1}(s,\alpha) \neq 0$) will result on Γ_2^* if $\alpha^*(s)$ and $\alpha(s)$ are not identical. The magnitude of the normal velocity indicates how and how much the angle of attack distribution must be changed.

The next step is the development of the potential in cylindrical coordinates. We refer to Figure 1c where the coordinates of a fixed point P^o on the surface of the body according to the assumptions are given in body-fixed coordinates as:

$$x^o \approx x; \quad y^o \approx r \sin \omega; \quad z^o \approx z_1(s) + r \cos \omega; \quad s^o = s. \tag{5.4}$$

A simple integration from the separation point s_B to a field point s yields the function by which the wake is shifted

$$z_1(s) = \int_{s_B}^{s} \delta(s)\, ds. \tag{5.5}$$

Since the arc length is approximately the same as in the axisymmetric case we keep s as the independent variable. For the summing point Q^o on the surface of the wake one obtains similar to (5.4)

$$\xi^o = \xi; \quad \eta^o \approx \rho \sin \omega', \quad \zeta^o \approx z_1(\sigma) + \rho \cos \omega'; \quad \sigma^o \approx \sigma. \tag{5.6}$$

The potential of the undisturbed flow field, represented by the first term on the right side of equation (5.2), can now be written as $r(s) \cos \omega \sin \alpha$. The denominator of the integral expression (5.3) contains the distance between point P^o and Q^o:

$$\bar{R} = \sqrt{(x^o-\xi^o)^2 + (y^o-\eta^o)^2 + (z^o-\zeta^o)^2}. \tag{5.7}$$

If we introduce (5.4) and (5.6) into the square root expression for $\bar{R}$, we obtain finally for

$$\frac{1}{\bar{R}} = \frac{1}{\sqrt{(x-\xi)^2+r^2+\rho^2-2r\rho \cos(\omega-\omega')+2(z_1(s)-z_1(\sigma))(r \cos \omega-\rho \cos \omega')+0(\delta^2)}} \tag{5.8}$$

The relation between the angle $\delta(s)$ which we call camber and the angle of attack $\alpha(s)$ can be seen in Figure 1c:

$$\alpha = \alpha(s) + \delta(s). \tag{5.9}$$

Consequently, the function $z_1(s)$ in (5.5) becomes

$$z_1(s) = \alpha \int_{s_B}^{s} \left(1 - \frac{\alpha(s)}{\alpha}\right) ds. \tag{5.10}$$

For small values of the angle of attack α, one can develop the reciprocal distance $\bar{R}$ into a series which we will truncate after the second term:

$$\frac{1}{\bar{R}} = \frac{1}{\sqrt{(x-\xi)^2+r^2+\rho^2-2r\rho\cos(\omega'-\omega)}} - \frac{2\alpha(z_1(s)-z_1(\sigma))(r\cos\omega-\rho\cos\omega')/\alpha}{[(x-\xi)^2+r^2+\rho^2-2r\rho\cos(\omega'-\omega)]^{3/2}} . \tag{5.11}$$

For the source distribution of the body and the cavity for a small angle of attack, we choose the symbol $\mu(s,\alpha) = q_1(s)\alpha(s)/\alpha$. After we insert $\mu(s,\alpha)$ and equation (5.11) into the perturbation potential (5.3), we obtain the approximate potential of the body with a cambered cavity in normal flow.

$$\varphi_1(s,\alpha,\omega) \approx -\frac{1}{4\pi}\int_0^{s_E}\int_0^{2\pi}\left(\frac{\alpha\mu(\sigma,\alpha)\ \rho\cos\omega'}{\sqrt{(x-\xi)^2+r^2+\rho^2-2r\rho\cos(\omega'-\omega)}} - 0(\alpha^2)\right)d\omega'\,d\sigma.$$

The comparison of this expression with equation (1.1) reveals that the first term under the untegral is equal to the perturbation potential of the body with a straight cavity. The next higher terms are at least proportional to α^2. If we apply partial differentiation and obtain the velocity terms depending on α^2, we can prove that these terms do not contribute to the total lift, since the exponent of cos ω is even, and the integral of the expression for the normal force vanishes. We consider, therefore, from now on, only the perturbation potential

$$\varphi_1(s,\alpha,\omega) = -\frac{\alpha}{4\pi}\int_0^{s_E}\int_0^{2\pi}\frac{\mu(\sigma,\alpha)\ \rho\cos\omega'\,d\omega'\ d\sigma}{\sqrt{(x-\xi)^2+r^2+\rho^2-2r\rho\cos(\omega'-\omega)}},$$

which is the potential of the axisymmetric forebody-cavity combination with a variable angle of attack distribution along the wake line Γ_2^*. The total potential is now given as

$$\phi_1(s,\alpha,\omega) = r(s)\cos\omega\sin\alpha + \varphi_1(s,\alpha,\omega). \tag{5.12}$$

On the surface of the fixed forebody, the angle of attack is constant and we set sin $\alpha = 1$. Along Γ_2^* the angle of attack $\alpha(s)$ is determined by (5.9). The angle α is still a constant; however, it consists now of two variable contributions.

Partial differentiation with respect to the arc length s yields the tangential velocity for meridian plane $\omega = 0$:

$$V_{T_1}(s,\alpha) = (\sin \alpha + v_1(s,\alpha))\, r'(s) + u_1(s,\alpha)\, x'(s). \tag{5.13}$$

The normal velocity for the same plane is given by

$$V_{N_1}(s,\alpha) = (\sin \alpha + v_1(s,\alpha))\, x'(s) - u_1(s,\alpha)\, r'(s) \tag{5.14}$$

and obtained by partial differentiation with respect to $\bar{v}$.

These velocity components as written above are valid and exact only along Γ_1, the contour of the forebody. For obtaining the velocity components on the cambered cavity we have to insert (5.9) into (5.13) and (5.14), linearize according to assumption (4) and the resulting approximation velocities are:

$$V_{T_1}(s,\alpha) = (\alpha(s) + v_1(s,\alpha))\, r'(s) + u_1(s,\alpha)\, x'(s) \tag{5.15}$$

and

$$V_{N_1}(s,\alpha) = (\alpha(s) + v_1(s,\alpha))\, x'(s) - u_1(s,\alpha)\, r'(s). \tag{5.16}$$

The terms $\alpha(s)r'(s)$ and $\alpha(s)x'(s)$ are in this form the tangential and normal velocity components of the normal velocity $u_\infty \sin(\alpha(s))$ of the undisturbed flow field respectively. The perturbation velocities $u_1(s,\alpha)$ and $v_1(s,\alpha)$ are those of the straight cavity with variable angle of attack distribution.

The linearized problem consists now in finding the angle of attack distribution $\alpha(s)$ along the straight and rotational symmetric wake or cavity which produces a vanishing normal force $C_n(s,\alpha) = 0$ along the line Γ_2^*.

(2) The System of Integral Equations

An integral equation with which we are able to determine the source strength on Γ_1 is given by equation (5.14) with $V_{N_1}(s,\alpha) = 0$. We introduce the perturbation velocities, linearize, and obtain

$$\mu(s,\alpha) = -2\alpha x'(s) - \frac{1}{\pi}\int_{o}^{s_E} \mu(\sigma,\alpha)\, K_q(s,\sigma)\, d\sigma. \tag{5.17}$$

The Kernel is represented by equation (1.28), where n = 1.

For the cavity boundary Γ_2^*, we use the total potential $\phi_{1B}(s,\alpha)$ expressed in terms of the perturbation potential with unknown source strength. With assumption (c) the potential $\phi_{1B}(s,\alpha)$ is known. With equation (5.12) for the meridian plane $\omega = 0$ and α replaced by $\alpha^*(s)$, the assumed angle of attack distribution, the integral equation for the region Γ_2^* can be written then as

$$\phi_{1B}(s,\alpha) - r'(s)\,\alpha^*(s) = \frac{1}{2\pi}\int_{o}^{s_E} \mu(\sigma,\alpha)\, K_\varphi(s,\sigma)\, ds, \tag{5.18}$$

where the Kernel function is in accordance with equation (1.9) and n = 1 given as

$$K_\varphi(s,\sigma) = \frac{-2\rho F_1(k^2)}{\sqrt{(x-\xi)^2 + (r+\rho)^2}}\,.$$

In both integral equations, (5.17) and (5.18), all functions except the source strength $\mu(s,\alpha)$ are known or assumed to be known. The Kernel functions depend only on the geometry of the forebody and the cavity. We employ according to assumption (a) the geometry of the axial symmetric flow case. Thus, $K_q(s,\sigma)$ and $K_\varphi(s,\sigma)$ do not change any more, and we need to determine them only once at the beginning of the iteration. The angle of attack along Γ_1 is constant and $\alpha = 1$. Along Γ_2^*, however, $\alpha(s)$ must be assumed first.

On the left side of equation (5.18) the potential $\phi_{1B}(s,\alpha)$ has to be evaluated. The next step toward a solution is therefore to relate the potential to the normal force coefficient. We start out from the definition of the local normal force coefficient:

$$C_n(s,\alpha) = -r(s) \int_0^{2\pi} C_p(s,\alpha,\omega) \cos\ \omega\ d\omega. \tag{5.19}$$

The pressure coefficient again can be expressed by the tangential velocity. In conjunction with the velocities of the axial flow case, we obtain the total tangential velocity as

$$V_{TG}^2(s,\alpha,\omega) = (V_T(s) \cos\ \alpha + V_{T1}(s,\alpha) \sin\ \alpha \cos\ \omega)^2$$

$$+ V_{T2}^2(s,\alpha) \sin^2\alpha \sin^2\omega, \tag{5.20}$$

where the velocity component in circumferential direction is given as

$$V_{T2}(s,\alpha) = (-\sin\ \alpha(s) + w_1(s,\alpha)).$$

Since in the equations the velocities $V_{T1}(s,\alpha)$ and $V_{T2}(s,\alpha)$ are connected with the angle of attack, these functions are therefore based on $\sin\ \alpha = 1$. The perturbation velocity $w_1(s,\alpha)$ is given that value which it will attain in the meridian plane $\pi/2$. For a positive angle of attack, this value will, in general, be negative. With the retention of all terms, the pressure coefficient becomes

$$C_p(s,\alpha,\omega) = C_p(s,\alpha=0) - \sqrt{1-C_p(s,\alpha=0)} \left[V_{T1}(s,\alpha) \sin\ 2\alpha \cos\ \omega \right]$$

$$+ (1-C_p(s,\alpha=0) - V_{T1}^2(s,\alpha)) \cos^2\omega - V_{T2}(s,\alpha) \sin^2\omega) \sin^2\alpha. \tag{5.21}$$

Insertion of this expression into (5.19) produces no contribution of the first term, and third (α^2) term, only the term linear in α contributes to the normal force; hence

$$C_n(s,\alpha) = 2\alpha\pi\ r(s) \sqrt{1 - C_p(s,\alpha=0)}\ V_{T1}(s,\alpha). \tag{5.22}$$

The integration of $V_{T_1}(s,\alpha)$ along s yields

$$\phi_1(s,\alpha) = \frac{1}{2\pi} \int_{s_B}^{s} \frac{C_n(s,\alpha)}{r(s)\,\alpha\,\sqrt{1-C_p(s,\alpha=0)}}\,ds + \phi_1(s_B,\alpha). \quad (5.23)$$

The normal force shall vanish along the exact free streamline Γ_2, hence the potential becomes

$$\phi_{1B}(s,\alpha) = \phi_1(s_B,\alpha). \quad (5.24)$$

The cavity boundary is thus an equipotential line, which means that the tangential velocity vanishes on Γ_2. We set $V_{T_1}(s,\alpha) = 0$, also $V_{N_1}(s,\alpha) = 0$, since Γ_2 is a streamline and we arrive at a condition that

$$u_1(s,\alpha) = \alpha(s) + v_1(s,\alpha) = 0. \quad (5.25)$$

The constant $\phi_1(s_B,\alpha)$ in equations (5.23) and (5.24) is the value of the total potential at the separation point s_B.

The left side of the integral equation (5.18) contains the expression $(\phi_{1B}(s,\alpha) - r(s)\,\alpha^*(s))$ which could be construed as the perturbation potential of the cavity in normal flow, if $\alpha^*(s)$ would be identical with $\alpha(s)$. However, we are using for the numerical calculation the assumed angle of attack distribution and therefore $\phi_{1B}(s,\alpha) - r(s)\,\alpha^*(s)$ is only approximately equal to $\varphi_{1B}(s,\alpha)$. For a convergent procedure $\Gamma_2^* \to \Gamma_2$ and $\alpha^*(s) \to \alpha(s)$ and, consequently, we define

$$\varphi_{1B}(s,\alpha) = \phi_{1B}(s,\alpha) - r(s)\,\alpha^*(s) = \overline{\varphi_1(s,\alpha)} + C. \quad (5.26)$$

The barred term represents all known functions

$$\overline{\varphi_1(s,\alpha)} = -r(s)\,\alpha^*(s), \quad (5.27)$$

and the constant becomes

$$C = \phi_{1B}(s_B,\alpha).$$

Similar to the axial flow case, we can represent the perturbation potential of (5.26) with the perturbation potential $\varphi_1^*(s,\alpha)$ of the assumed angle of attack distribution plus some corrective terms. After combining

$$\varphi_1^*(s,\alpha) = \phi_1^*(s_B,\alpha) - r(s)\,\alpha^*(s) + \int_{s_B}^{s} V_{T1}^*(s,\alpha)\,ds$$

and

$$\phi_{1B}(s_B,\alpha) - \phi_1^*(s_B,\alpha) = C,$$

we add and subtract in equation (5.26) the terms

$$\phi_1^*(s_B,\alpha) \quad \text{and} \quad \int_{s_B}^{s} V_{T1}^*(s,\alpha)\,ds$$

to obtain finally, with equation (5.23),

$$\varphi_{1B}(s,\alpha) = \varphi_1^*(s,\alpha) - \frac{1}{2\pi\alpha}\int_{s_B}^{s} \frac{C_n^*(s,\alpha)\,ds}{r(s)\sqrt{1-C_p(s,\alpha=0)}} + C. \qquad (5.28)$$

The constant C depends again only on the potential difference at the separation point s_B. The perturbation potential $\varphi_1^*(s,\alpha)$ and the normal force coefficient $C_n^*(s,\alpha)$ of the approximate free streamline Γ_2^* are obtained with the solution $\mu(s,\alpha)$ of the integral equation (3.1) with $n = 1$ and $q_1(s,\alpha) = -x(s)\alpha^*(s)$. Since (3.1) was obtained with the

condition $V_{N_1}(s,\alpha) = 0$ along the entire boundary Γ_1, Γ_2^* and Γ_3, Γ_2^* is consequently for this case a streamline. We combine again all known functions and obtain

$$\overline{\varphi_1(s,\alpha)} = \varphi_1^*(s,\alpha) - \frac{1}{2\pi\alpha} \int_{s_B}^{s} \frac{C_n^*(s,\alpha)\, ds}{r(s)\sqrt{1-C_p(s,\alpha=0)}} \,. \tag{5.29}$$

If the assumed angle of attack distribution $\alpha^*(s)$ is approaching the exact one $\alpha(s)$, the integral in equation (5.29) and the constant C in equation (5.28) will disappear. For the evaluation of the integral in (5.28) the integrated Lagrange interpolation polynomial with n = 4 points, two on each side of the intervals, was used.

The representation of the potential $\varphi_{1B}(s,\alpha)$ with the assumed perturbation potential $\varphi_1^*(s,\alpha)$ and additional correction terms had advantages for the numerical solution of the integral equations. The discussion of these advantages follows the same line as that of chapter 4 of the zero angle of attack case. A repetition is therefore not intended here.

Next, we continue with the discussion of the procedure to obtain a solution of the integral equations for the lifting body.

Equation (5.28) is inserted into the left-hand side of the integral equation (5.18). For determining the constant C, one other equation must be furnished; temporarily we might set C = 1 for the numerical calculation.

The system of integral equations (5.17) and (5.18) is converted to a set of N linear algebraic equations which are satisfied in N points on the contours Γ_1 and Γ_2^*. We introduce summation signs instead of the integral signs and obtain now for the integral equation (5.17) of the region Γ_1 with points $1 \leq \nu \leq i$

$$-x'_\nu \alpha_\nu = \frac{\mu_\nu}{2}\left[1 - \frac{1}{2\pi r_\nu} \sum_{\mu=1}^{N}{}' \left\{x'_\nu \left(\ln \frac{8r_\nu}{|s_\mu - s_\nu|} - 3\right) - r_\nu \kappa_\nu\right\} A_\mu \right.$$

$$\left. + \frac{1}{2\pi r_\nu}\left\{x'_\nu \left(s_E \ln \frac{8r_\nu}{|s_\nu - s_E|} + s_\nu \ln \left|1 - \frac{s_E}{s_\nu}\right| - 2s_E\right) - r_\nu \kappa_\nu s_E\right\}\right]$$

(equation (5.30) continued on next page)

$$+\frac{1}{2\pi}\sum_{\mu=1}^{N}{}' 2\mu_\mu r_\mu \frac{[r_\nu x'_\nu - r'_\nu(x_\nu - x_\mu)]G_1(k^2_{\nu\mu}) - r_\mu x'_\nu (G_0(k^2_{\nu\mu}) + G_2(k^2_{\nu\mu}))/2}{[(x_\nu - x_\mu)^2 + (r_\nu + r_\mu)^2]^{3/2}} A_\mu .$$

(5.30)

Along Γ_1, the angle of attack distribution is constant, and $\alpha_\nu = 1$. The primed summation sign indicates that the summation at the point $\mu = \nu$ is left out.

For the region Γ_2^* with points $j \leq \nu \leq N$, the following equation determines the source distribution μ_ν. The constant C, as mentioned above, is set equal to unity.

$$(\varphi_1)_\nu + 1 = \frac{\mu_\nu}{2\pi}\left[\sum_{\mu=1}^{N}{}' \left(\ln\frac{8r_\nu}{|s_\mu - s_\nu|} - 2\right) A_\mu - \left\{ s_E \ln\frac{8r_\nu}{|s_\nu - s_E|} + s_\nu \ln\left|1 - \frac{s_E}{s_\nu}\right| - s_E \right\}\right] - \frac{1}{2\pi}\sum_{\mu=1}^{N}{}' \frac{\mu_\mu 2r_\mu F_1(k^2_{\nu\mu})A_\mu}{[(x_\nu - x_\mu)^2 + (r_\nu + r_\mu)^2]^{1/2}} . \qquad (5.31)$$

The two equations (5.30) and (5.31) are solved for the source strength according to a special procedure. In matrix notation, we obtain

$$\begin{bmatrix} a_{11} & a_{12} & \cdots & a_{1N} \\ \cdot & \cdot & \cdots & \cdot \\ a_{i1} & a_{i2} & \cdots & a_{iN} \\ - & - & - & - \\ a_{j1} & a_{j2} & \cdots & a_{jN} \\ \cdot & \cdot & \cdots & \cdot \\ a_{N1} & a_{N2} & \cdots & a_{NN} \end{bmatrix} \begin{bmatrix} \overline{\mu_1} + \Delta\mu_1 \\ \cdot \\ \overline{\mu_i} + \Delta\mu_i \\ - \\ \overline{\mu_j} + \Delta\mu_j \\ \cdot \\ \overline{\mu_N} + \Delta\mu_N \end{bmatrix} = \begin{bmatrix} -2x'_1 + 0 \\ \cdot \\ -2x'_i + 0 \\ - \\ \overline{\varphi_{1j}} + 1 \\ \cdot \\ \overline{\varphi_{1N}} + 1 \end{bmatrix} . \qquad (5.32)$$

The elements are formed by the right sides of equations (5.30) and (5.31). In particular, we obtain:

$$a_{\nu\nu} = \left[1 + \frac{1}{2\pi r_\nu}\left\{x'_\nu\left(\ln\frac{8r_\nu}{|s_\nu - s_E|} - s_\nu \ln\left|1 - \frac{s_E}{s_\nu}\right| - 2s_E\right) - r_\nu \kappa_\nu s_E\right.\right.$$

$$\left.\left. - \sum_{\mu=1}^{N}{}' \left[x'_\nu\left(\ln\frac{8r_\nu}{|s_\mu - s_\nu|} - 3\right) r_\nu \kappa_\nu\right] A_\mu\right\}\right]$$

for the region $1 \leq \nu \leq i$;

$$a_{\nu\mu} = \frac{r_\mu A_\mu}{\pi/2} \frac{[r_\nu x'_\nu - r'_\nu(x_\nu - x_\mu)]G_1(k^2_{\nu\mu}) - r_\mu x'_\nu (G_o(k^2_{\nu\mu}) + G_2(k^2_{\nu\mu}))/2}{[(x_\nu - x_\mu)^2 + (r_\nu + r_\mu)^2]^{3/2}}$$

for the region $1 \leq \nu \leq i$ and $\nu \neq \mu$;

$$a_{\nu\nu} = \frac{1}{2\pi}\left[\sum_{\mu=1}^{N}{}' \left(\ln\frac{8r_\nu}{|s_\mu - s_\nu|} - 2\right) A_\mu - \left(s_E \ln\frac{8r_\nu}{|s_\nu - s_E|} + s_\nu \ln\left|1 - \frac{s_E}{s_\nu}\right| - s_E\right)\right]$$

for the region $j \leq \nu \leq N$; and

$$a_{\nu\mu} = -\frac{A_\mu}{\pi} \frac{r_\mu F_1(k^2_{\nu\mu})}{[(x_\nu - x_\mu)^2 + (r_\nu + r_\mu)^2]^{1/2}}$$

for the region $j \leq \nu \leq N$ and $\nu \neq \mu$.

We solve the system (5.32) twice in order to obtain the particular contributions. For the first solution, we employ the right sides

$$b_\nu = -2x'_\nu$$

for the region $1 \leq \nu \leq i$ with $\alpha_\nu = 1$, and

$$b_\nu = \overline{\varphi_{1\nu}}$$

for the region $j \leqq \nu \leqq N$, where $\overline{\varphi_{1\nu}}$ is given by equation (5.29). The particular solution of the system yields the source strength $\overline{\mu_\nu}$. For obtaining the second part of the solution, the right sides of the system are altered. The elements $a_{\nu\mu}$ are the same as for the first part. Analogous to the zero angle of attack case, the right sides of the system become now

$$b_\nu = 0$$

for the region $1 \leqq \nu \leqq i$ and

$$b_\nu = 1$$

for the region $j \leqq \nu \leqq N$.

The particular solution of this system is $\Delta\mu_\nu$, which is normalized to one. Since the geometry of the free streamline Γ_2 of the axisymmetric flow case does not change any more, the elements of the matrix which consist only of geometric functions will remain the same throughout the iteration. The same is true for the second right sides (0; 1). Therefore, the second system needs to be solved only once. The solution $\Delta\mu_\nu$ can be stored and used for the iterations.

After the particular solutions have been obtained, we combine them to form the general solution with an arbitrary constant C.

$$\mu_\nu = \overline{\mu_\nu} + C\ \Delta\mu_\nu. \tag{5.33}$$

However, before we discuss the determination of the constant C, we want to write the summation expressions for the tangential velocity. We use equation (2.10), replace the integral sign by a summation sign, and paying attention to equation (4.13) for the tangential velocity, obtain

$$(V_{T1})_\nu = r'_\nu \alpha_\nu - \frac{\mu'_\nu A_\nu}{2\pi} + \frac{\mu_\nu}{2\pi}\left[\sum_{\mu=1}^{N}{}' \left\{\frac{1}{s_\mu - s_\nu} + \frac{r'_\nu}{2r_\nu}\left(4 - \ln\frac{8r_\nu}{|s_\mu - s_\nu|}\right)\right\} A_\mu\right.$$

(equation (5.34) continued on next page)

$$- \left\{\left(1 - \frac{s_\nu r'_\nu}{2r_\nu}\right) \ln \left|1 - \frac{s_E}{s_\nu}\right| + \frac{r'_\nu s_E}{2r_\nu}\left(3 - \ln \frac{8r_\nu}{|s_\nu - s_\mu|}\right)\right\}\Bigg]$$

$$+ \frac{1}{2\pi} \sum_{\mu=1}^{N}{}' 2\mu_\mu r_\mu \frac{[x'_\nu(x_\nu - x_\mu) - r_\nu r'_\nu]G_1(k^2_{\nu\mu}) - r_\mu r'_\nu(G_0(k^2_{\nu\mu}) + G_2(k^2_{\nu\mu}))/2}{[(x_\nu - x_\mu)^2 + (r_\nu + r_\mu)^2]^{3/2}} A_\mu .$$

(5.34)

The general solution (5.33) is now inserted into expression (5.34). We set $(V_{T1}) = (V_{T1B}) = 0$, choose the special point for which this equation is to be satisfied at $\nu = j$, which is immediately downstream of s_B and solve for C:

$$C = \frac{\mu'_j A_j - \mu_j F_2 - \sum_{\mu=1}^{N}{}' \overline{\mu_\mu} K_{j\mu} A_\mu - \alpha_j r'_j}{\sum_{\mu=1}^{N} \Delta\mu_\mu K_{j\mu} A_\mu + \Delta\mu_j F_2 - \Delta\mu'_j A_j} , \qquad (5.35)$$

with the special functions

$$F_2 = \sum_{\mu=1}^{N}{}' \left\{\frac{1}{s - s_j} + \frac{r'_j}{2r_j}\left(4 - \ln \frac{8r_j}{|s_\mu - s_j|}\right)\right\} A_\mu$$

$$- \left\{\left(1 - \frac{s_j r'_j}{2r_j}\right) \ln \left|1 - \frac{s_E}{s_j}\right| + \frac{r'_j s_E}{2r_j}\left(3 - \ln \frac{8r_j}{|s_j - s_E|}\right)\right\}$$

and

$$K_{j\mu} = 2r_\mu \frac{[x'_j(x_j - x_\mu) + r_j r'_j]G_1(k^2_{j\mu}) - r_\mu r'_j[G_0(k^2_{j\mu}) + G_2(k^2_{j\mu})]/2}{[(x_\mu - x_j)^2 + (r_\mu + r_j)^2]^{3/2}} .$$

Once the constant C is known, we insert the general solution into the expression for the normal velocity (2.9), which is now

$$(V_{N1})_\nu = \alpha_\nu x'_\nu + \frac{\mu_\nu}{2}\left[1 - \frac{1}{2\pi r_\nu}\sum_{\mu=1}^{N}{}' \left\{x'_\nu\left(\ln\frac{8r_\nu}{|s_\mu - s_\nu|} - 3\right) - r_\nu K_\nu\right\} A_\mu\right.$$

$$\left. \frac{1}{2\pi r_\nu}\left\{x'_\nu\left(s_E \ln\frac{8r_\nu}{|s_\nu - s_E|} + s_\nu \ln\left|1 - \frac{s_E}{s_\nu}\right| - 2s_E\right) - r_\nu K_\nu s_E\right\}\right]$$

$$+ \frac{1}{2\pi}\sum_{\mu=1}^{N}{}' 2\mu_\mu r_\mu \frac{[r_\nu x'_\nu - r'_\nu(x_\nu - x_\mu)]G_1(k^2_{\nu\mu}) - r_\mu r'_\nu[G_o(k^2_{\nu\mu}) + G_2(k^2_{\nu\mu})]/2}{[(x_\nu - x_\mu)^2 + (r_\nu + r_\mu)^2]^{3/2}} A_\mu . \tag{5.36}$$

The boundary condition $V_N(s,\alpha) = 0$ is not satisfied on Γ_2 until the iteration cycle converges within a prescribed tolerance. Then $\mu(s,\alpha)$ is also a solution of (3.1), and $C_n(s,\alpha)$ vanishes on the cavity boundary. In analogy to the axisymmetric flow case, one can construct, with the aid of the velocity diagram of Figure 1b, an approximate expression for the normal velocity on Γ_2^*:

$$V_{N1}(s,\alpha) = V_T(s)(\theta^{**}(s,\alpha) - \theta^*(s,\alpha)), \tag{5.37}$$

where $\theta^{**}(s,\alpha)$ is the new improved slope of the contour Γ_2^{**}. This slope can be approximated by the local angle of attack

$$\theta^{**}(s,\alpha) = \alpha - \alpha^{**}(s). \tag{5.38}$$

We insert this expression into (5.37) and obtain a new angle of attack distribution along the cavity or wake:

$$\alpha^{**}(s) \approx \alpha^*(s) - \frac{V_{N1}(s,\alpha)}{V_T(s)} . \tag{5.39}$$

This distribution forms the basis for the next iteration step. The new angle of attack distribution $\alpha^{**}(s)$ is inserted into equation (3.1) which is then solved for $\mu^{**}(s,\alpha)$. With this source strength, we determine a new normal force coefficient $C_n^{**}(s,\alpha)$ on Γ_2^{**}. The perturbation potential (5.29) can now be improved. For this improvement we need to solve the system (5.32) for $\mu(s,\alpha)$. This procedure is repeated until condition (5.1) is sufficiently satisfied and the constant C is small enough.

At the beginning of the discussion, we mentioned that the representation of the potential in terms of the perturbation potential of the assumed line Γ_2^* plus corrective terms received preference over any other approach. According to the calculated cases, we found out that the matrix is not as well conditioned as that of the zero angle of attack case. The jump of the function (0, 1) of the right side again caused fluctuations of the solution $(\Delta\mu_1)_\nu$ in the neighborhood of the separation point s_B. These fluctuations entered the general solution with finite constant in all its severity. However, if the approach with vanishing constant C was used, these fluctuations vanished with C.

For those cases for which the cavity is subjected to an underpressure, we employ exclusively the dissipation model for the angle of attack case. In the axisymmetric flow case, we treat the boundary Γ_3 as a rigid stream tube with $V_N(s,\alpha) = 0$. For the angle of attack case, however, Γ_3 will shift and attain a position in space to satisfy condition (5.1). Thus, it does not differ from Γ_2. Both Γ_2 and Γ_3 are therefore subjected to a varying angle of attack distribution $\alpha(s)$.

(3) The Direct Solution of the Problems by Specifying V_{T_1B} on Γ_2^*

For the case under consideration, the second approach is definitely possible by prescribing the tangential velocity V_{T_1B} on the cavity boundary as indicated in the previous chapter. For the region Γ_2^* enclosing the boundary points $j \leq \nu \leq N$, we replace (5.31) by (5.34):

$$(V_{T_1B})_\nu - \alpha_\nu^* r'_\nu = -\frac{\mu'_\nu}{2\pi} A_\nu + \frac{\mu_\nu}{2\pi}\left[\sum_{\mu=1}^{N}{}' \left\{\frac{1}{s_\mu - s_\nu} + \frac{r'_\nu}{2r}\left(4 - \ln\frac{8r_\nu}{|s_\mu - s_\nu|}\right)\right\} A_\mu \right.$$

$$\left. - \left\{\ln\left|1 - \frac{s_E}{s_\nu}\right|\left(1 - \frac{s_\nu r'_\nu}{2r_\nu}\right) + \frac{r'_\nu s_E}{2r_\nu}\left(3 - \ln\frac{8r_\nu}{|s_\nu - s_E|}\right)\right\}\right]$$

$$+ \frac{1}{2\pi}\sum_{\mu=1}^{N}{}' 2\mu_\mu r_\mu \frac{[(x'_\nu(x_\nu - x_\mu) + r_\nu r'_\nu]G_1(k^2_{\nu\mu}) - r_\mu r'_\nu[G_0(k^2_{\nu\mu}) + G_2(k^2_{\nu\mu})]/2}{[(x_\nu - x_\mu)^2 + (r_\nu + r_\mu)^2]^{3/2}}\,.$$

The unknown function of the integro differential equation is the source intensity μ_ν whose derivative is also sought. The geometry of the body-cavity configuration of the axisymmetric flow case is again employed here. The derivative of the source strength is obtained with a differentiated Lagrange interpolation formula [18]:

$$\mu'_\nu = L'_{\nu-1}\mu_{\nu-1} + L'_\nu\mu_\nu + L'_{\nu+1}\mu_{\nu+1}.$$

The elements of the matrix for the region Γ_2 with the boundary points $j \leqq \nu \leqq N$ are now given by

$$a_{\nu\nu} = -\frac{L'_\nu A_\nu}{2\pi} + \frac{1}{2\pi}\left[\sum_{\mu=1}^{N}{}' \left\{\frac{1}{s_\mu - s_\nu} + \frac{r'_\nu}{2r_\nu}\left(4 - \ln\frac{8r_\nu}{|s_\mu - s_\nu|}\right)\right\} A_\mu \right.$$

$$\left. - \left\{\left(1 - \frac{s_\nu r'_\nu}{2r_\nu}\right)\ln\left|1 - \frac{s_E}{s_\nu}\right| + \frac{r'_\nu s_E}{2r_\nu}\left(3 - \ln\frac{8r_\nu}{|s_\nu - s_E|}\right)\right\}\right],$$

and for $\nu \neq \mu$ and $\mu \neq \nu \pm 1$, the elements are

$$a_{\nu\mu} = \frac{A_\mu r_\mu}{\pi} \cdot \frac{(x'_\nu\{x_\nu - x_\mu\} - r_\nu r'_\nu)G_1(k^2_{\nu\mu}) - r_\mu r'_\nu(G_0(k^2_{\nu\mu}) + G_2(k^2_{\nu\mu}))/2}{[(x_\nu - x_\mu)^2 + (r_\nu + r_\mu)^2]^{3/2}}.$$

The elements neighboring the principal diagonal contain, however, one additional term. It is the differentiated coefficient of the Lagrange interpolation formula

$$a^*_{\nu(\nu\pm1)} = L'_{\nu\pm1} + a_{\nu(\nu\pm1)}.$$

This method was used for different numerical examples. The solution $\mu(s,\alpha)$ showed extremely severe fluctuations; thus, the normal velocity on Γ_2^* could not be used to improve the angle of attack distribution. The procedure diverged, and it was therefore dropped. Even an increase in significant figures did not improve the situation.

The Forces on the Body

To determine the total drag coefficient of the body, the component of the pressure coefficient in x-direction is integrated along the meridian angle ω and along the body contour Γ_1 up to the separation point s_B. In addition, one has to add the base pressure coefficient which is considered to be constant over the entire base area. If we choose the base as the reference area, the expression for the total drag coefficient becomes

$$C_D\sigma_m = \int_0^{s_B}\int_0^{2\pi} C_p(s)r(s)r'(s)\, d\omega ds - r^2(s_B)\,\pi\, C_{pB}, \tag{6.1}$$

where $\sigma_m = R^2\pi$ is the dimensionless reference area.

The drag of a body can also be determined with the cavity radius R^* of the dissipation model. The radius R^* is identical with the radius of the stream tube Γ_3. We consider the body-wake configuration as a half body of radius R^*. We ask for the pressure drag of this half-body in potential flow. The drag is undetermined as long as the base pressure is not specified. We assume for this purpose that the half-body contour is interrupted by a slot in which the base pressure acts. Since the x-component of the integrated pressure along the contour disappears, only the suction force of the wake remains. We therefore obtain

$$C_p = R^{*2}(V_{TB}^2 - 1). \tag{6.2}$$

Additional forces and moments are the total normal force, the induced drag, and the moment coefficient.

The force normal to the body axis, the normal force coefficient, is obtained by integrating the r-component of the pressure coefficient along the meridian and arc length direction:

$$\frac{1}{\alpha} C_N\sigma_M = -\int_0^{s_B} r(s)x'(s) \int_0^{2\pi} C_p(s,\omega,\alpha)\cos\omega\, d\omega\, ds. \tag{6.3}$$

The major contribution to the moment coefficient is obtained by multiplying the above equation (6.3) by the moment arm about a reference point x(s):

$$\frac{1}{\alpha} C_{M_N} \sigma_M = - \int_0^{s_B} r(s)x'(s)x(s) \int_0^{2\pi} C_p(s,\omega,\alpha) \cos \omega \, d\omega \, ds. \tag{6.4}$$

One other contribution to the moment coefficient is obtained by integrating the angle of attack dependent pressure coefficient about the body. In the angle of attack case, C_p is a function of the meridian angle ω. The pressure coefficient therefore changes the sign with increasing ω, and a force couple exists.

$$\frac{1}{\alpha} C_{M_T} \sigma_M = - \frac{1}{2} \int_0^{s_B} r(s)r'(s) \, C_n(s) \, ds, \tag{6.5}$$

where $C_n(s)$ is given by equation (5.22).

Converting equation (5.22) to the pressure coefficient form, one term proportional to $\bar{\alpha}^2$ will appear which gives one contribution to the tangential force:

$$\frac{1}{\alpha^2} C_T \sigma_M = \int_0^{s_B} r(s)r'(s) \, \{2\pi(1-C_p(\alpha=0)) - \pi[(u_1 \cos \theta + (1 + v_1) \sin \theta)^2 + (-1 + w_1)^2]\} \, ds. \tag{6.6}$$

Considering all the contributions to the particular total force coefficients, one obtains for the induced drag of the body at angle of attack

$$C_D(\alpha) = C_{N_\alpha}(\sin \alpha \cos \alpha) \sin \alpha + C_T(\alpha) \cos \alpha,$$

and for the lift coefficient

$$C_L(\alpha) = C_{N_\alpha}(\sin \alpha \cos \alpha) \cos \alpha - C_T(\alpha) \sin \alpha,$$

where the lift coefficient per unit angle of attack is given by equations (6.3) and (6.6):

$$C_T(\alpha) = C_{D_o} + C_T(\alpha^2).$$

Finally the moment coefficient becomes

$$C_M(\alpha) = (C_{M_{N_\alpha}} + C_{M_{T_{\dot{\alpha}}}}) \sin \alpha \cos \alpha, \tag{6.7}$$

where $C_{M_{T_{\dot{\alpha}}}}$ is given by equation (6.5). The neutral point of the force is given by

$$\Delta x/L = C_{M_{N_\alpha}}/C_{N_\alpha}.$$

The Numerical Calculation Procedure

The excessive amount of calculations required for the solution of the problem necessitates the use of fast electronic computers. The problem was therefore coded for the CDC 3200 and the UNIVAC 1108. Before the problem is discussed in detail, the preparation of the necessary input of body coordinates and elliptic integral tables is presented.

For the integration of the integral equations, we employ the quadrature procedure of Gauss [19]. The abscissas of the quadrature are the zeros of Legendre's polynomials. The body under investigation as sketched in Figure 1 is subdivided into NT characteristic sections. The JT-points of the quadrature procedures are distributed within each section; in Figure 1, we set JT = 8. In this manner NT × JT points are placed along Γ_1, Γ_2 and Γ_3. By choosing the right distribution of characteristic sections, it is possible to place a larger number of points in the vicinity of the separation point. For instance, in

Figure 1, sections 2 and 3 are smaller than the others. The separation point was always an end point and starting point of a new section. For an abrupt separation, this section remained constant; however, for smooth separation, the point s_B is for a constant base pressure coefficient obtained by an iteration.

The complete elliptic integrals $G_n(k^2)$ and $F_n(k^2)$ are calculated with the aid of Landen's transformation [19]. This avenue of calculation proved to be the shortest and best. Only a few iterations were necessary to obtain an accuracy up to 12 digits. In most cases the number of iterations remained below 8.

The geometry of the forebody and the assumed cavity are read into the computer in terms of the characteristic sections s_A and r_A, where s_A and r_A are the arc length and the radius of the particular characteristic section, respectively. A subroutine specifically developed for the particular body distributes the points s_ν of Gauss' quadrature procedure within the characteristic sections up to the separation point. In Figure 1, there are, for instance, two characteristic sections, 1 and 2, with three boundary values s_A and i = 16 points; 8 for each section. For these points the subroutine determines the values x_ν, r_ν, x'_ν, x''_ν, r''_ν, κ_ν and the angle of attack $\alpha_\nu = 1$. For the cavity or wake, starting with the point j = 17 in Figure 1 and ending with N = 48, a table with (N-i) values is read into the computer; these are s^*_ν, r'^*_ν, α^*_ν. With these initial data, the following are calculated: r^*_ν, x'^*_ν, r''^*_ν, x^*_ν, x''^*_ν, κ^*_ν. These data are either assumed or approximated.

We can now start to determine the source distribution $q_o(s)$ of the axial flow case.

(a) We consider Γ^*_2 as a streamline on which condition (1.21) is satisfied. With equation (3.1) and n = 0, we obtain the set of N linear algebraic equations which is solved for $(q_o)^*_\nu$ and which satisfies the boundary condition (1.21) in N points on $\Gamma_1 + \Gamma^*_2$.

(b) The next step leads to the determination of the velocities $(u^*_o)_\nu$, $(v^*_o)_\nu$ with the help of equations (3.3) and (3.4), where we set n = 0. Thereafter, we calculate $(c^*_p)_\nu$ and the perturbation potential $(\varphi^*_o)_\nu$. We add to the perturbation potential the corrective terms of equation (4.6).

(c) Then we solve the system (4.11) with the corresponding right-hand sides twice. We obtain the complete solution (4.12) with an unspecified constant C. The partial solution $(\Delta q_o)_\nu$ is normalized to C = 1.

(d) The function $(q_o)_\nu$ is inserted into equation (4.16), and the constant C is changed in such a fashion that the tangential velocity V_{Tj} at $\nu = j$ downstream of the separation point s_B is equal to the specified tangential velocity V_{TB}. In Figure 1, j was set equal to 17. If the condition for V_{TB} is satisfied in one point on Γ_2^* then it is satisfied approximately on the entire length of Γ_2^*.

(e) The general solution $q_{o\nu}$ now with specified constant C is inserted into equation (4.15), and a normal velocity $V_{N\nu}$ is calculated on Γ_2^*. With the equations (4.19) and (4.20), a new line Γ_2^{**} will be calculated. This line is then the new free streamline for a new iteration step, and we start at point (a). If the absolute value of the difference of $|C_p^*(s) - C_{pB}|$ is equal to or less than .001, we terminate the iteration process and consider this case as solved.

For the body under normal flow, similar conditions prevail. A rough approximation of the angle of attack distribution was already stored in the machine. The geometry of the cavity stays fixed as obtained in the zero angle of attack case; therefore, the Kernel of the integral equation does not change during the angle of attack iteration.

(a) We consider for the first step of the angle-of-attack iteration the cavity or wake as a body with solid contours. This makes Γ_2^* a streamline. The normal velocities diminish on the contour Γ_2^*. We solve for the source distribution μ_ν^* which satisfies, for the given angle-of-attack distribution, the condition (1.21) in N points on the body and cavity.

(b) With this source distribution μ_ν^*, we can calculate the velocities $u_{1\nu}^*$, $v_{1\nu}^*$, and $w_{1\nu}^*$ with the aid of equations (3.3) through (3.5), the local normal force $C_{n\nu}^*$ with equation (5.22), and the perturbation potential $\overline{\varphi_1}$ with equation (5.29), where φ_1^* is given by equation (2.2).

(c) The solution of (5.32) provides us with the complete expression of the source strength with a partial solution $\Delta\mu_\nu$ based on C = 1. The partial solution $\Delta\mu_o$ needs only to be calculated once, since neither the right side nor the elements of the matrix change any more throughout the iteration.

(d) We determine the constant C which makes the tangential velocity V_{T1B} disappear on Γ_2^* at the point $\nu = j$, equation (5.35). Thus, the tangential velocity will approximately disappear over the entire length of Γ_2, since the potential function has changed accordingly.

(e) The constant C is determined, and one inserts the source distribution μ_ν into equation (5.36) and calculates a normal velocity component V_{N_1} along the cavity. Finally, one can compute an improved angle-of-attack distribution along Γ_2^* which represents the basis for a new iteration step, e.g., (5.39). If the absolute value of the normal force coefficient is $|c_n^*(s,\alpha)| \leq .001$, we terminate the procedure and the problem is solved.

This represents the basic procedure of the iteration scheme. In those cases where other models are employed, the corresponding equations have to be used; otherwise, the basic structure of the procedure remains the same.

IV. CALCULATED CASES AND COMPARISON WITH EXPERIMENTS

In order to gain an insight into the magnitude of the error which is involved by neglecting the infinitely long wake or cavity and by the numerical procedure, the flow field about a half-body with the potential $\phi(x,\rho^*,\varphi) = x-E/(4\pi\rho^*)$ is calculated, where E is the strength of the source at x_o on the x-axis. The strength of the source is determined in such a fashion that the radius of the body at infinity is equal to unity; then the distance of x_o from the stagnation point on the x axis is equal to one-half the radius. The spherical coordinates, the radius ρ^* is given by $\rho^* = \sin(\varphi/2)/\sin\varphi$. The pressure distribution is obtained by a simple calculation:

$$C_p = \frac{P-P_\infty}{q_\infty} = 1-4\sin^2(\varphi/2) + 3\sin^4(\varphi/2). \qquad (V.1)$$

The contour of the body is thus given by

$$r = \rho^* \sin\varphi; \quad x = x_o - \rho^* \cos\varphi. \qquad (V.2)$$

Since the numerical method employs the arc length s as the independent variable, we would like to represent the half-body in terms of the arc length:

$$s = \int_0^{\varphi} \sqrt{\rho^{*2} + (d\rho^*/d\varphi)^2}\, d\varphi.$$

We obtain finally, as the arc length,

$$s = \left[\frac{\sin(\varphi/2)}{\cos(\varphi)} \sqrt{1 - \frac{3}{4} \sin^2 \frac{\varphi}{2}} + F\left(\frac{\varphi}{2};k\right) - E\left(\frac{\varphi}{2},k\right) \right], \tag{V.3}$$

where $k^2 = 3/4$ is the modulus of the incomplete elliptic integrals $F(k,\theta)$ and $E(k,\theta)$. The integrals are known and tabulated in reference 19. For comparison with the numerical method, we need the first derivatives

$$x' = \frac{sp}{xp} = \frac{\cos\varphi + \frac{\sin\varphi}{2} \operatorname{tg}(\varphi/2)}{\sqrt{1 + \frac{1}{4} \operatorname{tg}^2(\varphi/2)}} \quad ; \quad r' = \frac{dr}{ds} = \frac{\sin\varphi - \frac{\cos\varphi}{2} \operatorname{tg}(\varphi/2)}{\sqrt{1 + \frac{1}{4} \operatorname{tg}^2(\varphi/2)}} \tag{V.4}$$

and the second derivative:

$$r'' = \frac{d^2r}{ds^2} = \frac{1}{\rho^* \sqrt{1 + (\operatorname{tg}^2(\varphi/2)/4)}} \left\{ \frac{\sin\varphi}{4\cos^2(\varphi/2)} + \frac{\cos\varphi}{2} \operatorname{tg}(\varphi/2) - \sin\varphi \right.$$

$$\left. - \frac{\operatorname{tg}(\varphi/2) \left(\cos\varphi + \frac{\sin\varphi}{2} \operatorname{tg}(\varphi/2) \right)}{8\cos^2(\varphi/2) \left(1 + \frac{1}{4} \operatorname{tg}^2(\varphi/2) \right)} \right\}. \tag{V.5}$$

After about 20R the body was truncated. The bow of the body was considered to be solid, Γ_1, and its separation point was placed at $s_B = 1$. The contour of the half-body downstream of the separation point was considered to be the free streamline Γ_2. The pressure distribution was given along Γ_2 and was identical with that of the half-body as given by equation (V.1). If we insert now the exact geometric functions, equations (V.2) through (V.5) of the free streamline Γ_2 into the numerical method, and if we compare the two pressure distributions as obtained by the numerical method and equation (V.1), we should obtain the error of the method. The stations of the characteristic sections $s_A(s)$, together with the pressure coefficient at the separation point $C_{PB}(s_B) = -.29422$, are listed in table 1. Following the arc length s of the 64 points along Γ_1 and Γ_2 are the source strength $q_o(s)$, the error (ERR)

$(C_{PB}(s) - C_P^*(s)/C_{PB}(s)$ on Γ_2^*, the given pressure coefficient CPW = $C_{PB}(s)$ of (V.1), the remaining normal velocity VN = $V_N(s)$, the calculated pressure coefficient CP = $C_P^*(s)$, the perturbation potential $\varphi_o(s)$ = PO, and finally the integral of equation (4.8). The error ERR becomes larger and larger toward the end of the truncated half-body, as we expected. The error, however, is even in the last point on Γ_2^*, less than 1.63 percent. The normal velocity VN is almost negligible. In the second part of table 1, the geometric functions of the exact half body, equations (V.2) through (V.5) are compared with those obtained by the numerical method. We notice that the radius of the body as calculated with the numerical method becomes greater than 1 close to the end of the body. The difference, however, is less than $\Delta R = .0006R$, at the end of the body. Looking at the source strength $Q = q_o(s)$, we notice that the strength attenuates rather fast on the nearly cylindrical part of the half body. We approximate the decaying curve by C/x^n, where $n > 8$. The absolute value of the source strength is very small $|q_o(s)| < 3.10^{-5}$ in the vicinity of the end of the body. Consequently, we surmise that the influence of the truncated part of the wake is negligibly small. An error estimation of appendix D also shows this clearly.

The exact drag coefficient of the forebody, which is in polar coordinates and according to (6.1),

$$C_D\sigma_M = 2\pi \int_o^{\varphi_B} C_p(\varphi) r(\varphi)\, dr(\varphi) - r_B^2\pi\, C_{PB} = \frac{\pi}{2}\left[\sin^2(\varphi/2) - 2\sin^4(\varphi/2) + 6\sin^6(\varphi/2)\right] - r^2\pi\, C_{PB},$$

was calculated for the wake pressure $C_{PB} = -.2942$, a radius $r_B = .7433$ and an angle of $\varphi_B = 1.676$ in radians as $C_D = .4944$. On the other hand, the drag coefficient obtained with the numerical method was $C_D = .4946$. The separation of s_B was smooth, and the curvature of the streamline Γ_2 was equal to the curvature of the forebody.

The sequence of convergence for successive iteration steps is shown in Figure 2. Plotted are the coordinates of Γ_2^* for the axisymmetric flow and the position of the wake centerlines z_1/R for the angle of attack case α = 10 degrees. Even with a rough zeroth approximation (a cylinder), only about six iterations were necessary to determine the free streamline up to about 15 radii behind the separation point s_B. For the angle of attack case, the angle of attack distribution changes barely at all after nine iterations. The zeroth approximation was tentatively assumed to be $\alpha^*(s)/\alpha = 0$.

In reference 13, Garabedian determined the flow field around a disk using the Riabouchinsky model for two base pressures. For the disk with $C_{PB} = 0$ (the infinite streamline model), he obtained the drag coefficient $C_D(0) = .827$. The corresponding drag coefficient calculated with the present method for the same base pressure yielded $.824 < C_D(0) < .829$ depending on the position of s_E. (The number in parentheses designates from now on the base pressure at which the drag coefficient was determined.) For the calculation, the boundary condition was satisfied at discrete points along the arc length of the contour; 16 points were distributed on the forebody and 64 points on the free streamline up to a downstream distance of 60 radii. The points were more closely placed at the separation point; 8 points were placed upstream and 8 points downstream of s_B. The maximum error of the remaining normal velocity was on the order of $V_N < .001$ up to about 30R behind the disk. Further downstream, the error in the normal velocity increased to about $V_N < .009$. The corresponding discrepancy in the pressure coefficient distribution amounted to about $|C_P(s) - C_{PB}| < .001$ up to $s \approx 30R$. In table 2 the calculated pressure distribution and the geometric functions for the cavity behind a disk for $C_{PB} = 0$ are tabulated. We notice that in the region of 30-60 radii the curvature frequently changes the sign; the value, however, stays relatively small so that the influence of the error on the pressure distribution of the forebody remains small. Similar fluctuations occurred in the source strength $q_o(s)$ in the same region.

The pressure distribution of a disk approached normally by the flow is plotted in Figure 3. At the stagnation point, the pressure distribution starts with a horizontal tangent. At the separation point s_B, the pressure coefficient has a vertical tangent on Γ_1; on the free streamline, however, it has a horizontal tangent. The derivative of the pressure coefficient $C_{PB}(s)$ along Γ_1 has a square-root singularity similar to the curvature on Γ_2.

Figure 4a shows the difference in the location of the free streamlines of plane and rotational symmetric flow for zero base pressure, and shows one main feature of the rotational symmetric flow field. The wake is narrower than that of the plane flow field. For different truncation positions s_E, the free streamline Γ_2 was calculated. The marked points are those which were used in the numerical calculations; we hardly notice any influence on the position of Γ_2 at least up to 3R behind the separation point.

An asymptotic representation of the curvature $\kappa(s)$ and the second derivative of the streamline radius $r''(s)$ of the axisymmetric as well as the plane case is shown in Figure 4b. The two asymptotes were determined by equation (4.26) and (4.29). The constant a_1 was calculated to be $a_1 = 4.526$. Since also the following points closely follow the asymptotes, we can surmise that the assumption of the square-root singularity and the representative expression for the asymptotes are

justified. The second derivative of the radius of the free streamline Γ_2 approaches, for vanishing $\epsilon = (s-s_B)$, the value $-a_1/2 = -2.26$. The circled points are calculated. The first point is placed about $\epsilon = 4.10^{-4}R$ downstream of s_B. With the help of this point and the one following in the r(s)-distribution along Γ_2, the constants a_1 and b_1 are determined. The curvature and the other calculated functions were not always so smooth as in Figure 4b; however, if the upstream distribution of points was made approximately the same as the downstream distribution, the functions were always smooth. The reason for this is to be sought in the determination of $q_o(s_B)$ by extrapolation of the upstream values of the strength.

The second drag coefficient, obtained by Garabedian with a different method, was for a base pressure of $C_{PB} = -.2235$. The modified drag coefficient $C_D'(-.2235) = C_D/(1-C_{PB})$ had the bounds $.85 < C_D' < .88$. His best estimate was $C_D' = .865$. A recalculation of this case produced $C_D' = .830$, a rather marked difference, though the maximum cavity diameter in both cases agreed much better: $D_C/2R = 2.3$ as compared with 2.28 obtained by the present method. Figure 5a shows the shape of the forward half of the cavity, and Figure 5b shows the pressure distribution over the front part of the disk and a part of the free streamline Γ_2 along which the pressure was assumed constant. For our calculation 16 points were distributed on the meridian of the body Γ_1 and 40 more on the forward half of the free streamline. An approximation of the position of the symmetry point s_R was obtained with the aid of the dissipation model. The point s_D, where Γ_2 joins Γ_3, was used as the zeroth approximation. With the procedure discribed in chapter 4 (section (4)) the calculation was continued. The half-length of the cavity was $L/D_C \approx 6.4$.

Figure 6 compares the drag coefficient obtained from water tunnels [16] with that obtained by the present numerical method. Cones of different vertex angles were placed into a water tunnel, and their bases were ventilated to obtain different base pressures. The theoretical results reproduce perfectly the experimental data. Some numerical results for the drag of cones are given in table 3. The numbers designated with an asterisk are obtained with the Riabouchinsky model; whereas, the remaining ones were obtained by the dissipation model. All models, despite their differences, converge to the infinite streamline model for a base pressure of $C_{PB} = 0$. A comparison of the two drag coefficients for $C_{PB} = -.41$ and the disk, $\beta = 90$ degrees, gives an indication of the difference between the Riabouchinsky and the dissipation model. However, for smaller C_{PB}, the difference in the drag coefficient will definitely become greater.

Figure 7 shows the pressure variation in the wake of a disk as it was measured in the water tunnel [20] and in the wind tunnel [21]. In reference 20 different torpedo head forms were tested. In the case shown, a blunt cylinder in axial flow was tested; therefore, the comparison is not quite justified, since the thick cylinder had a tremendous

effect on the wake. A better comparison was obtained from reference 22. On the whole, both wake pressure distributions have the same character. The theoretical curves were obtained with the dissipation model for a base pressure of $C_{PB} = -.41$. Across the front part of the disk, again the pressure agrees very well with the tests. Along the wake, the theory is right only in tendency. The shape of the pressure distribution suggests that a stream tube with a smaller radius than that of the dissipation model should be devised. For this model, the free streamline will be followed a little bit longer until it meets the line Γ_3. At this point a free stagnation point is formed.

Two additional points obtained from wind tunnel tests of reference 21 were drawn into the drag plot of Figure 7. The Reynolds number of these tests was 7×10^4. The drag coefficient obtained with the numerical method and the Riabouchinsky model for $C_{PB} = -.41$ was $C_D = 1.176$. The drag coefficient obtained with dissipation model and the same C_{PB} was $C_D = 1.177$.

The cavity behind a disk, photographed in reference 22, is reproduced in Figure 8. The measured base pressure, $C_{PB} = -.188$, was remarkably constant throughout the cavity up to a distance of six disk diameters downstream. The free streamline for the same C_{PB} was drawn on the photograph, and a very good result was obtained. The free streamline corresponds to the dissipation model, and therefore the streamlines run parallel from the maximum cavity diameter on downstream.

The flow field and the wake behind a disk with a base pressure of $C_{PB} = -.41$ were surveyed in a wind tunnel [21]. The pressure and velocity profiles in radial direction were measured, and the corresponding mean streamline $\psi = 0$ was calculated. The theoretical free streamlines obtained with two different models were compared with the experimental one in Figure 9. The measured drag coefficient was given as $C_D(-.41) = 1.13$, whereas the theoretical yielded $C_D = 1.18$. The free streamline of the Riabouchinsky model was not plotted beyond $x/R \geq 3$, because the measured pressures along the wake centerline differed greatly from the assumption of constant pressure for the theoretical model.

We now come to the discussion of separation points for convex bodies, especially for spheres. For this purpose we refer to the schematic representation of possible separation points in Figure 10. On the surface of the sphere exists one region (S-A) beginning at the stagnation point S in which any of the separating free streamlines of the infinite wake (Helmholtz model) are convex and have infinite curvature at the separation point S. The streamline intersects the body contour within S-A, unless the body ends at s_B. The free streamline Γ_2 separating smoothly at point A, has a finite curvature, which is equal to the curvature of the body at s_B. The maximum wake occurs for a smooth separation. The separation angle belonging to the point of

smooth separation is designated as $\varnothing_s$ (smooth). Any free streamline separating between A and B has a point of inflection. Immediately downstream of the separation point Γ_2 is concave. A distance sufficiently downstream of s_B, Γ_2 will change the sign and become convex along the rest of Γ_2. The free streamline separating at point B approaches the x-axis asymptotically without changing the curvature of Γ_2, which is concave. The streamline forms a cusp at infinity, and therefore has a free streamline width of zero at infinity.

The free streamlines separating between points B and S' all form a cusp on the x-axis a finite distance downstream of the separation point. The tangential velocity V_{TB} and Γ_2 in this region decreases with increasing separation angle $\varnothing_s$ and becomes zero at the rear stagnation point S'. These cavities have zero drag. The corresponding cavities with a finite cavity width have negative drag.

A selection of different separation angles and the peculiarities of the associated free streamline are given in the following figures, which we will discuss mutually. Figure 11 shows the behavior of the free streamline Γ_2 immediately downstream of the separation point s_B (smooth), $\varnothing_s$ (smooth) = 57.57 degrees. The cycled points are calculated. The solid lines represent the asymptote for the curvature $\kappa(s)$ and the second derivatives $x''(s)$ and $r''(s)$. The curvature approaches $\kappa_o = \kappa(s_B) = -1$. The other two functions are consequently finite and approach their respective x''_o and r''_o value of the contour Γ_1. The infinite wake from a point $s_E = 50R$ was neglected. The procedure to determine the smooth separation point was as follows: The characteristic section downstream of the separation point s_B was for two separation angles $\varnothing_s = 57$ degrees and $\varnothing_s = 58$ degrees specified to be the same, $\Delta s_A = 0.01$; thus, the first point $\gamma = j$ had the same distance $(s_j - s_B)$ for both cases. The constants a_1 which were obtained were plotted versus $\varnothing_s$ and interpolated linearly for that $\varnothing_s$ for which $a_1 = 0$. This interpolated value was used for the next approximation. For a sufficiently small value $|a_1| < 10^{-9}$, a_1 was arbitrarily set equal to zero and the corresponding angle $\varnothing_s$ was defined as $\varnothing_s$ (smooth). The value of the constant b_1 was then $b_1 = .8817$. In addition to the geometric functions the source strength $q_o(s)$ is plotted. The constant c_1 vanishes correspondingly. The asymptotic expressions for the geometric functions, as well as for the source strength, represent the corresponding numerically obtained functions very well.

Figure 12 shows the indeterminancy of the separation point on a sphere for a base pressure coefficient of $C_{PB} = 0$. Three separation points are chosen. The corresponding pressure distributions on sphere surface and free streamline in the neighborhood of the separation points are plotted in figure 12a. The radial derivative with respect to the arc length is plotted in figure 12b for the three cases, and figure 12c shows the corresponding curvature $\kappa(s)$ of the free streamlines. The

curve with the index 2 indicates the case for smooth separation. Here the derivative of the pressure coefficient with respect to the arc length dC_p/ds is a continuous function on the sphere and free streamline, the condition for smooth separation. At this point the radial derivative and the curvature are smooth functions of the arc length. The curve with index 1 shows the case where the flow separates upstream of the point of smooth separation. The pressure coefficient $C_p(s)$ on the sphere vanishes with an infinite negative tangent at the separation point, and the curvature κ is convex and greater than the curvature of the sphere. Consequently, the free streamline penetrates the solid body, and this case of an abrupt separation is therefore physically unrealistic. One other abrupt separation is shown by the curve with the index 3 downstream of the point of smooth separation. The pressure vanishes at the separation point with a positive infinite tangent. The minimum pressure occurs on the sphere, and the pressure in the cavity is higher. The curvature of the free streamline at the separation point is concave for a short distance, has an inflection point, becomes convex further downstream, and decreases monotonically. For cavitational flow one can argue that the pressure must be a minimum in the cavity because, otherwise, even a small reduction in the pressure coefficient C_p would induce cavitation elsewhere. This implies that the free streamline must be convex toward the cavity. By Bernoulli's theorem, this is equivalent to the condition that the velocity is a maximum on the free streamline. Assuming convexity, for the free streamline not to penetrate the obstacle, the free streamline must have finite curvature. In fact, the local curvature of the obstacle cannot be exceeded. These Brillouin separation conditions point out that smooth separation should be the only physical possibility for cavitation to occur.

The curvature $\kappa(s)$ of some selected free streamline Γ_2 is shown in figure 13. For separation angles from ϕ_s (smooth) to $\overline{\phi_s} \approx 110$ degrees, the base pressure coefficient was arbitrarily selected as $C_{PB} = 0$. For higher separation angles $\phi_s > \overline{\phi_s}$ the pressure coefficient was limited and could no longer be chosen freely. We notice that the free streamline has a point of inflection within the region A-B (ϕ_s (smooth) $< \phi_s < \overline{\phi_s}$) which shifts downstream on Γ_2 with increasing ϕ_s. The concave region increases thus until at $\overline{\phi_s} \approx 110$ and $C_{PB} = 0.0$ the free streamline is only concave and is therefore forming a cusp at infinity. If the separation point shifts beyond B, the corresponding free streamline is only concave. In Figure 14a, we notice that the wake or cavity width decreases with increasing ϕ_s. For $\phi_s > \overline{\phi_s}$ the free streamline Γ_2 and the streamline Γ_3 of the dissipation model have a point of contact of first order. The diameter of the stream tube Γ_3 vanishes for a certain value of C_{PB}. We designate this value to be C_{PB} (lim). The free streamlines then form a cusp on the x-axis, and wake form I is obtained. The particular (C_{PB}, ϕ_s)-combination is plotted in Figure 14b. For C_{PB} values below the line designated as "C_{PB} (lim)," the free streamlines intersect the x-axis and each other. On the other hand, if we

choose C_{PB} values above $C_{PB}(lim)$, we obtain the wake form II with negative drag. On the line $C_{PB}(lim)$ the drag coefficient is zero because the corresponding wake width is zero. For $\phi_s > \overline{\phi_s}$, the free streamline Γ_2 is only concave, and one can prove with equation (C.16) that $V_{TB} < 1$. Therefore, only positive pressure coefficients are possible in this region. Since the mean curvature increases with increasing ϕ_s, the tangential velocity V_{TB} on Γ_2 decreases until it becomes zero for $\phi_s = 180$ degrees. Figure 15a shows, in addition to wake form I, also wake form II for the case $\phi_s = 130$ degrees. The pressure coefficient $C_{PB}(lim) = .222$ produces approximately zero drag. However, if we choose $C_{PB} = .25$, we obtain a finite wake width with the corresponding drag coefficient of $C_D = -.026$. In order to obtain the cusped wake form, the rearward region of the cavity had to be changed. The pressure coefficient on the fixed cone surface (its geneatrix is an exponential function) did change from the specified C_{PB} only slightly. Only in the region of the rearward stagnation point did the pressure change appreciably; therefore, the point of intersection between Γ_3 and the x-axis is quantitatively and qualitatively not quite right. One other possibility, however, to obtain the cusped cavity is the extrapolation of the wake form II to lower C_{PB} values.

Figure 15b shows an additional region where the separation angle ϕ_s and the wake pressure cannot be chosen arbitrarily. The corresponding wake forms for a $C_{PB} = -.1$ are plotted in Figure 16. If we hold, for instance, the base pressure constant ($C_{PB} = -.1$) and let the separation angle ϕ_s change to higher angles, then the wake width decreases and with it the drag coefficient. The curvature of Γ_2 is concave and becomes convex shortly before it joins the streamline Γ_2. The convex region finally disappears, and Γ_2 is only concave. A concave streamline cannot sustain $V_{TB} > 1$, and therefore the streamline model breaks down. For $C_{PB} = -.1$, the separation angle $\overline{\phi_s} \approx 99.6$ represents the limiting rearward angle possible for the model. One other try for $\phi_s = 99.75$ failed. Figure 13c also shows that, for decreasing ϕ_s, the contact point s_D between Γ_2 and Γ_3 moves forward. With decreasing C_{PB}, the separation angle ϕ_s (smooth) moves to higher angles. The limiting separation angle $\overline{\phi_s}$, however, moves forward from 110 degrees for $C_{PB} = 0$ to a position of 90 degrees for a $C_{PB} \approx -.525$. At this point, the free streamline Γ_2 has disappeared and Γ_1 leads directly into Γ_3. These investigations could be carried on almost without limit. Although there are still a number of interesting questions about separation from round bodies, we are presently content only with this limited investigation.

In Figure 17 an attempt was made to predict the laminar separation point of the sphere. (The boundary layer method used can be found in reference 23.) The boundary layer equation is solved by a series approximation of the "separated" velocity distribution, by the use of an iterative procedure. For a fixed base pressure coefficient of

$C_{PB} = -.45$, an arbitrary separation point around $\phi_s \approx 80$ degrees was chosen. The resulting velocity distribution on the sphere was developed into a polynomial containing terms of up to s^7, where s is again the arc length. The boundary layer equations were then solved, and a new separation point was obtained. The wind tunnel experiment yielded a separation point of $\phi_s \approx 81$ degrees; the iteration procedure predicted a separation point of $\phi_s \approx 77$ degrees plus. One of the difficulties was to reproduce the velocity distribution in the neighborhood of the separation point. A more modern procedure might have given a much closer result. Figure 17 shows the theoretical pressure distribution for a laminar separation at $\phi_s = 80$ degrees, and for turbulent separation at $\phi_s = 143$ degrees. Due to the laminar separation bubble (T) on the lee side of the sphere, the theory does not quite reproduce the actual pressure distribution over that portion of the surface. The theoretical pressure distribution was selected in such a fashion that the pressure distribution of test and theory coincided very well over the forward part of the sphere. For a separation angle of $\phi_s \approx 130$ degrees, we obtain the lowest possible pressure coefficient as $C_{PB}(\text{lim}) = .222$ with $C_D = 0$.

The Brillouin separation conditions were tested in a water tunnel [24] on a sphere. (The results are plotted in Figure 18.) The drag coefficients for spheres obtained by the use of axial singularities (flow past a half-body) were given as $C_D(0) = .30$ in reference 24. This result can be compared to the smooth separation occurring at an angle of about $\phi_s = 57$ to 58 degrees measured from the forward stagnation point. The corresponding drag coefficient obtained by the present method yields $C_D(0) = .31$. It seems, however, that cavitation does not occur at the point of smooth separation (Brillouin point), probably because of surface tension. The cavitation occurs, rather, at greater angles $\phi_s \approx 80$ degrees depending mildly on base pressure coefficient. Using these separation angles, the corresponding drag coefficients were calculated. Varying the separation angle by a few degrees and plotting the corresponding drag result, it was found that the drag coefficients, shown in figure 18a, were closer to the minimum drag coefficient of the sphere for fixed base pressure coefficient.

Figure 19 shows the behavior of the free streamline immediately downstream of the separation point $s_B = \phi_s = \pi/2$ from a sphere. For this point $r' = 0$, $r'' = -1$ and $x_o' = 1$. The curvature of the sphere is constant and $\kappa_o = -1$. With equation (4.29) and only a_1 considered, we obtain, for $\epsilon \to 0$,

$$\kappa(s) \approx \frac{a_1}{2\sqrt{\epsilon}} + \frac{r_o''}{x_o'} ,$$

where $a_1 = .3616$. This function is plotted in figure 19 as an asymptote. Close to the separation point the free streamline is very well represented by the asymptotic expression. For this point, only the second derivative of the radius r(s) contributes to the square root singularity. Consequently, the function x"(s) must approach a finite value:

$$\lim_{\epsilon \to 0} x''(s) = -\frac{a_1}{2} = -.1808,$$

which indeed will be approached.

The lift of cones was measured in the water tunnel [25]. Figure 20 plots the lift coefficient gradient $dC_L/d\alpha$ for zero angle of attack and a base pressure of $C_{PB} = .0$ and $-.1$. The base pressure, a function of the angle of attack, was held constant for these investigations. One notices that, with decreasing base pressure coefficient, the lift coefficient gradient also decreases. For very small cone half-angles, the lift slope approaches the "slender body" result of $dC_L/d\alpha = 2$. With increasing cone half angle, however, the lift gradient decreases and becomes negative until at $\beta = 90$ degrees only the drag component contributes to the lift.

In addition to the theoretical lift coefficient gradient obtained by the numerical procedure, some approximate theories are proffered which were obtained from reference 26. The curve for the modified slender body was obtained in the following way. For calculating the normal force of a slender body, only the change of the momentum in planes normal to the body is considered. For slender bodies, this plane moves with the velocity of U_∞ along the body axis, and the result is the well known $C_{L\alpha} = 2.0$. For cones with an appreciable half-angle β, the velocity along the cone surface will be less than U_∞. We assume that this velocity will be $V_T \cos \beta$. We obtain with section 6, for the lift gradient,

$$C_{L_\alpha} = C_{N_\alpha} - C_{D_o},$$

where

$$C_{N_\alpha} = 2V_T^2 \cos^2\beta = 2(1 - C_{P_o}) \cos^2\beta.$$

Finally, we obtain with

$$C_{L_\alpha} = 2(1 - C_{P_o}) \cos^2\beta - C_{D_o}$$

an expression which shows a relatively good coincidence with tests for all half-angles including the disk.

One other method, termed "strip theory," was taken from reference 26 and plotted into Figure 20. The theory resembles a correspondence theory, where two-dimensional results are applied to bodies of revolution.

The lift, moment, and drag coefficient of cones with half-angles of β = 15, 45, and 90 degrees and a constant base pressure coefficient of C_{PB} = -.1 are plotted as a function of the angle of attack in Figure 21. The disk is here considered as a cone of 90 degrees half-angle. For technical reasons the angle of attack was chosen to be negative. The drag coefficient $C_D(\alpha)$ as a function of the angle of attack is fairly well reproduced by the linearized theory except for the cone of β = 15 degrees, where the theory does not quite predict the increase in drag with angle of attack. It is possible that some higher terms in α which are neglected here play a certain role. The lift coefficient is satisfactorily reproduced as is the moment coefficient over the angle-of-attack range where separation of the flow from the lee side of the body is not expected, $\alpha \leqq \beta$. The reference point for the moment coefficient was in all cases the center of the cone bases and the stagnation point of the disk.

Figure 22 shows the lift and drag coefficient of a 15-degree cone plotted versus the base pressure coefficient. Even for an angle of attack of $\alpha = \pm 20°$, the theory is still predicting the right lift coefficient. Also, the tendency with varying base pressure coefficient is well reproduced. At an angle of attack of α = 0 degrees, the cavity was subjected to a hydrostatic lift which was noticed again on the forebody. The theoretical result was therefore shifted toward the experimental for α = 0. The change of the drag coefficient with the angle of attack is very good for small angles; for higher values of α, however, the theory yields smaller values. This was already noticed in Figure 21.

In Figures 23 and 24 the same coefficients are plotted as in Figure 22 for a 45-degree cone and a disk, respectively. In these cases, the cavity had little or no effect on the α = 0 shift for the lift coefficient, since the normal force for a 45-degree cone is very small and that of a disk is zero.

The downwash angles behind cones of β = 15, 45, and 90 degree half-angles are compared in figure 25. With decreasing cone half-angle, which corresponds to increasing lift coefficient of the forebody, the ratio of the local wake angle of attack $\alpha(s)$ to the angle of attack of the forebody α increases. For a disk, therefore, the wake leaves the base essentially in the same direction as the free stream; whereas, for cones the downwash angle increases behind the base and approaches asymptotically a certain limiting value at infinity, according to the normal force of the forebody.

To obtain an idea of how good the approximate theory describes the wake of a body at zero and small angles of attack, the free streamlines were drawn into the shadowgraphs of the flow configurations of Figures 15 and 16. Figure 26 shows a cone of 50 degrees half-angle at an angle of attack of α = 10 and 0 degrees. The base pressure coefficient was measured at C_{PB} = -.4. The lower edge of the wake is fairly well reproduced close to the body base where the shear layer of the wake is relatively thin. Figure 27 shows the wake of a 15-degree cone at α = 10 and 0 degrees with a base pressure of approximately C_{PB} = -.32. Wake boundary and free streamline show again a fair coincidence, at least up to two diameters behind the base of the cone. The free streamlines for both cones were obtained with the dissipation model.

V. FURTHER APPLICATIONS

In the area of steady discontinuous flows, other applications of the theory are possible. In some engineering problems, the added or virtual masses of bodies at separated flow conditions -- for instance, meteorological balloons and parachute canopies -- must be known to determine their dynamical behavior. The theory yields these quantities readily. Furthermore, rotational symmetric bodies can be constructed whose surfaces have a certain prescribed pressure distribution. However, the given distribution must obey certain rules in order not to produce negative body radii. Into the same category falls the problem of designing the optimum shape of the cowl of a rotational symmetric jet intake. Another class of problems is the flow out of an orifice, jet penetration, and cavity and jet flows under the influence of gravity fields. The theory is directly applicable to some of the mentioned problems; whereas, for certain others, slight modifications in the boundary conditions have to be made.

VI. CONCLUSIONS

The flow about bodies of revolution with blunt bases separates and forms a free streamline which divides the flow field into an outer flow region and the wake region with zero velocities. In case of cavitational flow, this free streamline is clearly visible in flow pictures. For wake flows, the free streamline concept is merely an idealization of the free shear layer.

An integral equation method using singularities on the surface of the body and the free streamline was applied to obtain solutions for the mixed boundary-value problem. The problem contains two parameters for the case of separation from a smooth body: the base pressure P_B and the separation point s_B on the surface of the rigid body. With the help of boundary layer theory the second parameter can be eliminated as was proven with an example (laminar separation from a sphere). The base pressure P_B for wake flow must be obtained from experiment. For cavitational flow, P_B is equal to the vapor pressure of the liquid.

An approximate procedure for the body at small angles of attack analogous to the zero angle of attack case was developed in the second part of the report. The geometric shape of the cavity as obtained in the axial flow case was used for the angle of attack case. The sections of the wake are shifted to a position where the local normal force on the wake is zero. The potential of the bent wake could be reduced to that of a straight one after a series development and linearization where the angle of attack distribution varies along the boundary of the wake.

A number of examples are given, and theoretical and experimental results were compared. Excellent to good agreement of drag, lift, moment, and induced drag coefficients was achieved even at moderate angles of attack. The excellent agreement between theory and experiment proves further that the free streamline concept can be applied to wake flows, as long as one is concerned with the forces on the rigid body only.

TABLE 1. COMPARISON OF EXACT AND APPROXIMATE PRESSURE COEFFICIENTS ALONG THE HALF-BODY

SA

0
5.0000E-01
1.0000E 00
1.5000E 00
2.0000E 00
3.5000E 00
6.0000E 00
1.0000E 01
2.0000E 01

CPB =-2.94226E-01

			Exact			Approx.		
S	C	ERR	CPW	VS	CP	PO	I(DEL(VT))	
9.9275E-03	1.2921E 00	0	9.9885E-01	4.2385E-10	9.9885E-01	-4.9969E-01	0	
5.0833E-02	1.2878E 00	0	9.8962E-01	-3.7256E-10	9.8962E-01	-4.9927E-01	0	
1.1861E-01	1.2691E 00	0	9.4479E-01	3.6705E-10	9.4479E-01	-4.9653E-01	0	
2.0414E-01	1.2259E 00	0	8.4325E-01	1.4918E-10	8.4325E-01	-4.8966E-01	0	
2.9585E-01	1.1582E 00	0	6.9193E-01	5.7838E-11	6.9193E-01	-4.7911E-01	0	
3.8138E-01	1.0794E 00	0	5.2775E-01	-1.0586E-10	5.2775E-01	-4.6616E-01	0	
4.4916E-01	1.0090E 00	0	3.9258E-01	-1.7341E-10	3.9258E-01	-4.5423E-01	0	
4.9007E-01	9.6434E-01	0	3.1219E-01	1.4316E-10	3.1219E-01	-4.4645E-01	0	
5.0942E-01	9.4218E-01	0	2.7400E-01	-3.3538E-11	2.7400E-01	-4.4255E-01	0	
5.5083E-01	8.9591E-01	0	1.9786E-01	-1.0414E-11	1.9786E-01	-4.3424E-01	0	
6.1861E-01	8.1848E-01	0	8.1096E-02	6.8731E-11	8.1096E-02	-4.1966E-01	0	
7.0414E-01	7.2183E-01	0	-4.5722E-02	3.9455E-12	-4.5722E-02	-4.0094E-01	0	
7.9585E-01	6.2259E-01	0	-1.5352E-01	4.7118E-11	-1.5352E-01	-3.8017E-01	0	
8.8138E-01	5.3642E-01	0	-2.2799E-01	9.0317E-11	-2.2799E-01	-3.6088E-01	0	
9.4916E-01	4.7345E-01	0	-2.7065E-01	3.2430E-11	-2.7065E-01	-3.4965E-01	0	
9.9007E-01	4.3790E-01	0	-2.9017E-01	3.7262E-11	-2.9017E-01	-3.4367E-01	0	
1.0099E 00	4.2130E-01	-1.2205E-10	-2.9806E-01	-1.3582E-07	-2.9806E-01	-3.4237E-01	-1.4446E-10	
1.0508E 00	3.8862E-01	-1.9968E-06	-3.1145E-01	6.5472E-07	-3.1145E-01	-3.2394E-01	-1.0857E-09	
1.1186E 00	3.3872E-01	7.4785E-06	-3.2596E-01	-3.0468E-07	-3.2596E-01	-3.0943E-01	1.4896E-08	
1.2041E 00	2.8311E-01	-9.4598E-06	-3.3312E-01	-1.0377E-07	-3.3312E-01	-2.9231E-01	5.0744E-09	
1.2958E 00	2.3211E-01	5.8464E-06	-3.3046E-01	7.0427E-07	-3.3045E-01	-2.7498E-01	-1.7483E-08	
1.3813E 00	1.9190E-01	-2.4565E-06	-3.2129E-01	-2.2207E-07	-3.2129E-01	-2.5983E-01	1.3467E-08	
1.4491E 00	1.6454E-01	-6.0335E-07	-3.1095E-01	3.8246E-07	-3.1095E-01	-2.4831E-01	-4.2045E-09	
1.4900E 00	1.4978E-01	1.3424E-06	-3.0382E-01	9.6359E-08	-3.0382E-01	-2.4198E-01	4.6214E-10	
1.5138E 00	1.4174E-01	-1.7794E-06	-2.9943E-01	2.4431E-07	-2.9943E-01	-2.3879E-01	-1.0262E-10	
1.5711E 00	1.2404E-01	4.4357E-06	-2.8854E-01	1.9677E-07	-2.8856E-01	-2.2969E-01	2.5073E-09	
1.6666E 00	9.9205E-02	-5.2803E-06	-2.6918E-01	-3.1175E-08	-2.6918E-01	-2.1633E-01	9.2838E-09	
1.7857E 00	7.4588E-02	3.5704E-06	-2.4476E-01	5.1052E-07	-2.4476E-01	-2.0099E-01	-1.3977E-08	
1.9142E 00	5.4755E-02	-7.9658E-07	-2.1969E-01	-1.6347E-08	-2.1969E-01	-1.8627E-01	1.2187E-08	
2.0339E 00	4.0941E-02	-9.6505E-07	-1.9809E-01	8.3761E-07	-1.9809E-01	-1.7399E-01	-1.6015E-09	
2.1288E 00	3.2461E-02	9.6737E-07	-1.8238E-01	2.0386E-07	-1.8238E-01	-1.6515E-01	2.5333E-10	
2.1861E 00	2.8197E-02	-2.6027E-07	-1.7352E-01	1.4668E-07	-1.7352E-01	-1.6016E-01	1.7414E-09	
2.2254E 00	2.5561E-02	2.0635E-08	-1.6765E-01	2.5348E-07	-1.6765E-01	-1.5683E-01	1.1772E-09	
2.3321E 00	1.9671E-02	2.2735E-06	-1.5299E-01	3.3990E-08	-1.5299E-01	-1.4852E-01	9.8182E-09	
2.5084E 00	1.2772E-02	-5.1709E-06	-1.3107E-01	1.5015E-07	-1.3107E-01	-1.3676E-01	-5.2075E-10	
2.7307E 00	7.4403E-03	5.3598E-06	-1.1015E-01	3.3646E-07	-1.1015E-01	-1.2313E-01	-1.0904E-08	
2.9692E 00	4.1824E-03	-2.6444E-06	-9.1715E-02	1.2784E-06	-9.1715E-02	-1.1136E-01	1.4019E-08	
3.1915E 00	2.4486E-03	-4.5475E-08	-7.8078E-02	1.8756E-07	-7.8078E-02	-1.0211E-01	-2.0852E-09	
3.3678E 00	1.6018E-03	7.9118E-07	-6.9172E-02	1.4689E-07	-6.9172E-02	-9.5737E-02	1.5325E-09	
3.4741E 00	1.2393E-03	-5.3988E-07	-6.4467E-02	1.3865E-07	-6.4467E-02	-9.2235E-02	1.5771E-09	
3.5496E 00	1.0320E-03	5.9753E-07	-6.1396E-02	1.4894E-07	-6.1396E-02	-8.9894E-02	1.4915E-09	
3.7541E 00	6.3832E-04	-5.2623E-07	-5.4041E-02	1.1356E-07	-5.4041E-02	-8.4075E-02	3.9469E-09	
4.0930E 00	3.0379E-04	-7.5936E-07	-4.4353E-02	1.3401E-07	-4.4353E-02	-7.5867E-02	-2.7037E-09	
4.5207E 00	1.3556E-04	2.1707E-06	-3.5336E-02	1.2870E-07	-3.5336E-02	-6.7477E-02	2.4355E-09	
4.9792E 00	7.0414E-05	-2.1501E-06	-2.8344E-02	1.0356E-07	-2.8344E-02	-6.0275E-02	4.3056E-09	
5.4069E 00	4.8043E-05	1.0147E-06	-2.3502E-02	1.3636E-07	-2.3502E-02	-5.4768E-02	-3.1434E-11	
5.7458E 00	4.0386E-05	-1.8725E-07	-2.0479E-02	1.2056E-07	-2.0479E-02	-5.1068E-02	1.7156E-09	
5.9513E 00	3.7793E-05	5.3488E-08	-1.8925E-02	1.1921E-07	-1.8925E-02	-4.9566E-02	1.5862E-09	
6.0794E 00	3.6593E-05	-9.8152E-08	-1.8031E-02	1.1995E-07	-1.8031E-02	-4.7849E-02	1.5673E-09	
6.4066E 00	3.4747E-05	3.4203E-07	-1.6027E-02	1.1770E-07	-1.6027E-02	-4.5128E-02	1.7067E-09	
6.9489E 00	3.3202E-05	-4.2507E-07	-1.3364E-02	1.1349E-07	-1.3364E-02	-4.1174E-02	1.9342E-09	
7.6331E 00	3.2230E-05	3.1123E-07	-1.0846E-02	1.1449E-07	-1.0846E-02	-3.7067E-02	1.3051E-09	
8.3668E 00	3.1596E-05	-1.8752E-07	-8.8573E-03	1.1124E-07	-8.8573E-03	-3.3480E-02	1.6751E-09	
9.0510E 00	3.1193E-05	4.2354E-07	-7.4544E-03	1.0902E-07	-7.4544E-03	-3.0705E-02	2.0405E-09	
9.5933E 00	3.0953E-05	-6.2805E-07	-6.5651E-03	1.1120E-07	-6.5651E-03	-2.8812E-02	1.6173E-09	
9.9205E 00	3.0828E-05	6.4761E-07	-6.1030E-03	1.0927E-07	-6.1030E-03	-2.7778E-02	1.7064E-09	
1.0198E 01	3.0744E-05	-7.7353E-07	-5.7475E-03	1.0805E-07	-5.7475E-03	-2.6950E-02	1.7777E-09	
1.1016E 01	3.0672E-05	-5.6118E-06	-4.8636E-03	1.2083E-07	-4.8636E-03	-2.4796E-02	-6.5028E-09	
1.2372E 01	3.0791E-05	8.8581E-05	-3.7891E-03	-1.5042E-08	-3.7890E-03	-2.1889E-02	1.2023E-07	
1.4082E 01	3.1392E-05	-6.2091E-04	-2.8741E-03	8.9940E-07	-2.8759E-03	-1.9069E-02	-6.6408E-07	
1.5917E 01	3.2800E-05	2.5184E-03	-2.2170E-03	-2.5667E-06	-2.2114E-03	-1.6753E-02	1.6969E-06	
1.7627E 01	4.0520E-05	-6.2542E-03	-1.7878E-03	4.2839E-06	-1.7986E-03	-1.5059E-02	-1.8996E-06	
1.8983E 01	2.8652E-05	7.0186E-03	-1.5302E-03	-2.2511E-06	-1.5195E-03	-1.3921E-02	6.2966E-07	
1.9801E 01	1.0468E-04	-1.6276E-02	-1.4006E-03	5.8734E-07	-1.4236E-03	-1.3328E-02	8.4015E-08	

TABLE 1 (continued)

The Exact and Approximate Geometric Functions of the Half-Body

	Exact: Parallel Flow + Source				Approximate Numerical Procedure: (The region s ≥ 1 is defined as wake.)			
S	X	R	RP	RP2	X	R	RP	RP2
9.9275E-03	7.3914E-05	9.9271E-03	9.9988E-01	-2.2333E-02	7.3914E-05	9.9271E-03	9.9988E-01	-2.2333E-02
5.0833E-02	1.9363E-03	5.0784E-02	9.9709E-01	-1.1392E-01	1.9363E-03	5.0784E-02	9.9709E-01	-1.1392E-01
1.1861E-01	1.0503E-02	1.1799E-01	9.8434E-01	-2.6117E-01	1.0503E-02	1.1799E-01	9.8434E-01	-2.6117E-01
2.0414E-01	3.0829E-02	2.0101E-01	9.5458E-01	-4.3097E-01	3.0829E-02	2.0101E-01	9.5458E-01	-4.3097E-01
2.9585E-01	6.3808E-02	2.8652E-01	9.0781E-01	-5.8303E-01	6.3808E-02	2.8652E-01	9.0781E-01	-5.8303E-01
3.8138E-01	1.0413E-01	3.6189E-01	8.5311E-01	-6.9017E-01	1.0413E-01	3.6189E-01	8.5311E-01	-6.9017E-01
4.4916E-01	1.4200E-01	4.1808E-01	8.0418E-01	-7.4958E-01	1.4200E-01	4.1808E-01	8.0418E-01	-7.4958E-01
4.9007E-01	1.6714E-01	4.5034E-01	7.7298E-01	-7.7460E-01	1.6714E-01	4.5034E-01	7.7298E-01	-7.7460E-01
5.0992E-01	1.7992E-01	4.6553E-01	7.5751E-01	-7.8391E-01	1.7992E-01	4.6553E-01	7.5751E-01	-7.8391E-01
5.5083E-01	2.0737E-01	4.9586E-01	7.2514E-01	-7.9749E-01	2.0737E-01	4.9586E-01	7.2514E-01	-7.9749E-01
6.1861E-01	2.5589E-01	5.4317E-01	6.7074E-01	-8.0458E-01	2.5589E-01	5.4317E-01	6.7074E-01	-8.0458E-01
7.0414E-01	3.2181E-01	5.9760E-01	6.0239E-01	-7.8984E-01	3.2181E-01	5.9760E-01	6.0239E-01	-7.8984E-01
7.9585E-01	3.9735E-01	6.4958E-01	5.3156E-01	-7.5121E-01	3.9735E-01	6.4958E-01	5.3156E-01	-7.5121E-01
8.8138E-01	4.7139E-01	6.9235E-01	4.6941E-01	-7.0042E-01	4.7139E-01	6.9235E-01	4.6941E-01	-7.0042E-01
9.4916E-01	5.3204E-01	7.2260E-01	4.2349E-01	-6.5385E-01	5.3204E-01	7.2260E-01	4.2349E-01	-6.5385E-01
9.9007E-01	5.6934E-01	7.3938E-01	3.9734E-01	-6.2417E-01	5.6934E-01	7.3938E-01	3.9734E-01	-6.2417E-01
1.0099E 00	5.8762E-01	7.4715E-01	3.8510E-01	-6.0656E-01	5.8762E-01	7.4715E-01	3.8510E-01	-6.0745E-01
1.0508E 00	6.2557E-01	7.6240E-01	3.6079E-01	-5.7904E-01	6.2557E-01	7.6240E-01	3.6079E-01	-5.7895E-01
1.1186E 00	6.8927E-01	7.8556E-01	3.2325E-01	-5.2882E-01	6.8927E-01	7.8556E-01	3.2325E-01	-5.2802E-01
1.2041E 00	7.7081E-01	8.1135E-01	2.8071E-01	-4.6729E-01	7.7081E-01	8.1135E-01	2.8070E-01	-4.6730E-01
1.2958E 00	8.5936E-01	8.3523E-01	2.4081E-01	-4.0522E-01	8.5936E-01	8.3523E-01	2.4081E-01	-4.0517E-01
1.3813E 00	9.4270E-01	8.5441E-01	2.0853E-01	-3.5201E-01	9.4270E-01	8.5441E-01	2.0853E-01	-3.5203E-01
1.4491E 00	1.0091E 00	8.6777E-01	1.8604E-01	-3.1342E-01	1.0091E 00	8.6777E-01	1.8603E-01	-3.1354E-01
1.4900E 00	1.0493E 00	8.7512E-01	1.7367E-01	-2.9180E-01	1.0493E 00	8.7512E-01	1.7366E-01	-2.9169E-01
1.5138E 00	1.0728E 00	8.7918E-01	1.6686E-01	-2.7996E-01	1.0728E 00	8.7918E-01	1.6685E-01	-2.8001E-01
1.5711E 00	1.1294E 00	8.8829E-01	1.5162E-01	-2.5357E-01	1.1294E 00	8.8829E-01	1.5161E-01	-2.5361E-01
1.6660E 00	1.2233E 00	9.0160E-01	1.2954E-01	-2.1474E-01	1.2233E 00	9.0161E-01	1.2953E-01	-2.1466E-01
1.7857E 00	1.3422E 00	9.1569E-01	1.0654E-01	-1.7350E-01	1.3422E 00	9.1568E-01	1.0655E-01	-1.7352E-01
1.9142E 00	1.4700E 00	9.2805E-01	8.6823E-02	-1.3766E-01	1.4700E 00	9.2805E-01	8.6848E-02	-1.3757E-01
2.0339E 00	1.5894E 00	9.3754E-01	7.2117E-02	-1.1085E-01	1.5894E 00	9.3754E-01	7.2147E-02	-1.1087E-01
2.1288E 00	1.6841E 00	9.4391E-01	6.2497E-02	-9.3404E-02	1.6841E 00	9.4391E-01	6.2520E-02	-9.3521E-02
2.1861E 00	1.7412E 00	9.4734E-01	5.7423E-02	-8.4339E-02	1.7412E 00	9.4735E-01	5.7438E-02	-8.4488E-02
2.2258E 00	1.7809E 00	9.4956E-01	5.4191E-02	-7.8794E-02	1.7809E 00	9.4956E-01	5.4200E-02	-7.8922E-02
2.3321E 00	1.8871E 00	9.5490E-01	4.6550E-02	-6.6149E-02	1.8871E 00	9.5491E-01	4.6553E-02	-6.6157E-02
2.5084E 00	2.0632E 00	9.6218E-01	3.6555E-02	-4.9789E-02	2.0632E 00	9.6219E-01	3.6571E-02	-4.9697E-02
2.7307E 00	2.2854E 00	9.6923E-01	2.7426E-02	-3.5106E-02	2.2854E 00	9.6925E-01	2.7467E-02	-3.5025E-02
2.9692E 00	2.5238E 00	9.7491E-01	2.0576E-02	-2.4458E-02	2.5238E 00	9.7493E-01	2.0627E-02	-2.4438E-02
3.1915E 00	2.7462E 00	9.7895E-01	1.6022E-02	-1.7702E-02	2.7462E 00	9.7898E-01	1.6073E-02	-1.7726E-02
3.3678E 00	2.9224E 00	9.8157E-01	1.3290E-02	-1.3836E-02	2.9224E 00	9.8157E-01	1.3336E-02	-1.3871E-02
3.4741E 00	3.0287E 00	9.8286E-01	1.1925E-02	-1.1999E-02	3.0287E 00	9.8291E-01	1.1967E-02	-1.2036E-02
3.5496E 00	3.1042E 00	9.8373E-01	1.1065E-02	-1.0922E-02	3.1042E 00	9.8378E-01	1.1113E-02	-1.0952E-02
3.7541E 00	3.3087E 00	9.8578E-01	9.1010E-03	-8.6177E-03	3.3087E 00	9.8604E-01	9.1375E-03	-8.6221E-03
4.0930E 00	3.6476E 00	9.8844E-01	6.7336E-03	-5.9296E-03	3.6476E 00	9.8851E-01	6.7715E-03	-5.9256E-03
4.5207E 00	4.0752E 00	9.9086E-01	4.7674E-03	-3.8035E-03	4.0752E 00	9.9095E-01	4.8096E-03	-3.8041E-03
4.9792E 00	4.5338E 00	9.9272E-01	3.4138E-03	-2.4428E-03	4.5338E 00	9.9282E-01	3.4515E-03	-2.4466E-03
5.4069E 00	4.9614E 00	9.9398E-01	2.5721E-03	-1.6646E-03	4.9614E 00	9.9411E-01	2.6081E-03	-1.6642E-03
5.7458E 00	5.3003E 00	9.9477E-01	2.0895E-03	-1.2512E-03	5.3003E 00	9.9491E-01	2.1243E-03	-1.2543E-03
5.9503E 00	5.5049E 00	9.9517E-01	1.8549E-03	-1.0633E-03	5.5049E 00	9.9532E-01	1.8892E-03	-1.0699E-03
6.0794E 00	5.6339E 00	9.9540E-01	1.7245E-03	-9.6719E-04	5.6339E 00	9.9555E-01	1.7984E-03	-9.8992E-04
6.4066E 00	5.9612E 00	9.9592E-01	1.4439E-03	-7.7471E-04	5.9612E 00	9.9608E-01	1.4772E-03	-7.7644E-04
6.9489E 00	6.5034E 00	9.9660E-01	1.0981E-03	-5.4697E-04	6.5034E 00	9.9678E-01	1.1307E-03	-5.4826E-04
7.6331E 00	7.1876E 00	9.9725E-01	8.0214E-04	-3.6243E-04	7.1876E 00	9.9744E-01	8.3396E-04	-3.6336E-04
8.3668E 00	7.9214E 00	9.9775E-01	5.9146E-04	-2.4069E-04	7.9214E 00	9.9797E-01	6.2270E-04	-2.4137E-04
9.0510E 00	8.6056E 00	9.9811E-01	4.5640E-04	-1.6886E-04	8.6056E 00	9.9835E-01	4.8725E-04	-1.6935E-04
9.5933E 00	9.1478E 00	9.9833E-01	3.7709E-04	-1.2969E-04	9.1478E 00	9.9854E-01	4.0771E-04	-1.3008E-04
9.9205E 00	9.4751E 00	9.9845E-01	3.3792E-04	-1.1164E-04	9.4751E 00	9.9872E-01	3.6642E-04	-1.1196E-04
1.0198E 01	9.7530E 00	9.9854E-01	3.0879E-04	-9.9459E-05	9.7530E 00	9.9882E-01	3.3921E-04	-9.9673E-05
1.1016E 01	1.0571E 01	9.9876E-01	2.4028E-04	-7.3069E-05	1.0571E 01	9.9906E-01	2.7068E-04	-7.3073E-05
1.2372E 01	1.1926E 01	9.9903E-01	1.6518E-04	-4.5410E-05	1.1926E 01	9.9938E-01	1.9563E-04	-4.4931E-05
1.4082E 01	1.3637E 01	9.9926E-01	1.0907E-04	-2.6232E-05	1.3637E 01	9.9966E-01	1.4128E-04	-2.6728E-05
1.5917E 01	1.5471E 01	9.9943E-01	7.3876E-05	-1.5426E-05	1.5471E 01	9.9988E-01	1.0217E-04	-1.0581E-05
1.7627E 01	1.7182E 01	9.9953E-01	5.3488E-05	-9.8522E-06	1.7182E 01	1.0000E 00	1.0120E-04	-1.4805E-05
1.8983E 01	1.8537E 01	9.9960E-01	4.2353E-05	-7.1003E-06	1.8537E 01	1.0001E 00	6.5840E-05	2.3193E-05
1.9801E 01	1.9355E 01	9.9963E-01	3.7094E-05	-5.7561E-06	1.9355E 01	1.0002E 00	1.0914E-04	8.2674E-05

TABLE 2. THE PRESSURE COEFFICIENT AND THE GEOMETRY OF THE CAVITY BEHIND A DISK FOR $C_{PB} = 0$

SA 0

9.000000000E-01
1.000000000E 00
1.100000000E 00
1.400000000E 00
2.200000000E 00
5.000000000E 00
1.000000000E 01
6.000000000E 01

CDT =8.2898E-01
CPB = 0

LEGEND:

S = arc length
X = x-coordinate
R = wake radius (r(s))
RP = dr/ds
RP2 = d^2r/ds^2
CUR = curvature
Q = source strength
VN = remaining normal velocity on the streamline
CP = pressure coefficient

S	X	R	RP	RP2	CUR	Q	VN	CP
1.7a7.E=02	0	1.7a70E-02	1.0000E 00	0	0	1.7010E 00	-5.6653E-13	9.9937E-01
9.1500E=02	0	9.1500E-02	1.0000E 00	0	0	1.7012E 00	-1.4019E-11	9.9865E-01
2.1351E-01	0	2.1351E-01	1.0000E 00	0	0	-1.6983E-00	-1.6829E-11	9.9253E-01
3.6745E-01	0	3.6745E-01	1.0000E 00	0	0	1.6987E 00	1.6012E-11	9.7660E-01
5.3255E-01	0	5.3255E-01	1.0000E 00	0	0	1.6741E 00	2.5721E-11	9.4527E-01
6.8649E-01	0	6.8649E-01	1.0000E 00	0	0	1.6593E 00	1.4211E-11	8.9283E-01
8.0850E-01	0	8.0850E-01	1.0000E 00	0	0	1.6149E 00	-4.4910E-11	8.1699E-01
8.8213E-01	0	8.8213E-01	1.0000E 00	0	0	1.5849E 00	-3.1061E-11	7.3587E-01
9.0199E-01	0	9.0199E-01	1.0000E 00	0	0	1.5736E 00	-1.3173E-11	7.0438E-01
9.1017E-01	0	9.1017E-01	1.0000E 00	0	0	1.5641E 00	-2.1064E-11	6.8969E-01
9.2372E-01	0	9.2372E-01	1.0000E 00	0	0	1.5524E 00	-1.3360E-11	6.6075E-01
9.4183E-01	0	9.4183E-01	1.0000E 00	0	0	1.5316E 00	9.7213E-12	6.1700E-01
9.5917E-01	0	9.5917E-01	1.0000E 00	0	0	1.5076E 00	-4.9268E-12	5.5446E-01
9.7628E-01	0	9.7628E-01	1.0000E 00	0	0	1.4713E 00	-1.1755E-11	4.6813E-01
9.8983E-01	0	9.8983E-01	1.0000E 00	0	0	1.4213E 00	-3.8142E-11	3.5002E-01
9.9811E-01	0	9.9811E-01	1.0000E 00	0	0	1.3497E 00	-1.4254E-11	2.1714E-01
1.0420E 00	1.1744E-02	1.0420E 00	9.9744E-01	-1.7202E-02	-2.3864E 01	1.2623E 00	5.5753E-06	-9.0332E-02
1.0810E 00	1.2458E-02	1.0810E 00	9.8139E-01	-2.0137E 00	-1.0488E 01	9.8510E-01	-1.3772E-05	1.0155E-03
1.0837E 00	4.6752E-02	1.0837E 00	9.5292E-01	-2.0116E 00	-6.6343E 00	8.6450E-01	2.9779E-05	-9.5805E-03
1.0905E 00	1.0672E-02	1.0892E 00	9.2043E-01	-1.8410E 00	-4.7059E 00	7.8349E-01	-8.7916E-05	2.6374E-04
1.0992E 00	1.8213E-02	1.0956E 00	8.8781E-01	-1.6425E 00	-3.5085E 00	7.2258E-01	7.8059E-05	-4.6566E-04
1.0743E 00	2.6088E-02	1.0707E 00	8.5160E-01	-1.5206E 00	-4.0142E 00	6.8701E-01	-7.4966E-05	5.6911E-04
1.0898E 00	3.3912E-02	1.0823E 00	8.1603E-01	-1.3872E 00	-2.5640E 00	6.5782E-01	1.9776E-05	-5.1556E-04
1.0946E 00	3.8405E-02	1.0891E 00	8.0343E-01	-1.3470E 00	-2.4178E 00	6.4710E-01	-2.9085E-05	4.4491E-04
1.1060E 00	4.2874E-02	1.0957E 00	8.1933E-01	-1.3477E 00	-2.3508E 00	6.3317E-01	-4.3960E-05	-6.2726E-04
1.1305E 00	5.7580E-02	1.1154E 00	7.8998E-01	-1.1577E 00	-1.8682E 00	6.0575E-01	1.9911E-04	9.1742E-04
1.1712E 00	8.3553E-02	1.1466E 00	7.4547E-01	-1.0049E 00	-1.5476E 00	5.6376E-01	-2.7942E-04	-9.2667E-04
1.2225E 00	1.1980E-01	1.1837E 00	6.9970E-01	-8.2259E-01	-1.1911E 00	5.2942E-01	1.2624E-04	5.2529E-04
1.2775E 00	1.5947E-01	1.2210E 00	6.5855E-01	-6.9807E-01	-9.2763E-01	5.0082E-01	9.5574E-05	-2.6566E-04
1.3284E 00	1.9884E-01	1.2539E 00	6.2510E-01	-5.8969E-01	-7.5519E-01	4.7826E-01	3.6560E-04	-2.6188E-05
1.3695E 00	2.3894E-01	1.2789E 00	6.0312E-01	-5.4015E-01	-6.7718E-01	4.6633E-01	1.4003E-04	2.0851E-04
1.3940E 00	2.5894E-01	1.2915E 00	5.8987E-01	-5.0203E-01	-6.2246E-01	4.5726E-01	1.4571E-04	-1.8913E-04
1.4159E 00	2.6886E-01	1.3063E 00	5.7962E-01	-4.6401E-01	-5.7095E-01	4.5205E-01	2.9764E-04	2.6044E-04
1.4813E 00	3.2247E-01	1.3432E 00	5.5010E-01	-4.1527E-01	-4.9727E-01	4.3374E-01	6.6179E-05	-3.5226E-04
1.5809E 00	4.1434E-01	1.4007E 00	5.1149E-01	-3.3177E-01	-3.8609E-01	4.1415E-01	2.5915E-05	1.7054E-04
1.7206E 00	5.3306E-01	1.4676E 00	4.7126E-01	-2.6410E-01	-2.9914E-01	3.9914E-01	5.4729E-05	-4.5206E-04
1.8734E 00	6.6441E-01	1.5343E 00	4.3733E-01	-2.1036E-01	-2.3385E-01	3.8725E-01	1.4057E-04	3.9356E-04
2.0112E 00	7.8437E-01	1.5922E 00	4.1037E-01	-1.7570E-01	-1.9267E-01	3.7542E-01	-4.4057E-06	-2.5777E-04
2.1187E 00	8.8769E-01	1.6456E 00	3.9315E-01	-1.5457E-01	-1.6811E-01	3.6594E-01	1.3069E-04	1.2546E-04
2.1841E 00	9.4801E-01	1.6812E 00	3.8320E-01	-1.4308E-01	-1.5576E-01	3.5941E-01	-3.5213E-05	-6.7643E-05
2.2556E 00	1.0142E 00	1.6882E 00	3.7555E-01	-1.3143E-01	-1.4168E-01	3.5365E-01	-9.4654E-06	8.1124E-05
2.4847E 00	1.2279E 00	1.7705E 00	3.4606E-01	-1.0849E-01	-1.1563E-01	3.3524E-01	-1.0469E-04	-1.0759E-04
2.8643E 00	1.6865E 00	1.8951E 00	3.1213E-01	-7.9923E-02	-8.4128E-02	3.0933E-01	-2.7956E-04	1.9535E-04
3.3412E 00	2.0441E 00	2.0364E 00	2.7956E-01	-5.8759E-02	-6.1195E-02	2.8606E-01	-2.9110E-04	-2.4946E-04
3.8568E 00	2.5392E 00	2.1782E 00	2.5446E-01	-4.3635E-02	-4.5386E-02	2.6459E-01	-1.6599E-04	1.1616E-04
4.3357E 00	3.0145E 00	2.2984E 00	2.3572E-01	-3.4915E-02	-3.5927E-02	2.4809E-01	-5.2052E-04	2.1615E-07
4.7153E 00	3.3736E 00	2.3776E 00	2.2575E-01	-2.9995E-02	-3.0776E-02	2.3595E-01	-3.8515E-04	1.2254E-04
4.9444E 00	3.5906E 00	2.4280E 00	2.1709E-01	-2.7179E-02	-2.7643E-02	2.2850E-01	-3.7659E-04	-2.2221E-05
5.0993E 00	3.7476E 00	2.4613E 00	2.1308E-01	-2.5490E-02	-2.6057E-02	2.2477E-01	-3.8254E-04	2.7526E-05
5.5143E 00	4.1478E 00	2.5444E 00	2.0114E-01	-2.2602E-02	-2.3145E-02	2.1347E-01	-4.1742E-04	-5.8170E-05
6.1862E 00	4.8124E 00	2.6794E 00	1.8960E-01	-1.8355E-02	-1.8694E-02	1.9770E-01	-4.6220E-04	6.4818E-05
7.0414E 00	5.6515E 00	2.8353E 00	1.7566E-01	-1.4858E-02	-1.5093E-02	1.7437E-01	-4.6159E-04	-1.2774E-04
7.9586E 00	6.5372E 00	2.9786E 00	1.6365E-01	-1.1703E-02	-1.1946E-02	1.6237E-01	-5.0855E-04	1.177 E-04
8.8138E 00	7.4016E 00	3.1265E 00	1.5459E-01	-1.0194E-02	-1.0322E-02	1.5402E-01	-5.6510E-04	-6.8114E-05
9.4917E 00	8.0717E 00	3.2289E 00	1.4776E-01	-8.5291E-03	-8.6236E-03	1.4688E-01	-4.9751E-04	-2.9465E-05
9.9007E 00	8.4765E 00	3.2987E 00	1.4465E-01	-7.7050E-03	-7.7969E-03	1.4416E-01	-5.9105E-04	1.3677E-04
1.0093E 01	9.5576E 00	3.4420E 00	1.3593E-01	-7.2602E-03	-7.3513E-03	1.3471E-01	-5.8054E-04	-4.0251E-04
1.5083E 01	1.3616E 01	3.9219E 00	1.1741E-01	-5.9775E-03	-6.0151E-03	1.1719E-01	-2.8814E-04	7.6413E-04
2.1862E 01	2.0356E 01	4.6730E 00	9.6802E-02	-4.3079E-03	-4.3186E-03	9.6472E-02	-6.8456E-04	-3.8753E-04
2.8414E 01	2.8474E 01	5.4431E 00	8.4814E-02	-3.3161E-03	-3.3209E-03	8.4914E-02	-1.9254E-04	-1.3169E-03
3.9546E 01	3.8818E 01	6.1265E 00	7.3584E-02	-2.5310E-03	-2.5455E-03	7.1491E-02	-4.4046E-04	7.8774E-03
4.8138E 01	4.6534E 01	6.6540E 00	6.2160E-02	-1.9693E-03	-1.9777E-03	1.052 E-01	6.9372E-03	-2.0119E-02
5.4917E 01	5.3304E 01	7.3194E 00	5.6563E-02	-1.6398E-03	-1.6466E-03	5.1467E-02	-4.6991E-03	2.2226E-02
5.9007E 01	5.7374E 01	7.6867E 00	1.4417E-01	8.1493E-02	8.1785E-02	2.2579E-01	4.9743E-03	-4.9645E-02

TABLE 3. CONE AND SPHERE DRAG COEFFICIENTS

Cone Drag Coefficients

*(Riabouch. Mod.)

C_{PB}	.0	-.05	-.1	-.2	-.2235	-.3	-.41	-.6
β = 15°	.1460		.2014					
45°	.5042		.5694	.6360				
63.4°	.6679							
90°	.8238	.8664	.9092	.9955	1.0144*	1.0822	1.1777 1.1767*	1.3455

Sphere Drag Coefficients

C_{PB}	.0	-.2	-.45
ϕ_s = 52.32°	.3027		
54.04°	.3063		
55.75°	.3084		
57.48°	.3090		
63.03°	.3090		
80°		.3076	.4909
82°		.2907	.4797

TABLE 4. THE APPROXIMATE CALCULATION OF THE LAMINAR SEPARATION POINT FROM A SPHERE

s	V_T	V_T Calculated	Error
.027423	.055215	.040701	.2628
.140419	.203833	.207253	-.0167
.327660	.466285	.471754	-.0117
.563907	.769968	.769153	.0010
.817262	1.040140	1.032990	.0068
1.053509	1.218332	1.221146	-.0023
1.240750	1.289778	1.300160	-.0080
1.353746	1.285990	1.285045	.0007
1.382162	1.274379	1.269342	.0042
1.386253	1.272036	1.266597	.0042
1.393031	1.267721	1.261764	.0046
1.401584	1.261152	1.255147	.0047
1.410755	1.252393	1.247384	.0039
1.419308	1.241234	1.239498	.0013
1.426086	1.227846	1.232790	-.0040
1.430177	1.212065	1.228540	-.0135

$\overline{u_1} = 1.4845, \quad \overline{u_3} = -.4385, \quad \overline{u_5} = .2094, \quad \overline{u_7} = -.0706$

The determination equation for the separation point is:

$$1 - .6832s_B^2 + .4666s_B^4 - .2198s_B^6 = 0.$$

Solution:

$$s_B = 1.342, \quad \underline{\underline{\phi_s = 77°.}}$$

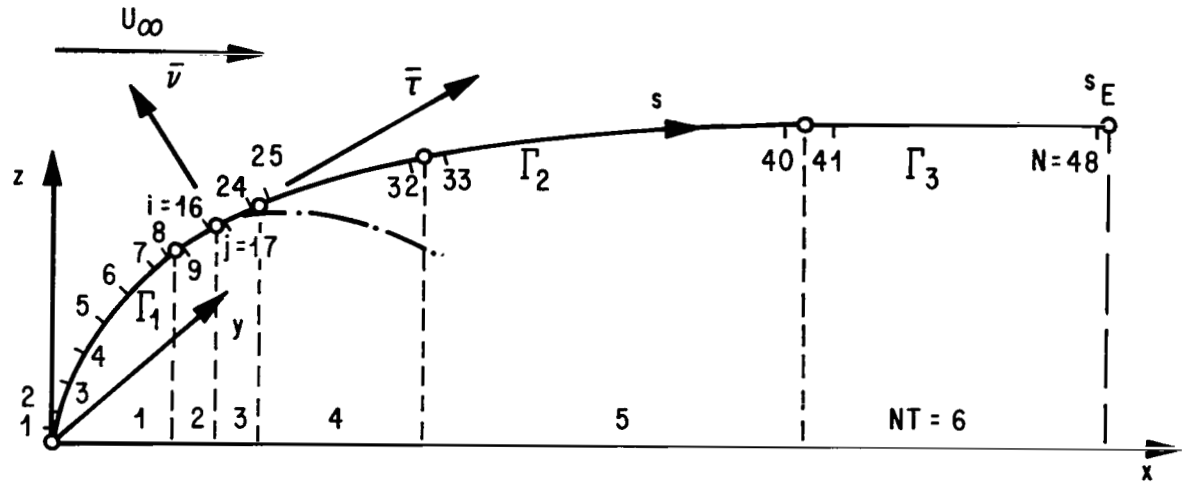

(a) The Coordinate System and the Distribution of Points

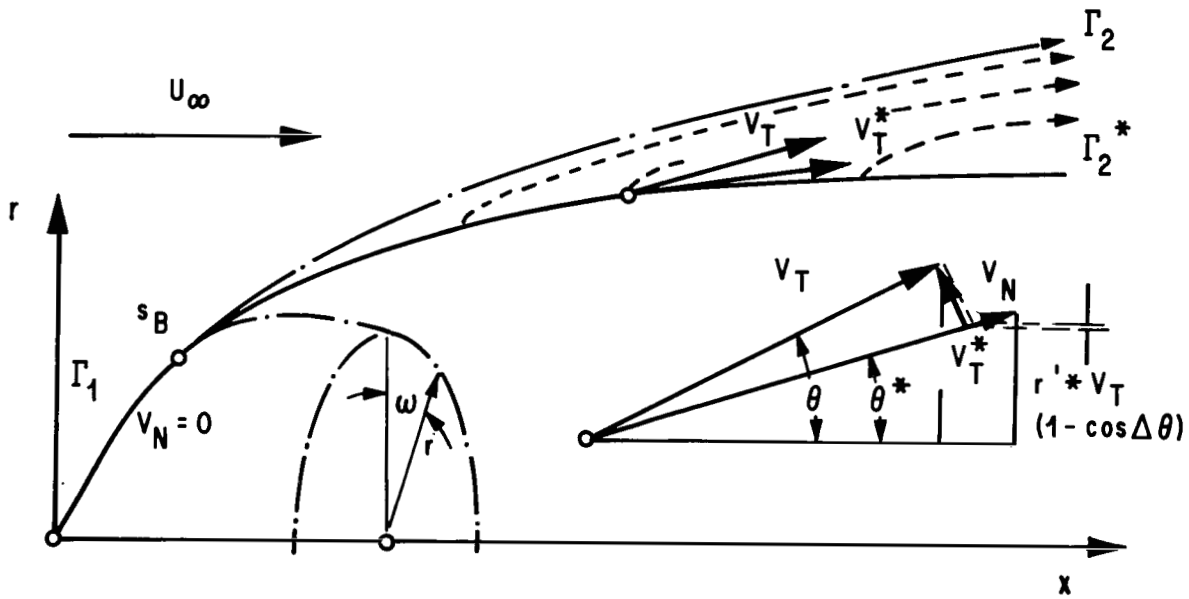

(b) Representation of Two Lines with $V_N = 0$ Along Γ_2^*

Figure 1. Notations and Schematic of Cavity or Wake Flow

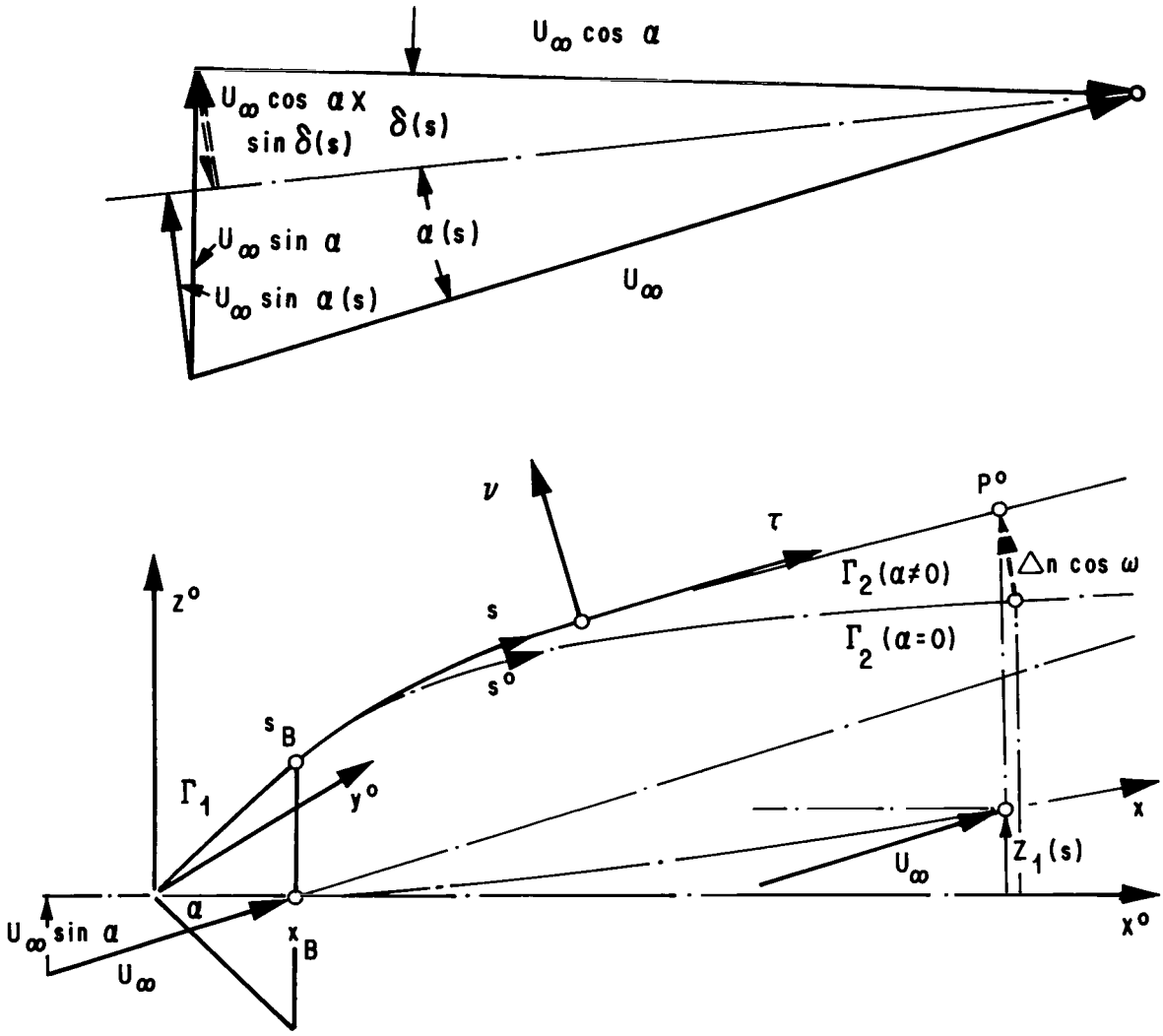

(c) The Bent Wake and Additional Notations

Figure 1. (Continued)

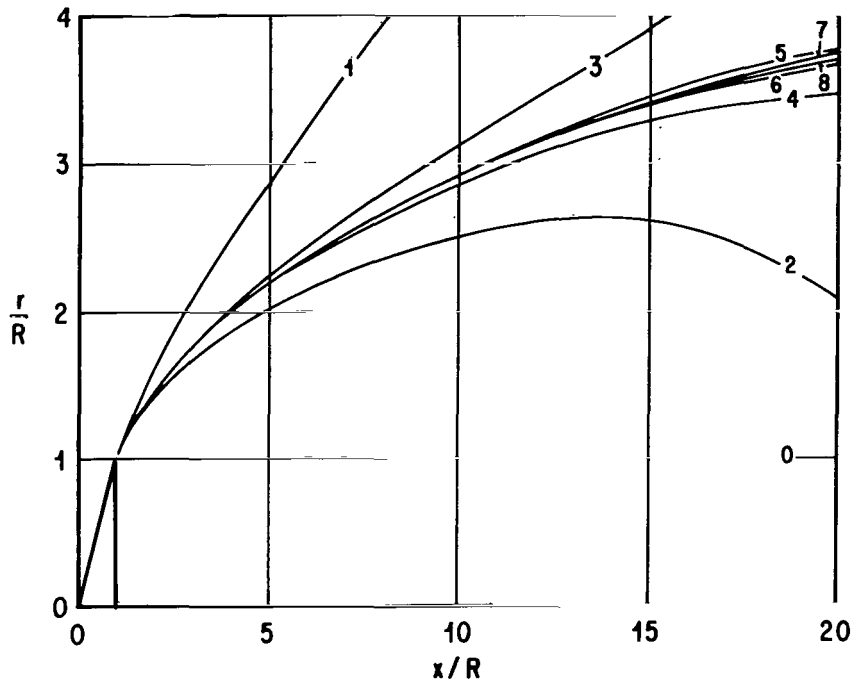

(a) The Axisymmetric Flow

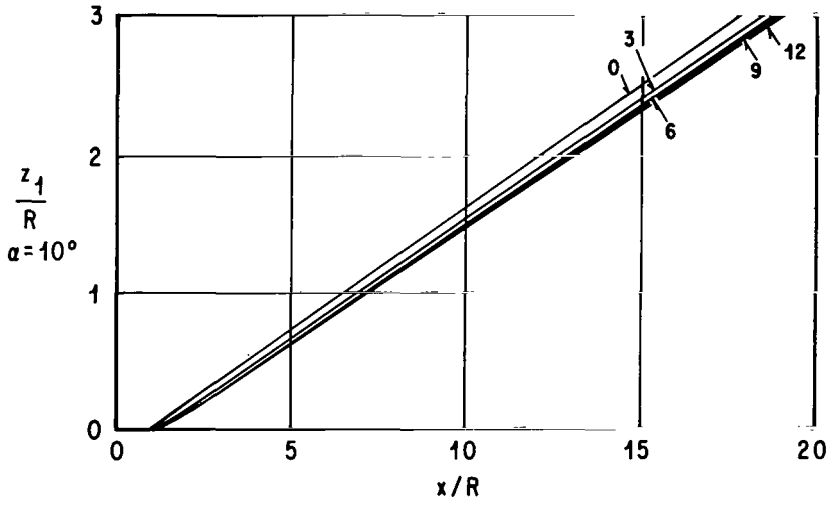

(b) Flow About the 10-Degree Inclined Cone

Figure 2. The Convergence of the Numerical Procedure. Representation of the First Iteration Steps for A 45-Degree Cone

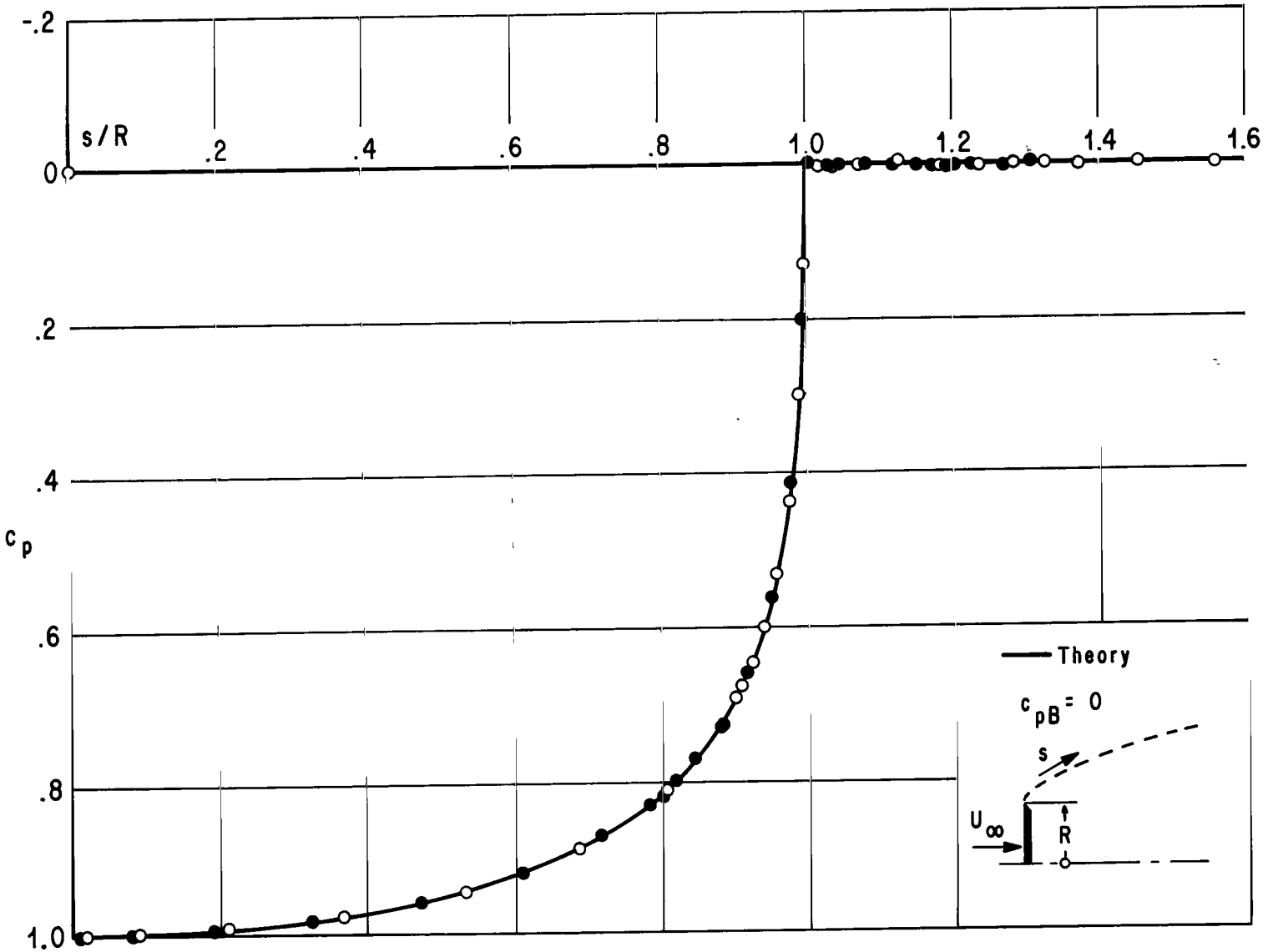

Figure 3. The Pressure Distribution Along the Disk in Normal Flow For $C_{PB} = 0$ and A Drag Coefficient of $C_D = .824$

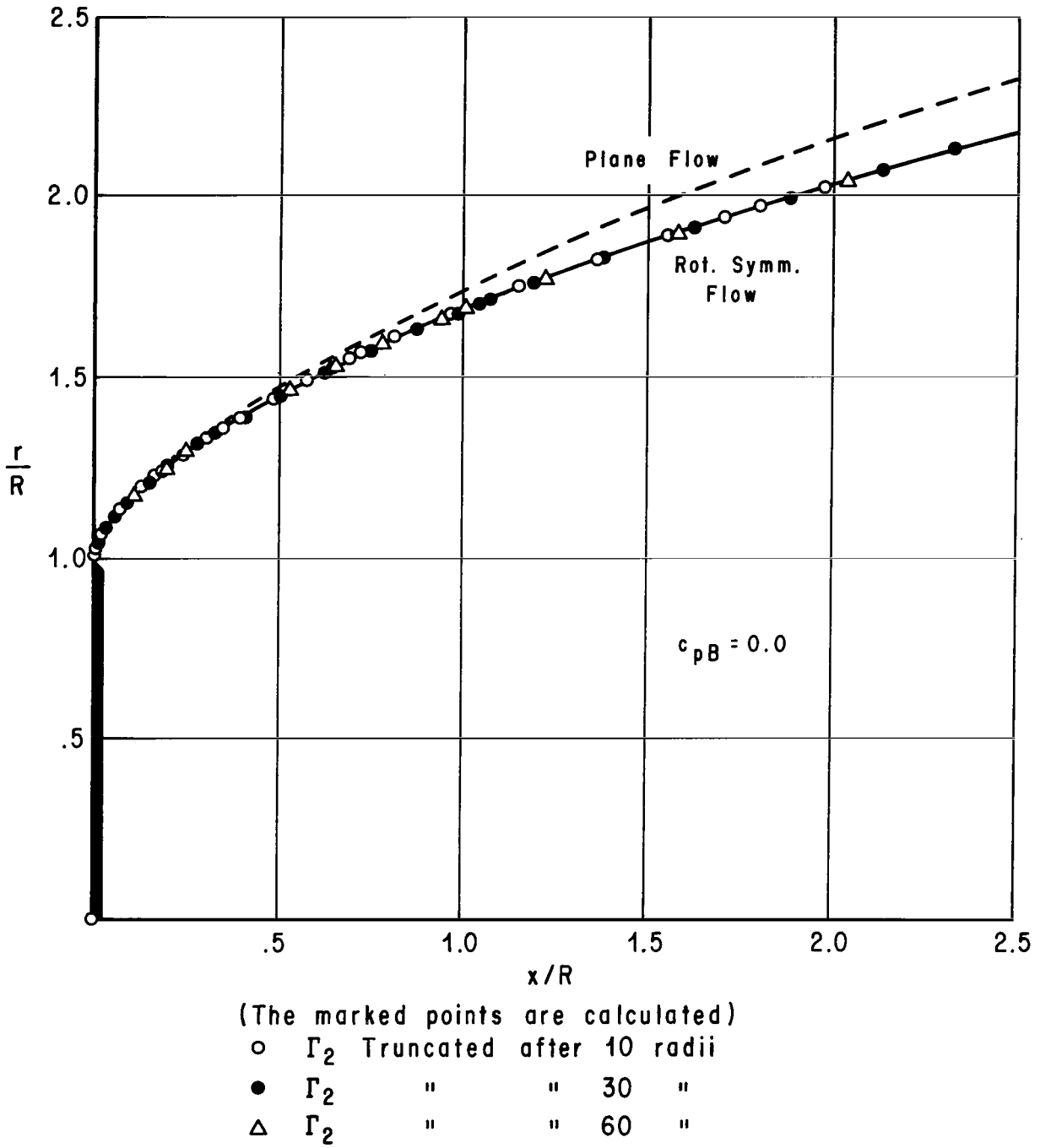

(a) The Free Streamline in the Neighborhood of s_B

Figure 4. The Free Streamline In Plane and Axisymmetric Flow About a Disk for a Base Pressure Coefficient of $C_{PB} = 0$

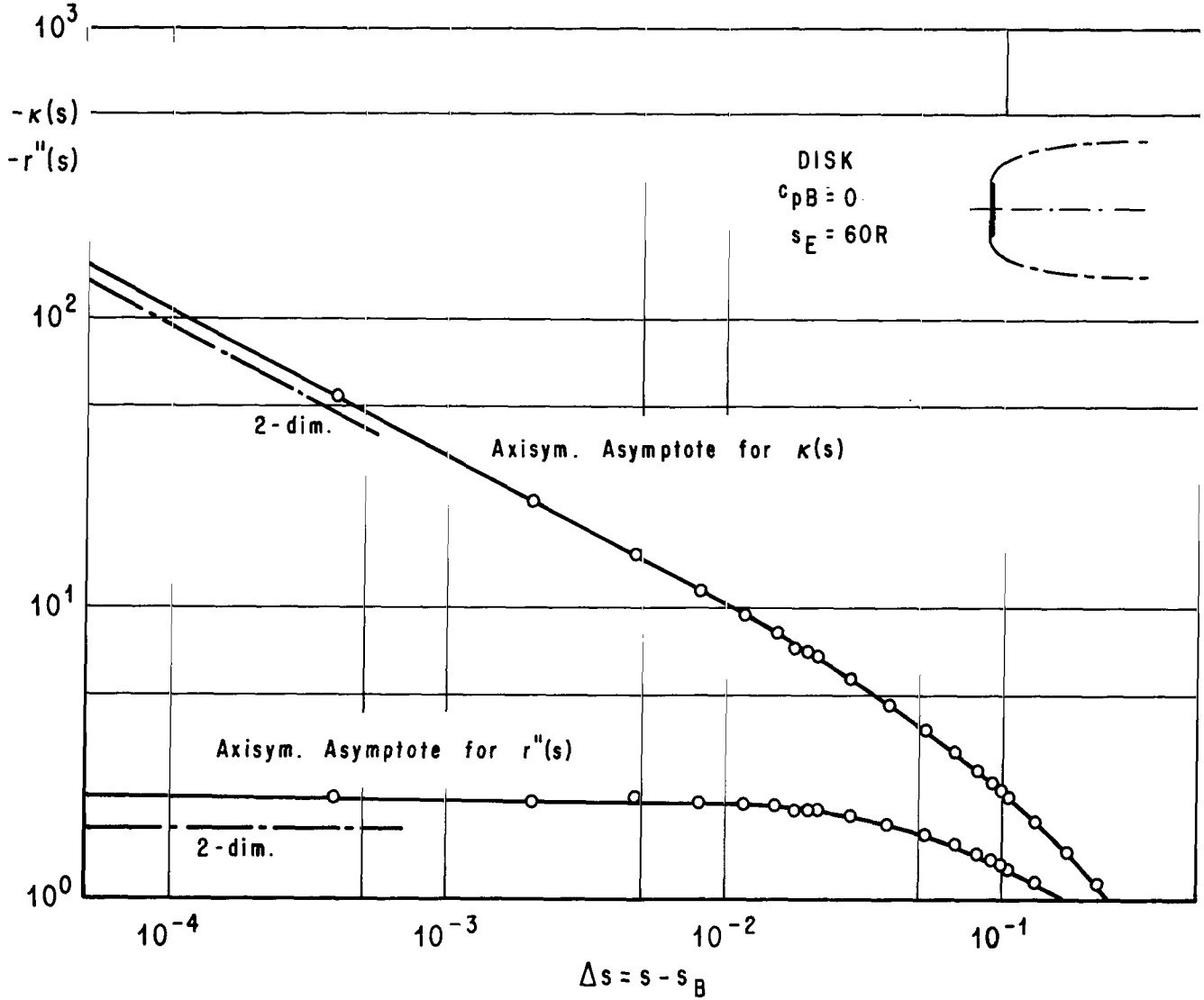

(b) The Asymptotic Representation of the Curvature and the Second Derivative of the Radius of the Free Streamline in the Vicinity of the Separation Point of the Disk

Figure 4. (Continued)

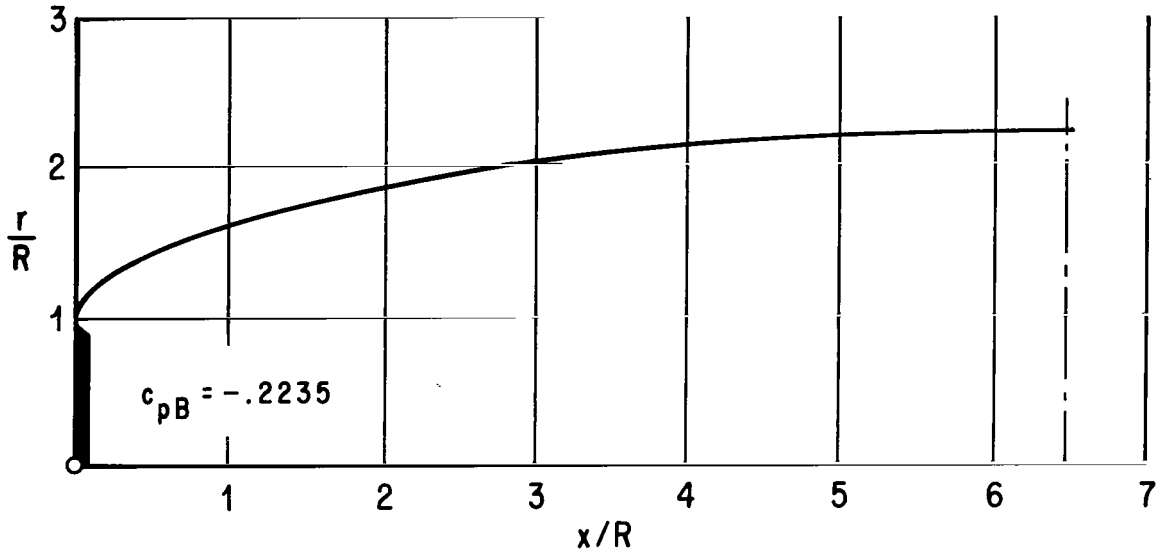

(a) The Free Streamline of the Half-Cavity (Riabouchinsky Model)

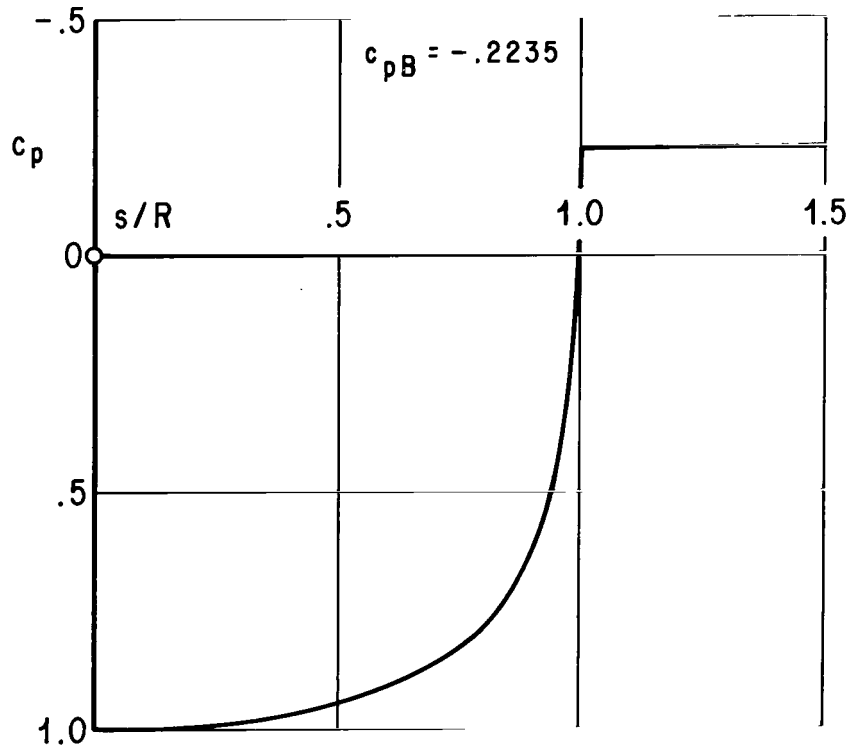

(b) The Pressure Coefficient on the Front Side of the Disk

Figure 5. The Geometry of the Cavity and the Pressure Distribution of the Disk (Riabouchinsky Model). $C_D = 1.015$

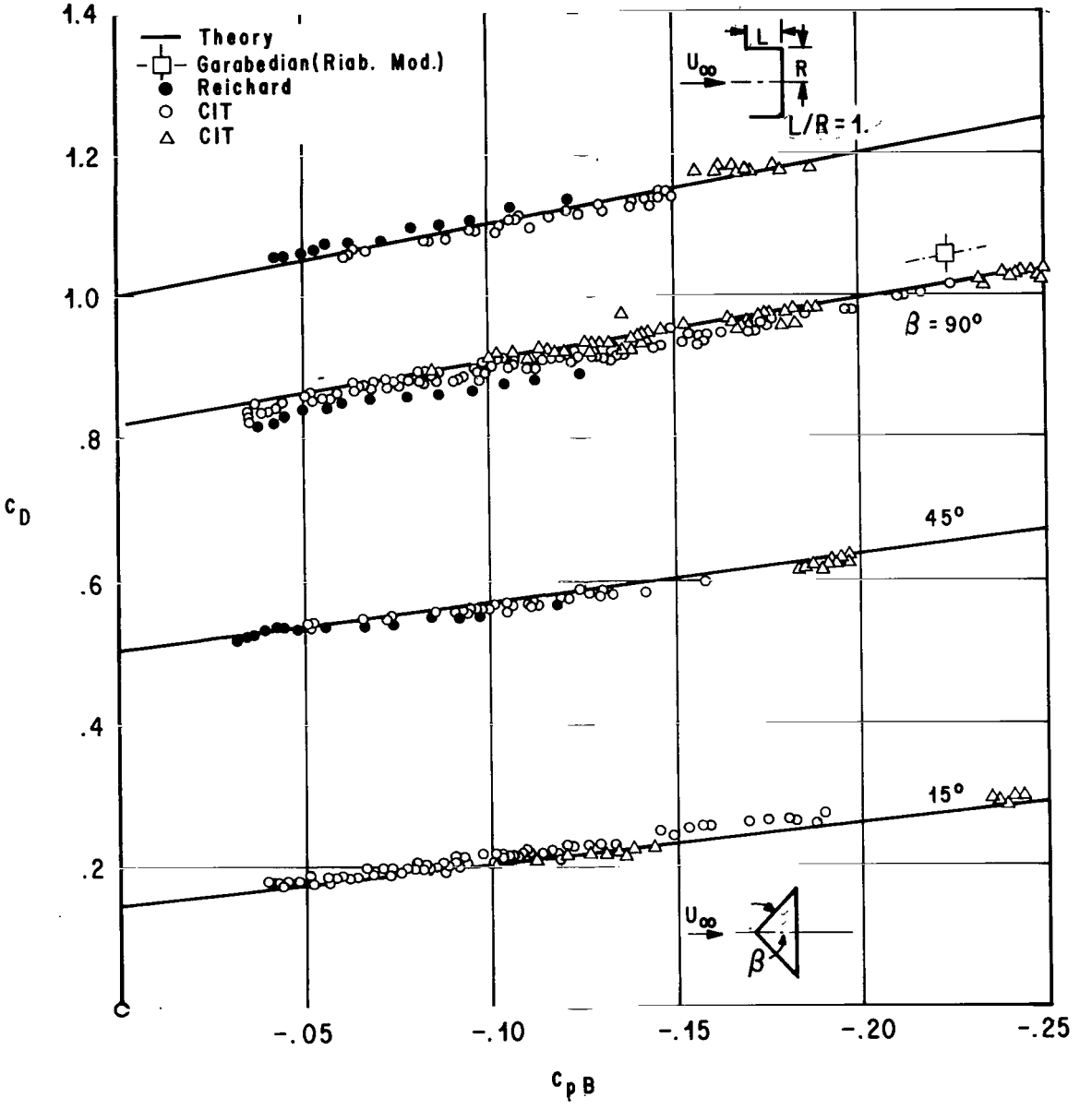

Figure 6. The Drag Coefficient of Different Cones as A Function of The Base Pressure Coefficient (Water Tunnel Tests) [16]

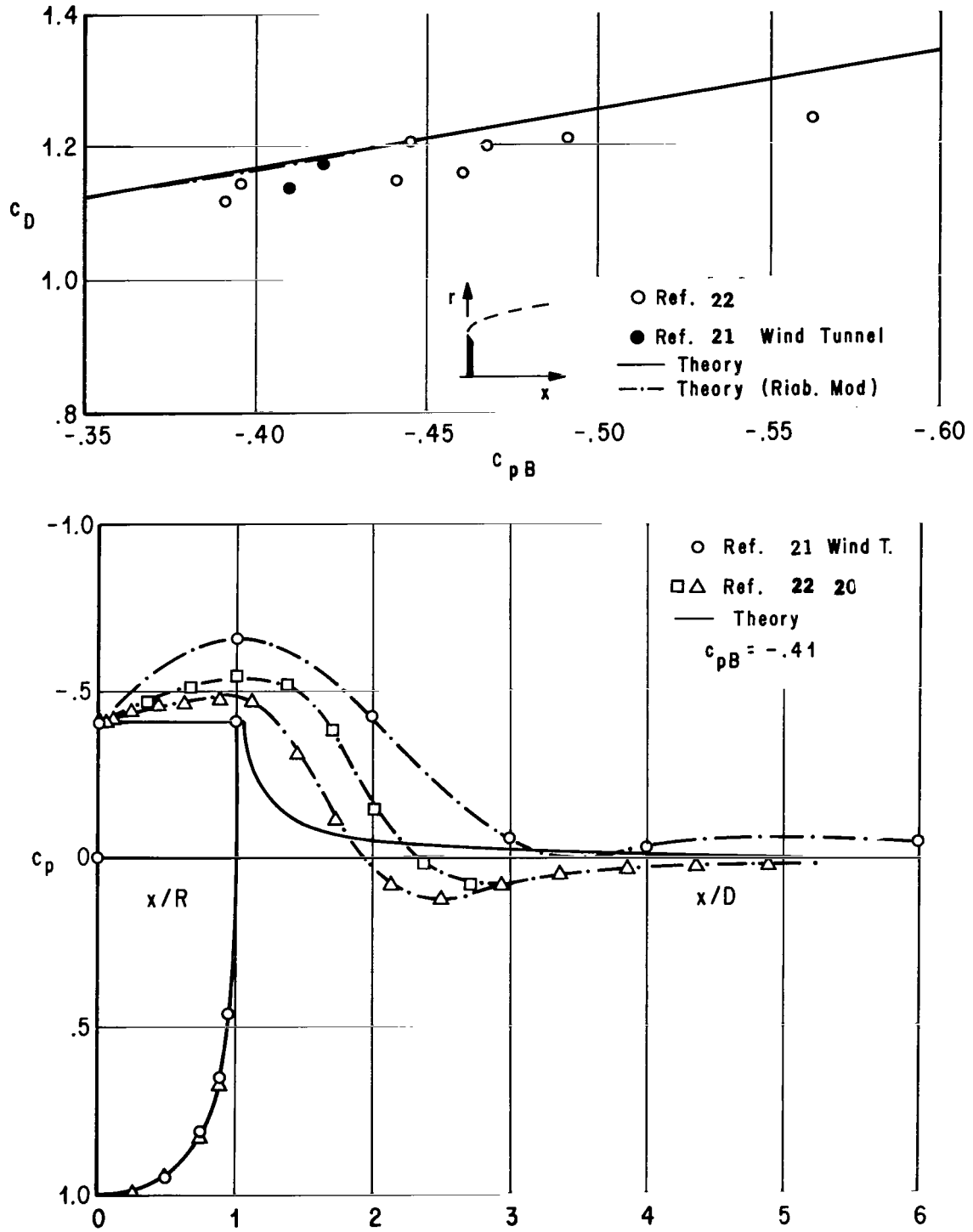

Figure 7. Drag Coefficients and Pressure Distributions of Disks for High Base Pressure Coefficients (Dissipation Model)

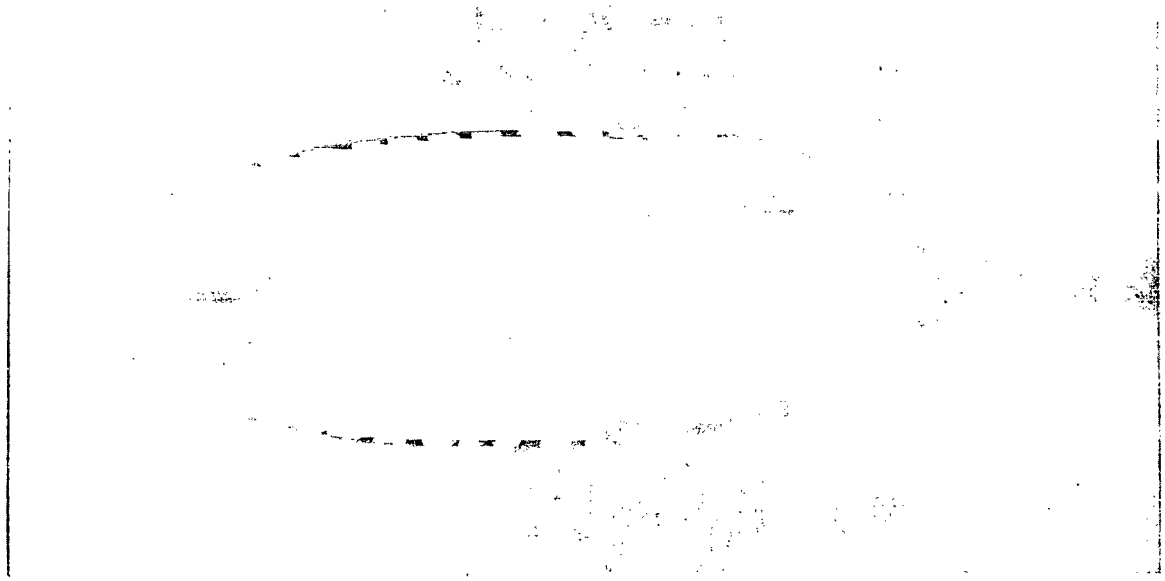

Figure 8. The Cavity Behind a Disk for C_{PB} = -.188 [22]
(Water Tunnel Test)

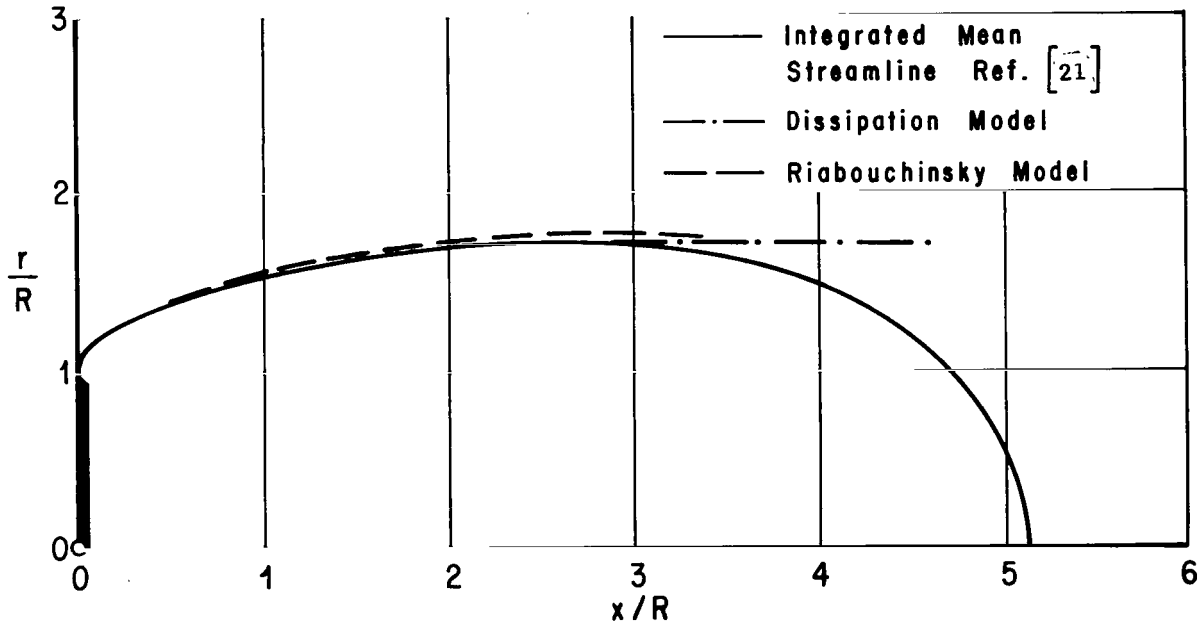

Figure 9. Comparison of the Streamline ψ = 0 Obtained from Wind Tunnel Tests and Theory for A Disk with C_{PB} = -.41

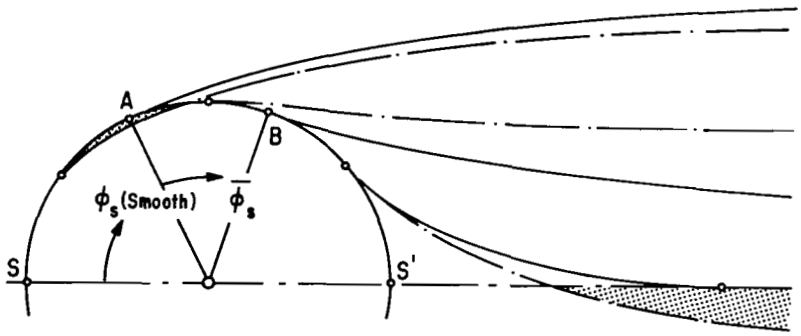

Figure 10. Schematic Representation of the Separation Points from a Sphere

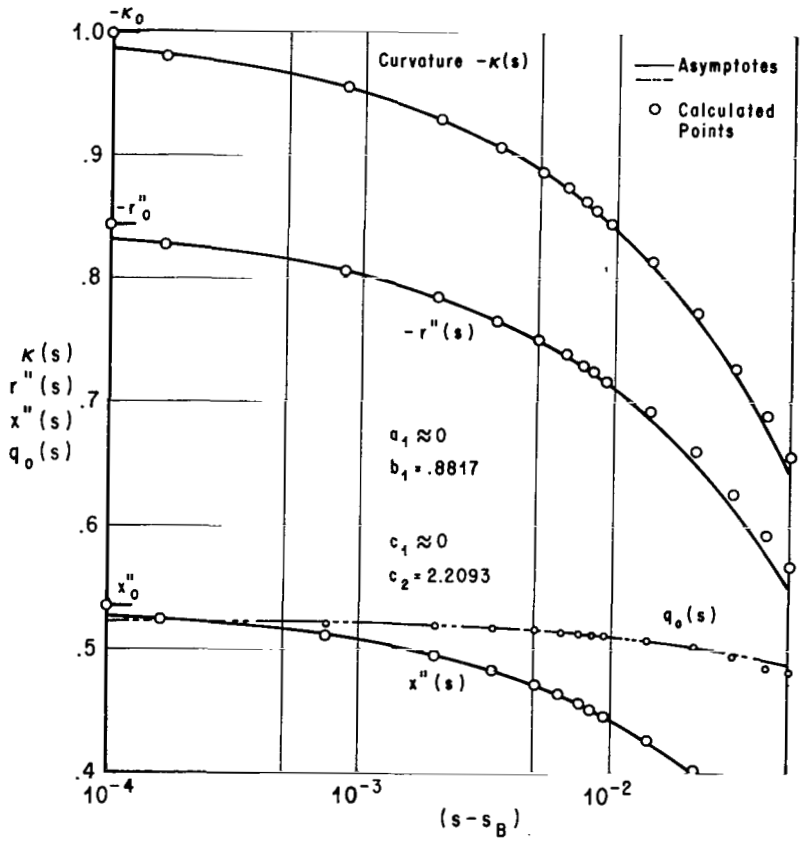

Figure 11. The Free Streamline in the Immediate Vicinity of the Smooth Separation Point of A Sphere for $C_{PB} = 0$

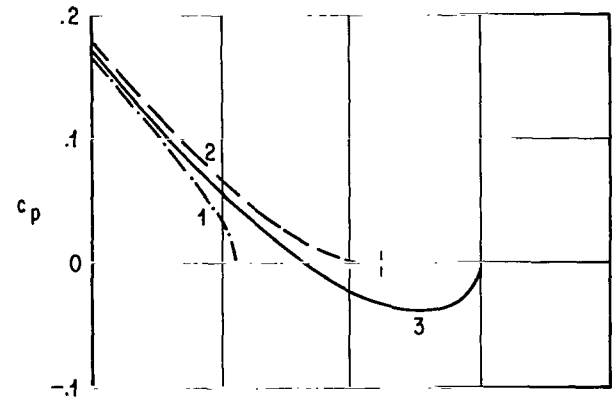

(a) Pressure Distribution

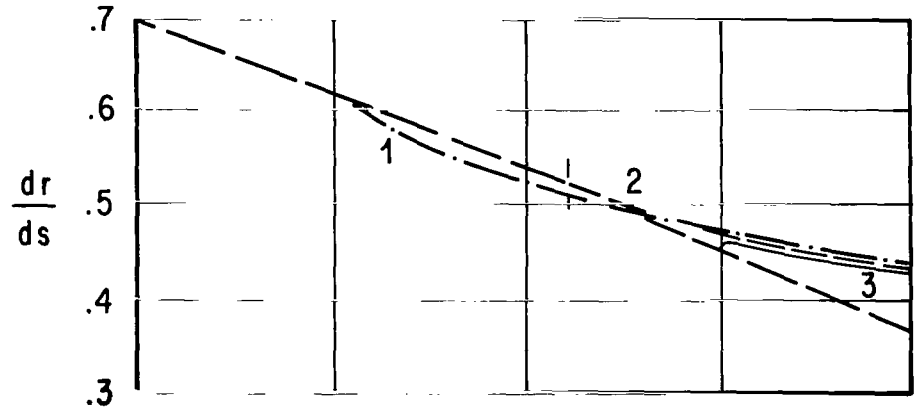

(b) Derivative of the Radius with Respect to s

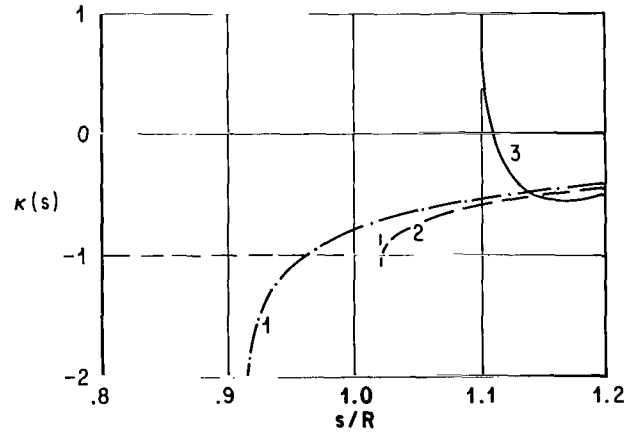

(c) Curvature of the Free Streamline

Figure 12. Representation of the Possibilities of Separation Close to the Point of Smooth Separation

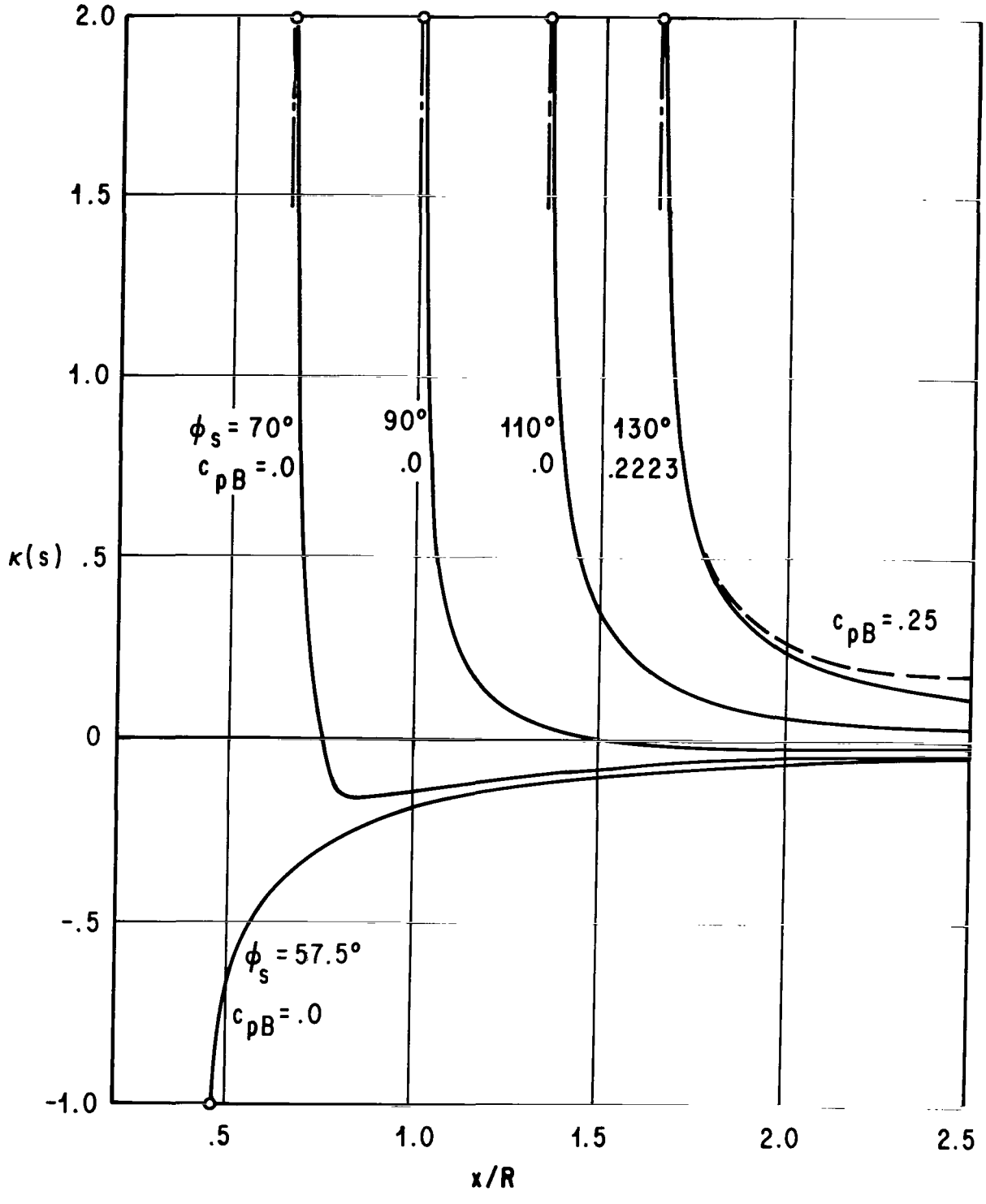

Figure 13. The Curvature of the Free Streamline Γ_2 for Different Sphere Separation Angles ϕ_s and Base Pressure Coefficients C_{PB}

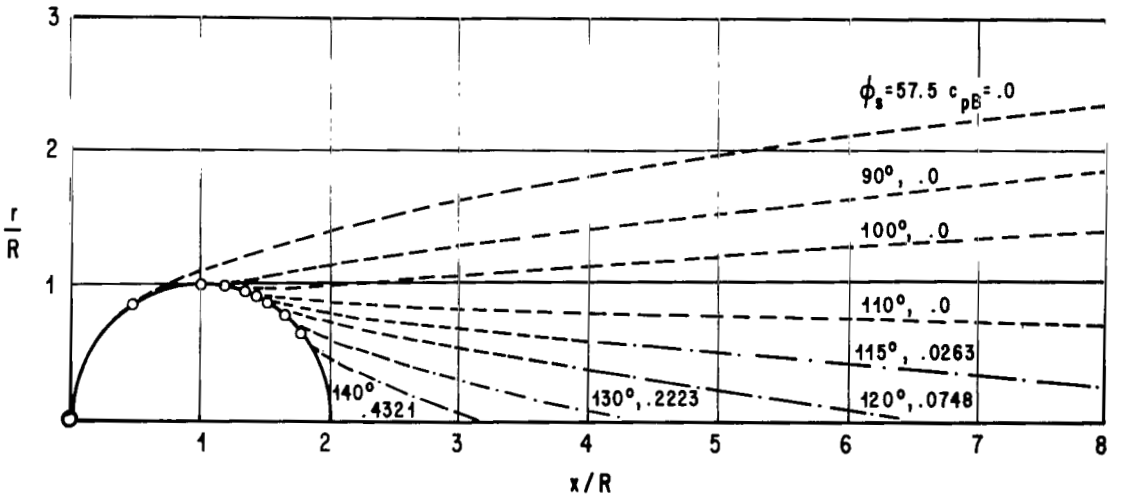

Figure 14a. The Free Streamline for the Rearward Separation from A Sphere

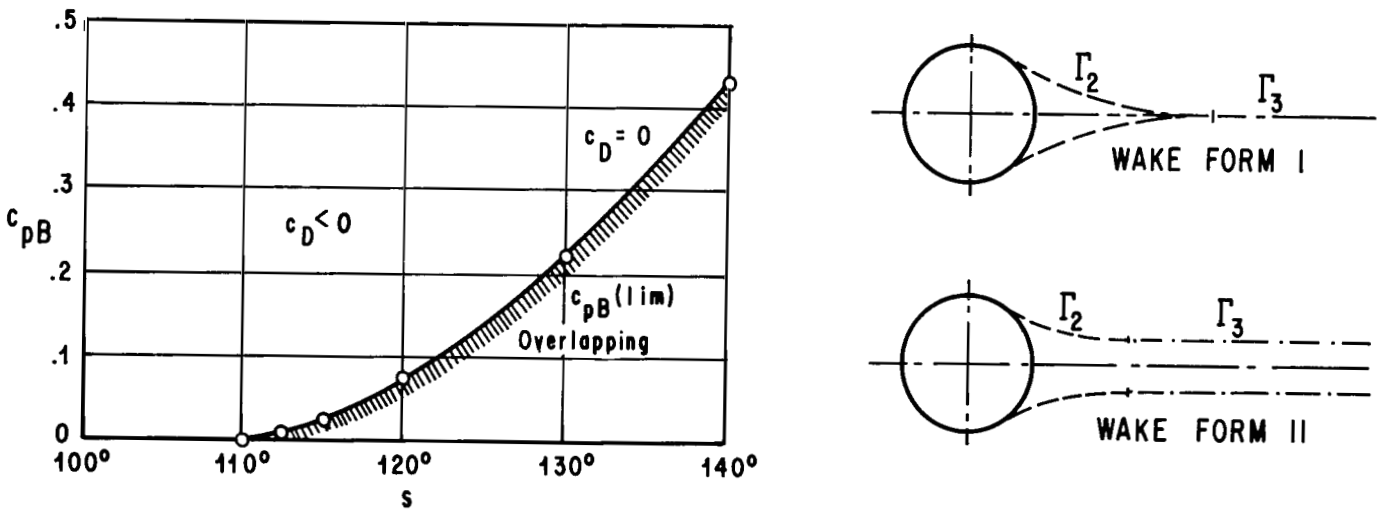

Figure 14b. The Region of the Possible (C_{PB},∅) Combination

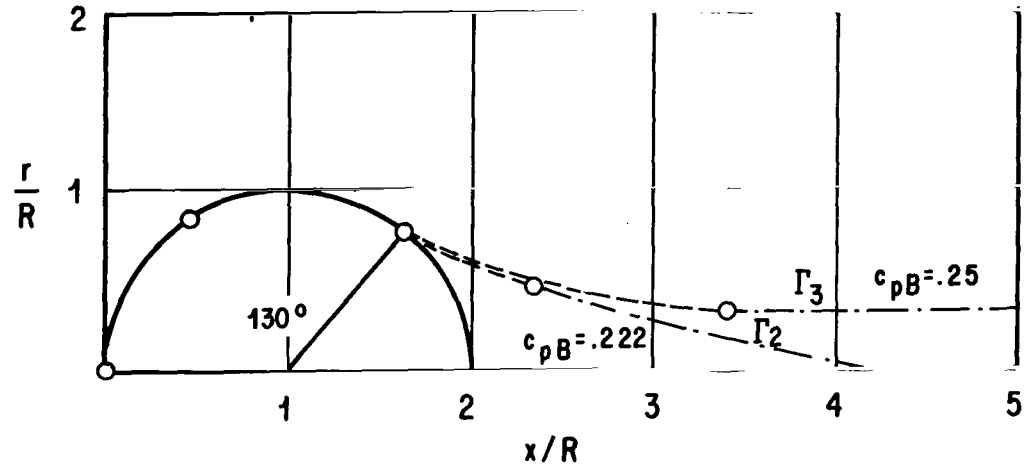

Figure 15a. The Possible Wake Forms for the Separation Angle ϕ_s = 130 Degrees

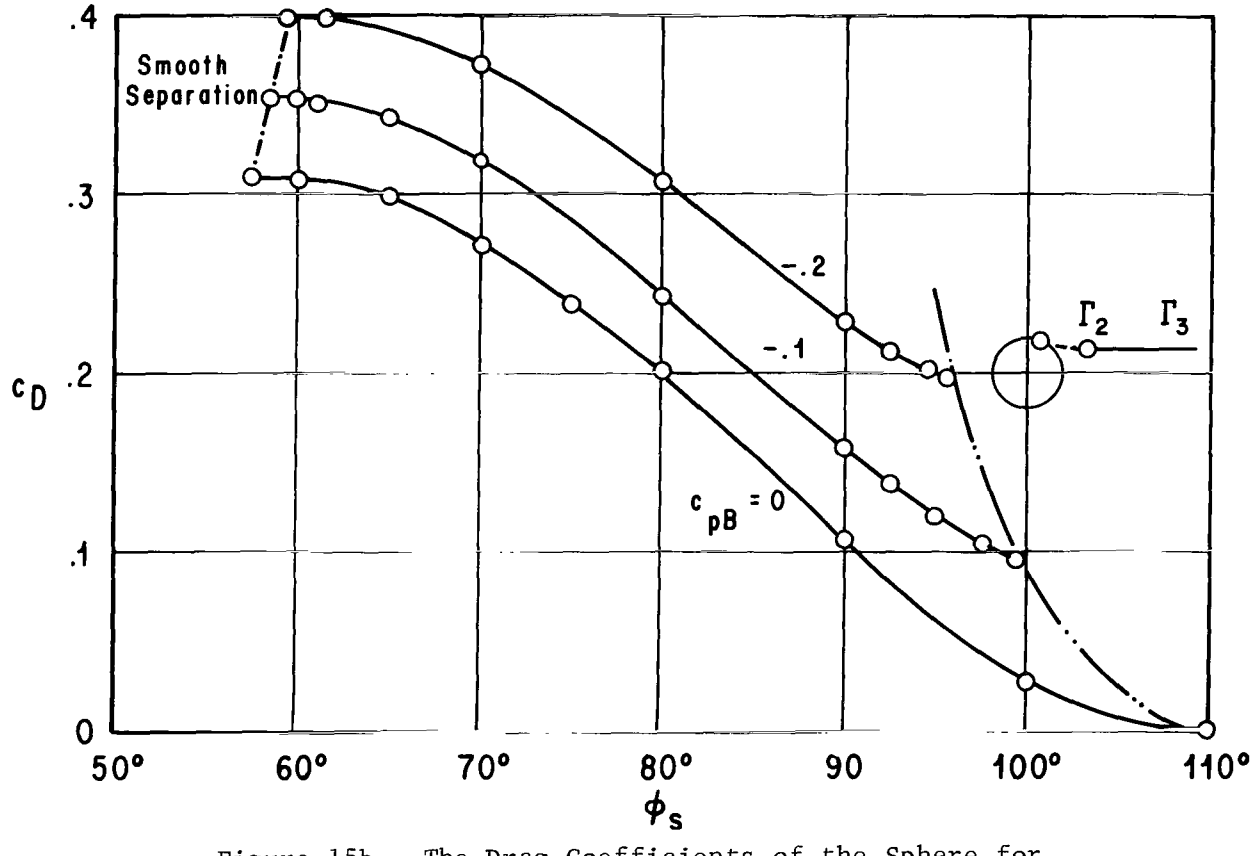

Figure 15b. The Drag Coefficients of the Sphere for Different Separation Angles ϕ_s in the Region ϕ_s(smooth)-$\overline{\phi_s}$

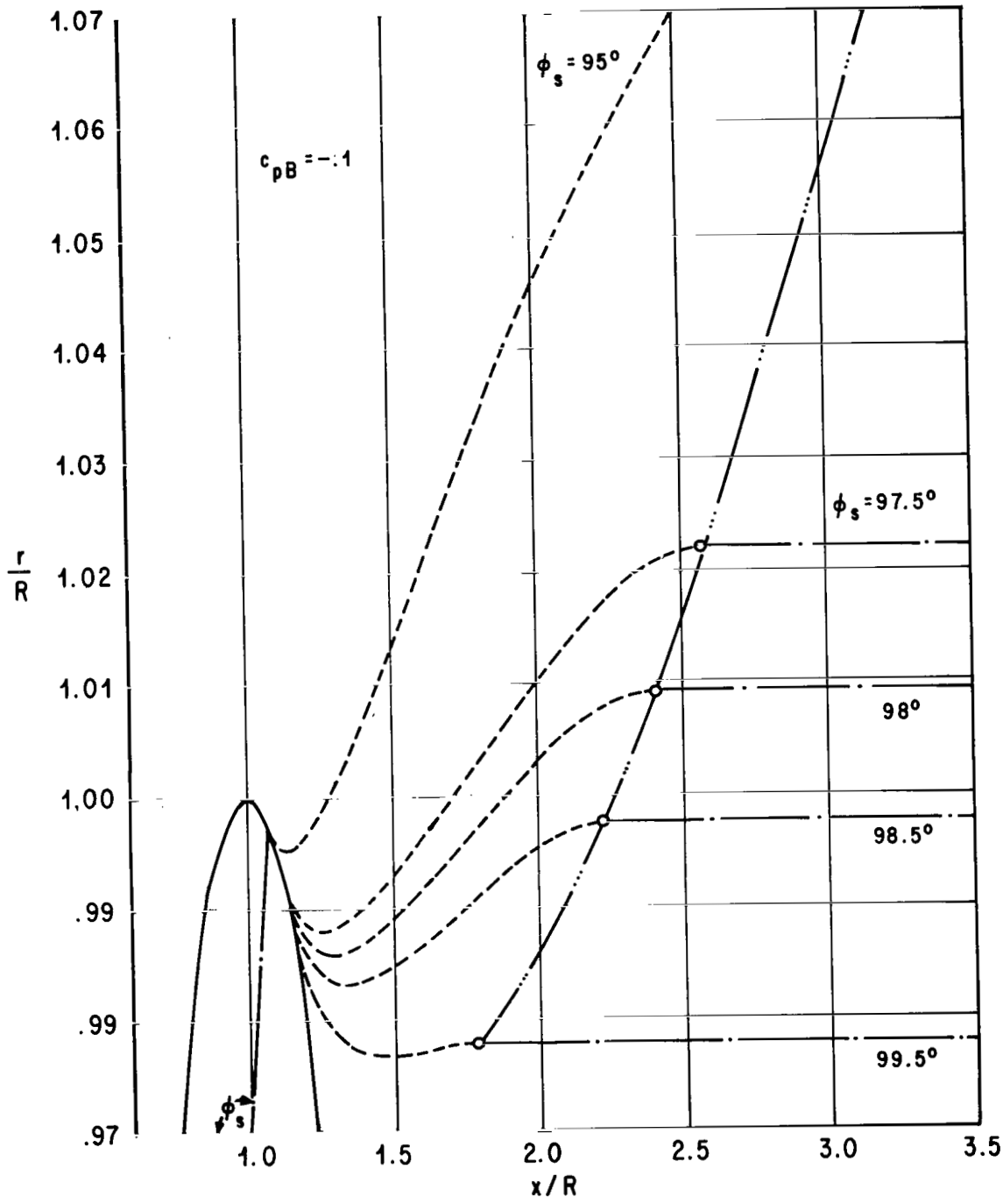

Figure 16. The Possible Wake Forms for Separation Angles ϕ_s Within the Region $\phi_s(\pi/2)$, $\overline{\phi_s}$ for the Pressure Coefficient $C_{PB} = -.1$

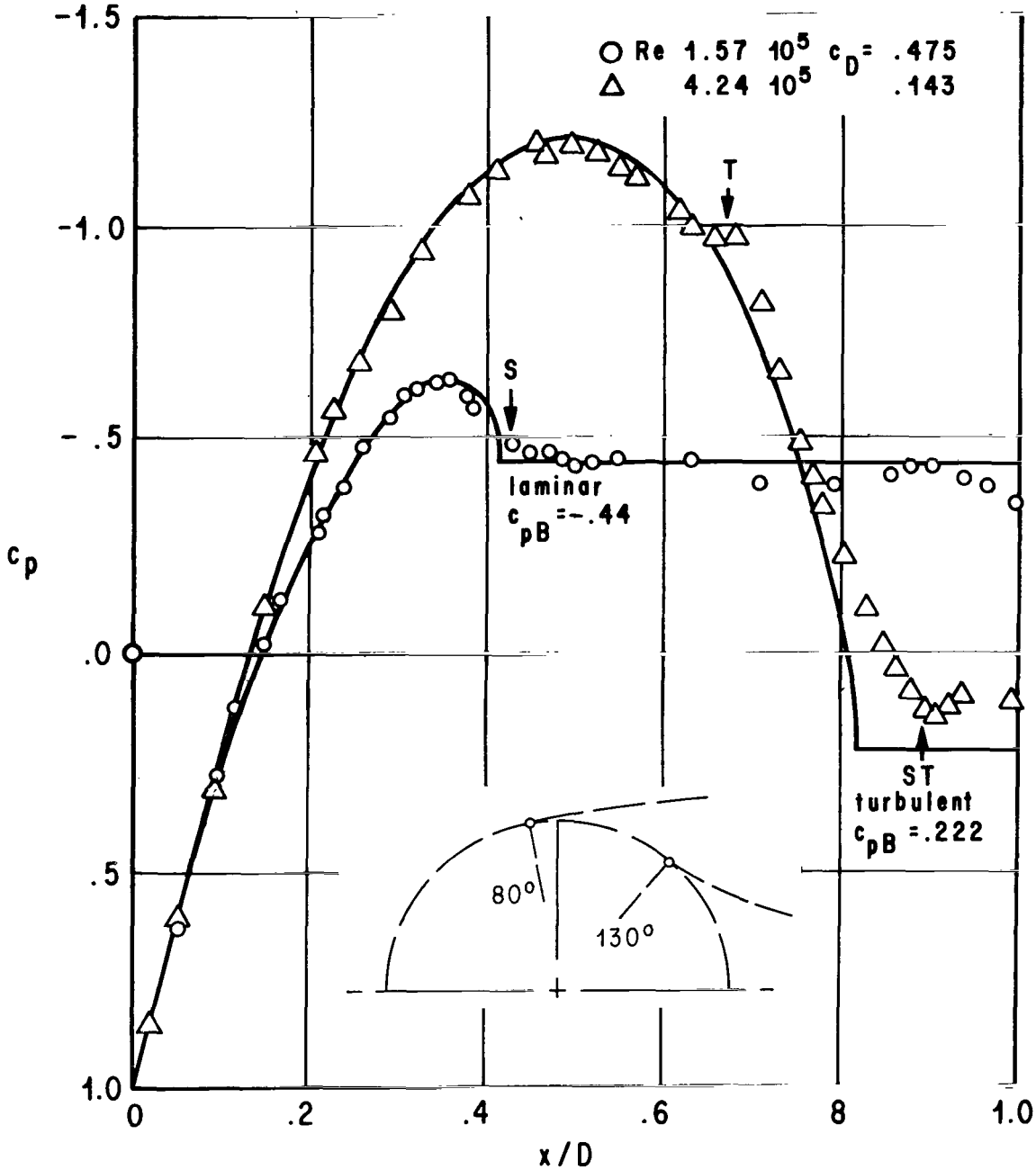

Figure 17. The Pressure Distribution Around A Sphere for Laminar and Turbulent Flow Separation (Dissipation Model) [27]

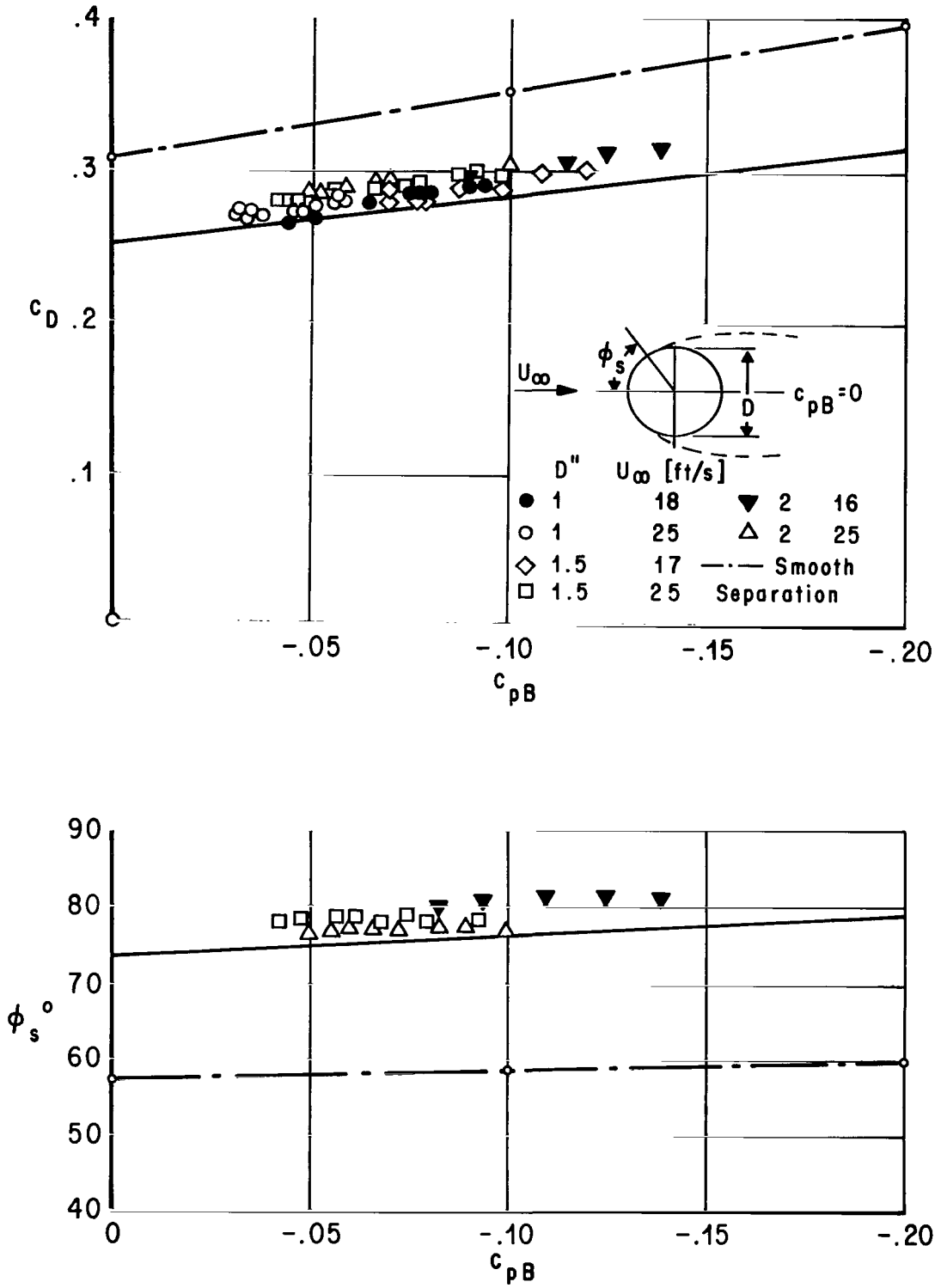

Figure 18. The Drag Coefficient and the Separation Angle of A Sphere as A Function of the Base Pressure [24]

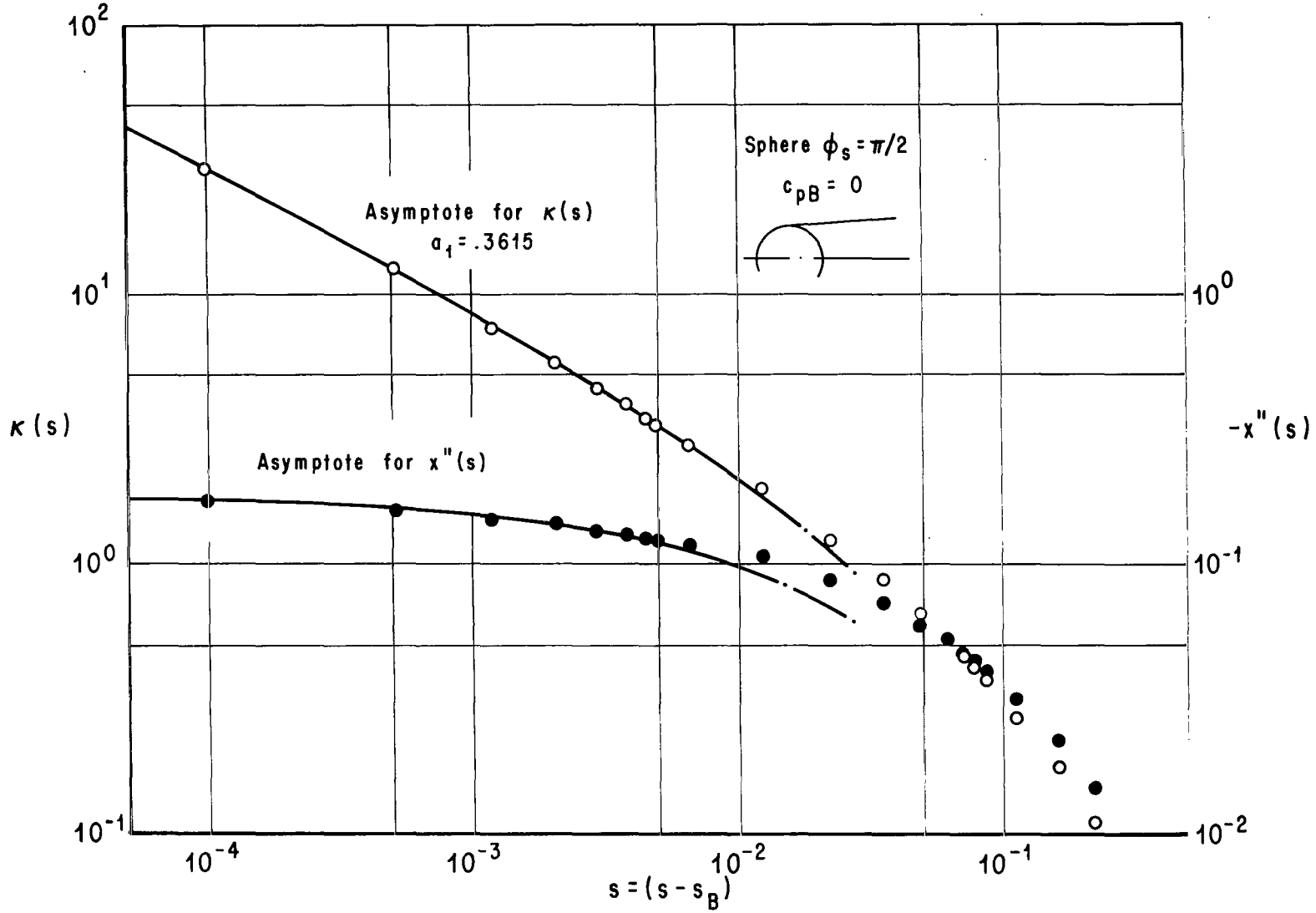

Figure 19. The Asymptotic Representation of the Curvature and the Second Derivative of the X-Coordinate of the Free Streamline in the Immediate Vicinity of the Separation Point of A Sphere $\phi_s = \pi/2$

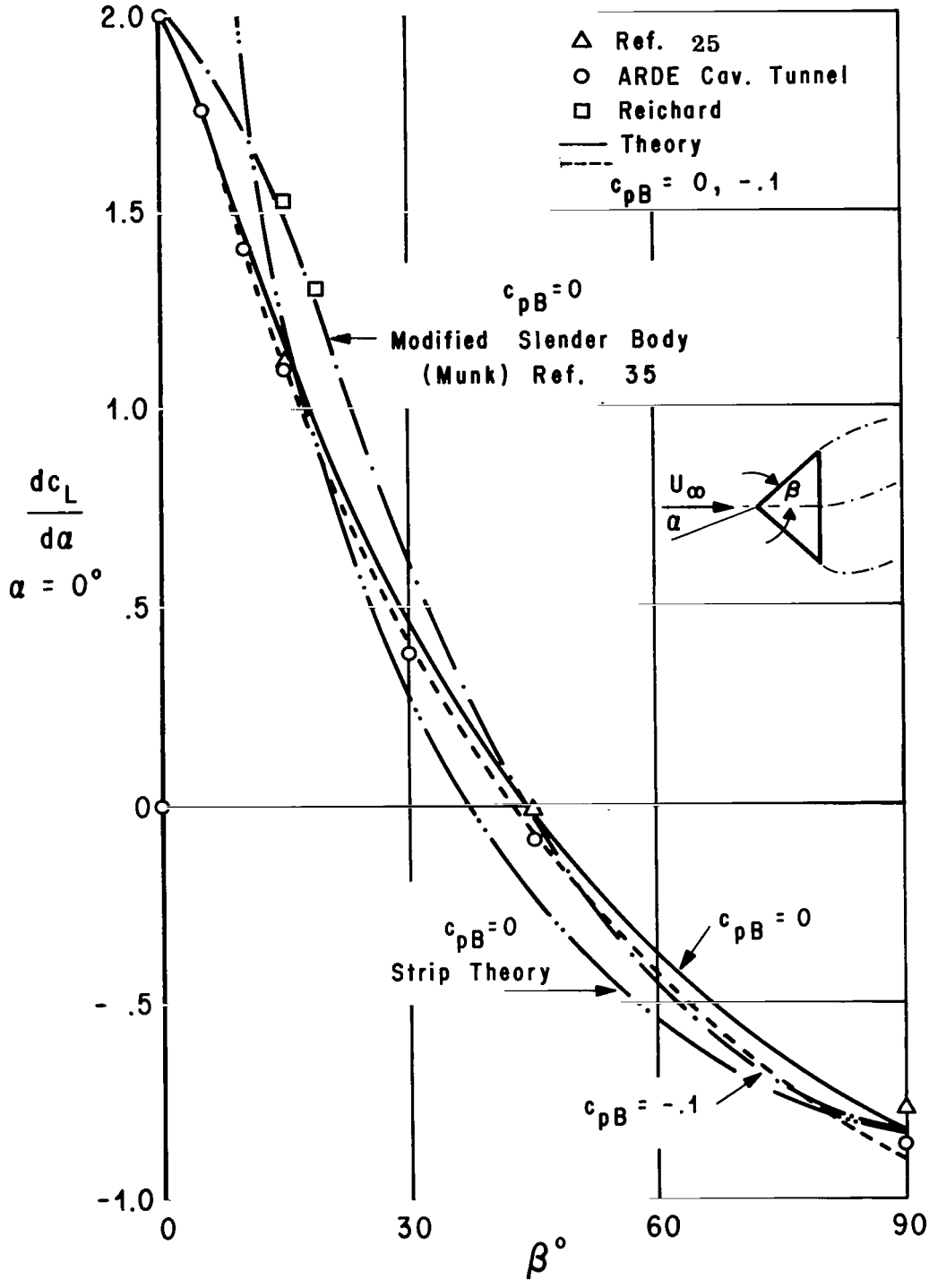

Figure 20. The Lift Gradient of Cones as A Function of the Half-Angle β and the Base Pressure C_{PB}

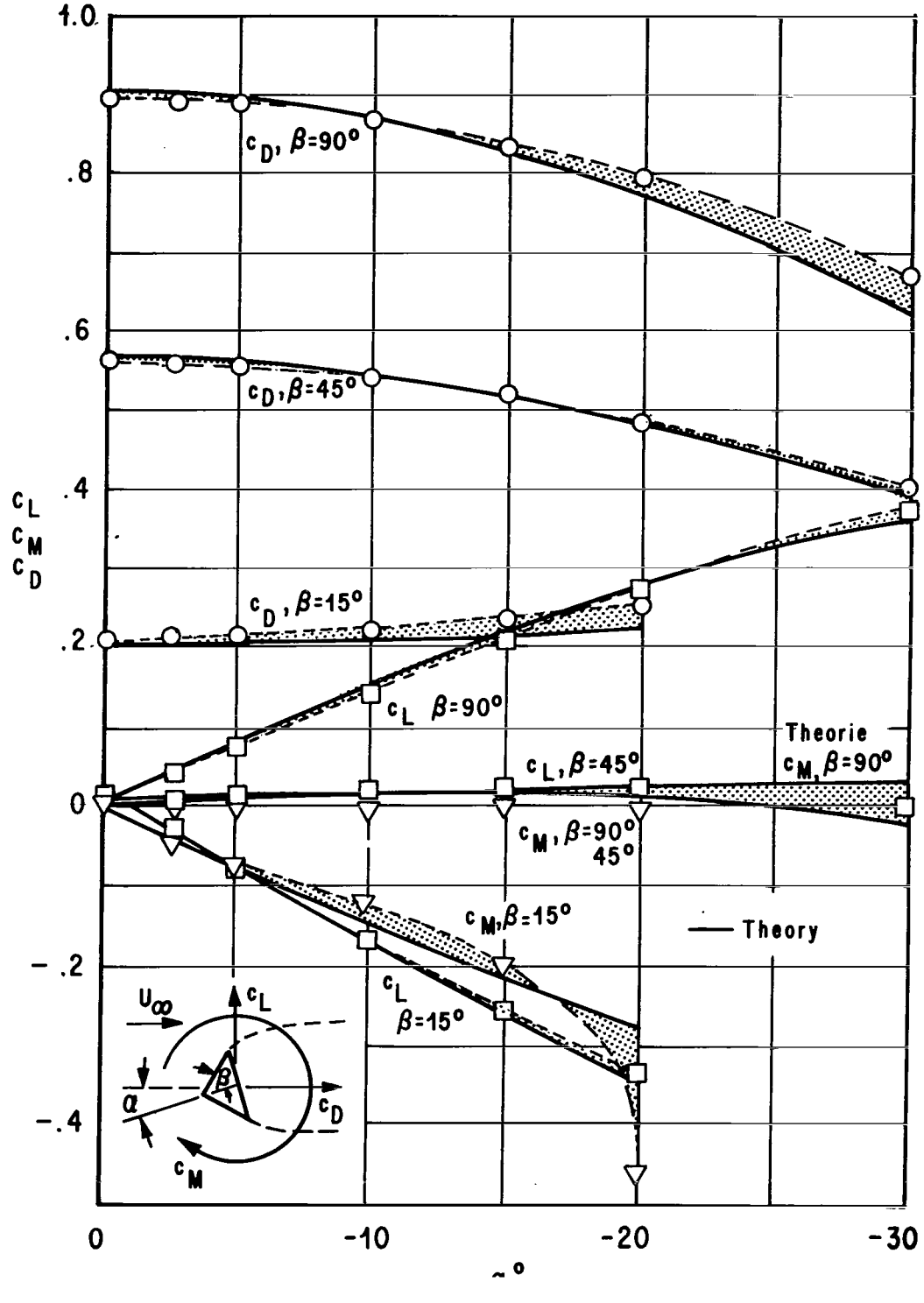

Figure 21. Drag, Lift and Moment Coefficients for Different Cones As A Function of the Angle of Attack for C_{PB} = -.1 [25]

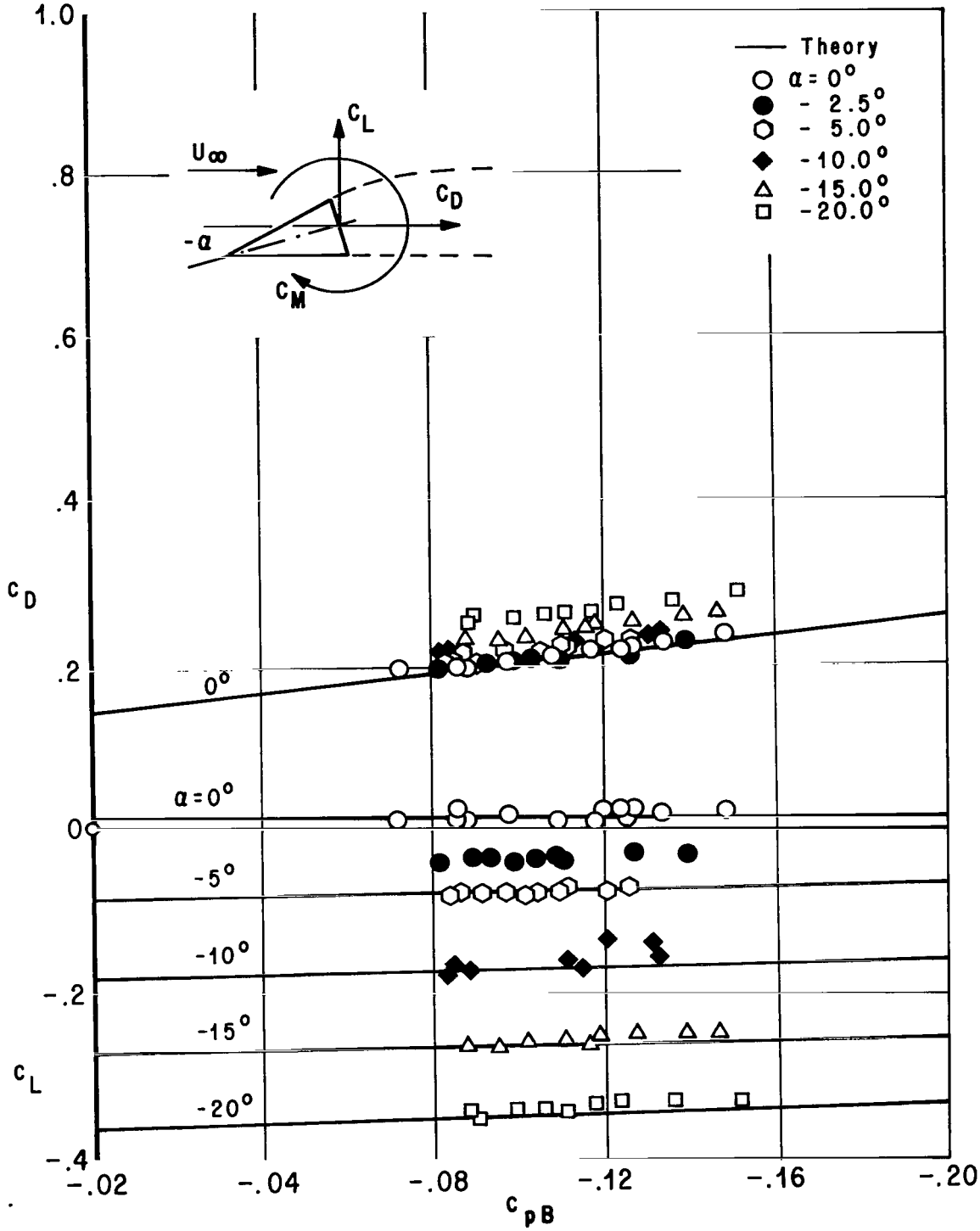

Figure 22. Lift and Drag Coefficients of a 15-Degree Cone for Different Base Pressures with α as Parameter [25]

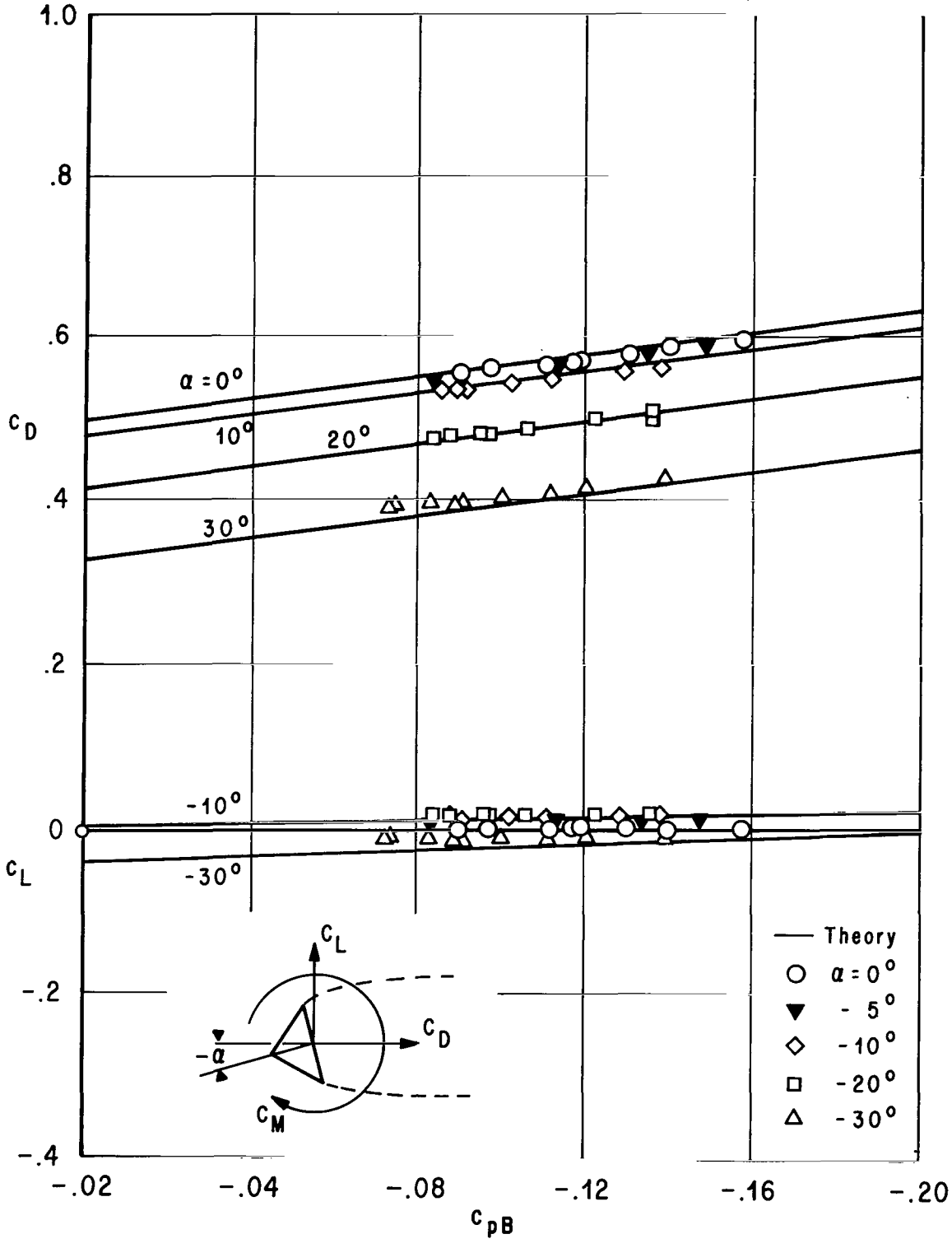

Figure 23. Lift and Drag Coefficients of a 45-Degree Cone for Different Base Pressures with α as Parameter [25]

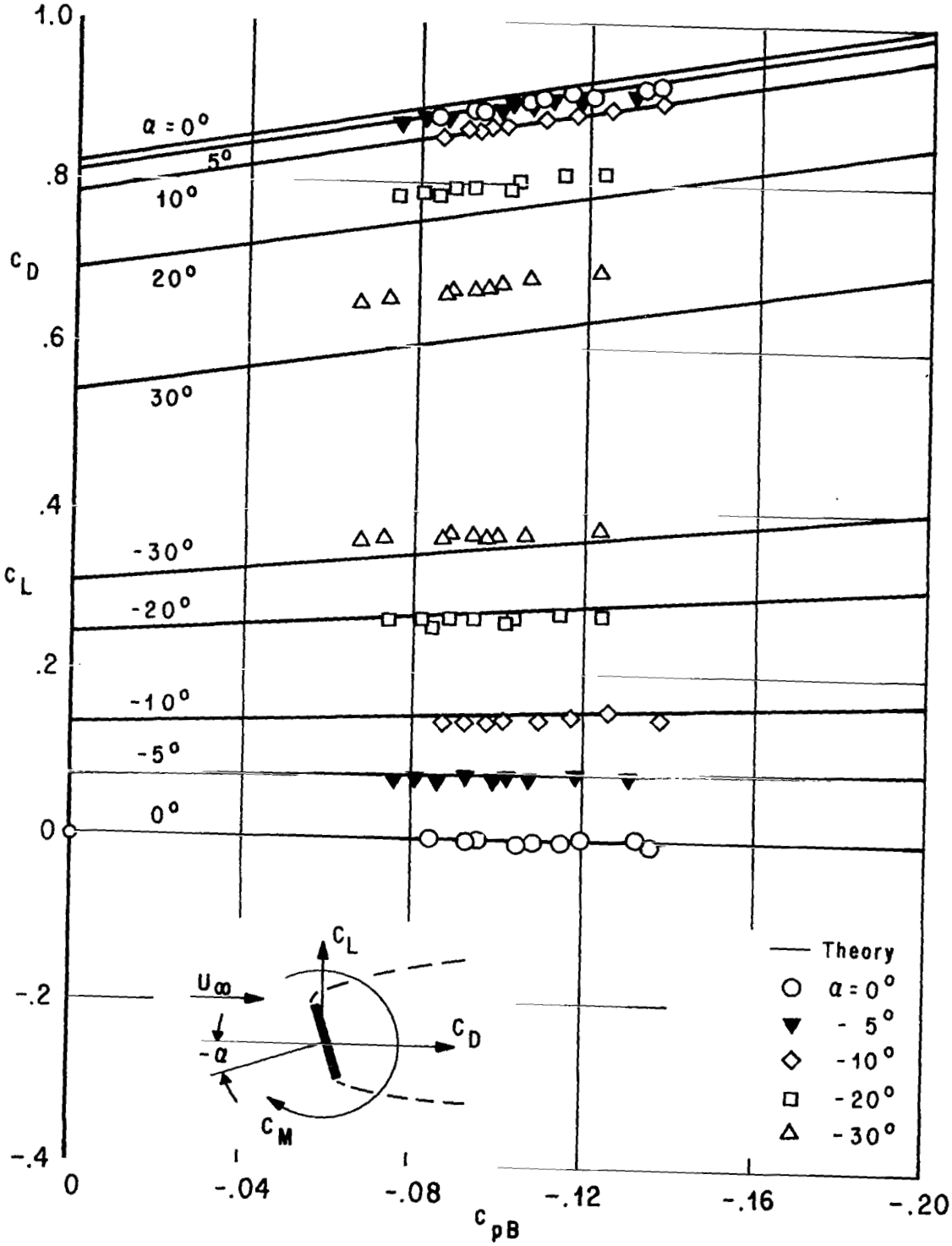

Figure 24. Lift and Drag Coefficients of a Disk for Different Base Pressures with α as Parameter [25]

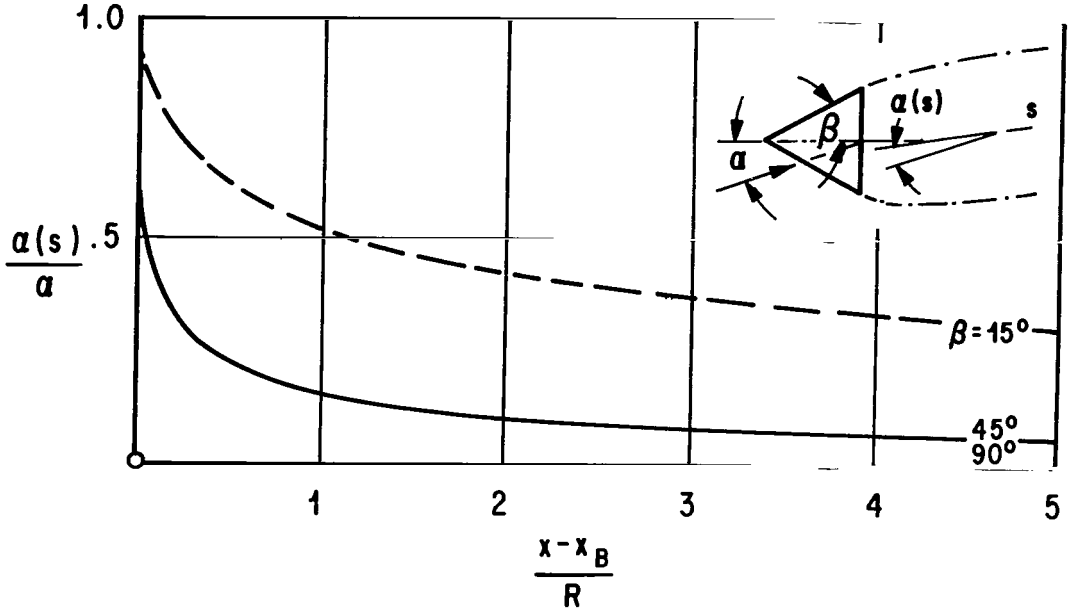

(a) The Dimensionless Angle of Attack Distribution Along Cone Wakes

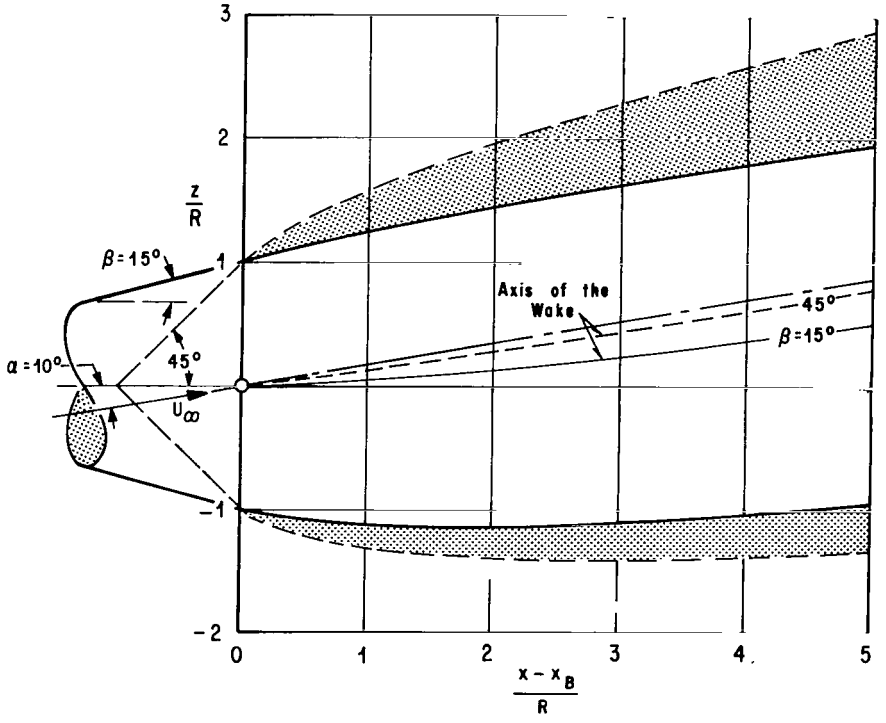

(b) The Shifted Wake

Figure 25. The Theoretical Angle of Attack Distribution and the Shifted Wake for Two Cones

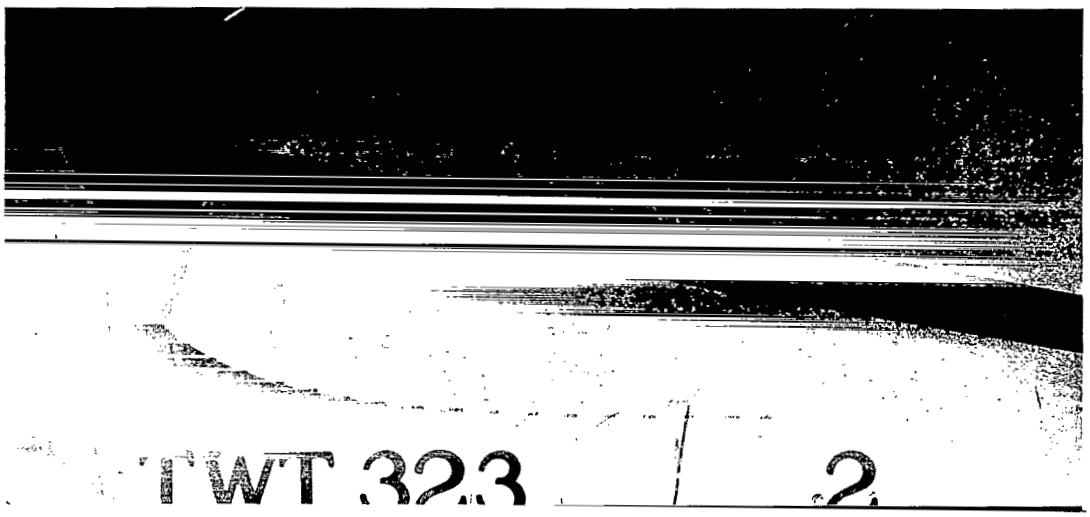

(a) The Inclined Cone, α = 10 Degrees

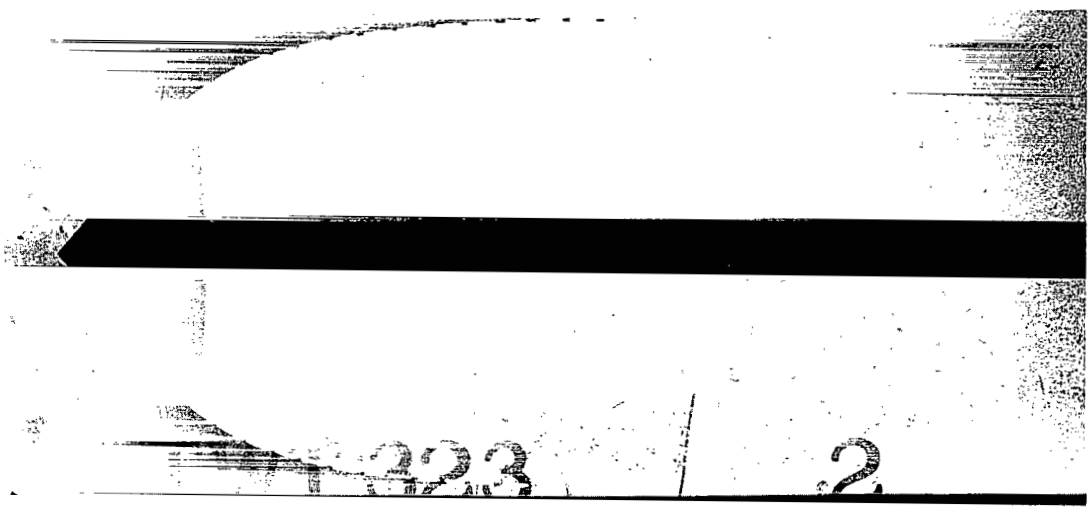

(b) The Axisymmetric Flow About A Cone

Figure 26. The Shadowgraph of the Flow About A 50-Degree Cone With A Superimposed Streamline for C_{PB} = -.4 (Dissipation Model)

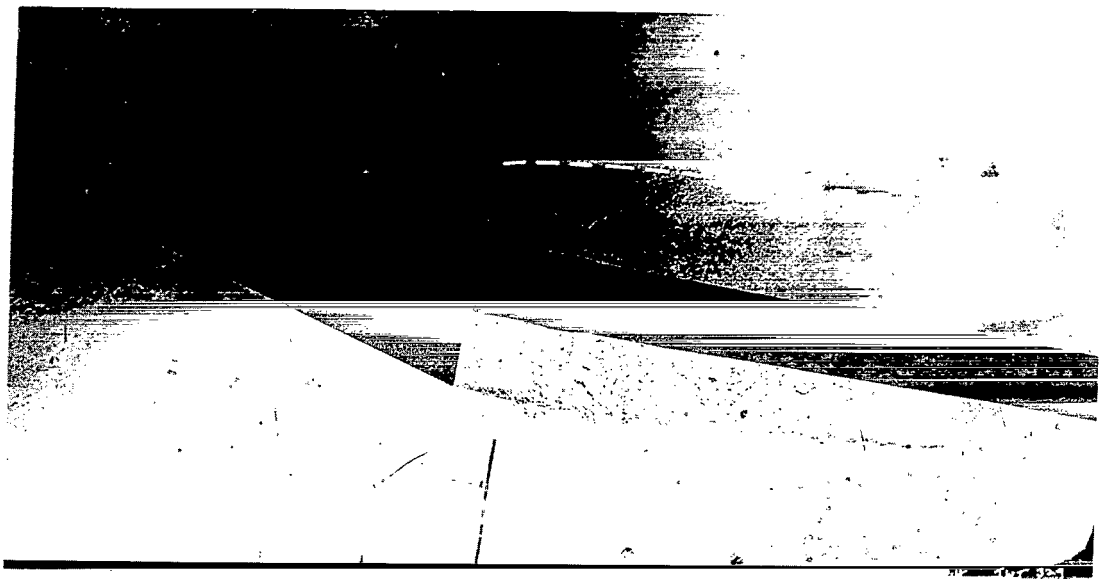

(a) The Inclined Cone, α = 10 Degrees

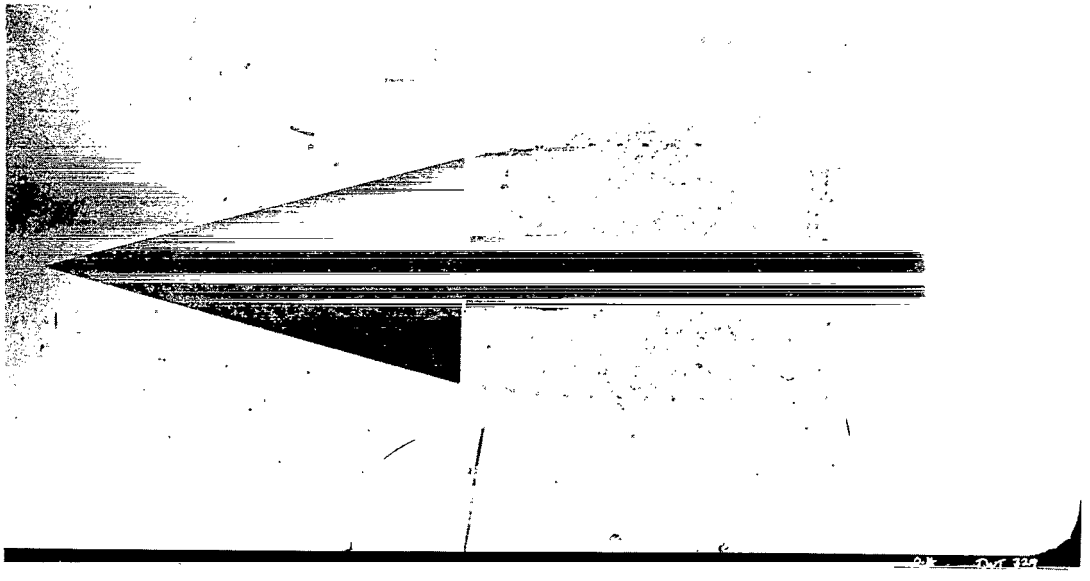

(b) The Axisymmetric Flow About the Cone

Figure 27. The Shadowgraph of the Flow About A 15-Degree Cone with A Superimposed Streamline for C_{PB} = -.32

REFERENCES

1. Rankine, W. J. M., Philosophical Trans., 1871.

2. Taylor, D. W., Transactions of the Inst. of Naval Archit., 35 (1894).

3. Fuhrmann, G., Jahrb. der Motorluftschiff-Studienges., (1911-1912).

4. Weinstein, A., Quart. of Appl. Math., 5 No. 4 (1948).

5. Van Tuyl, A., Quart. of Appl. Math., 7 No. 4 (1950).

6. Sadowsky, M. A. and E. Sternberg, Quart. of Appl. Math., 8 No. 2 (1950).

7. Karman, Th. v., NACA TM 574 (1930).

8. Lotz, I., NACA TM 675 or Ing. Arch. 2, p. 507 (1931).

9. Trefftz, E., Z. Math. Phys., 64, pp. 34-61 (1916).

10. Riegels, F., Mitteil. Max-Plank-Inst. f. Strömungsf., No. 5 (1952).

11. Bauer, W., Ann. der Physik, 80, pp. 232-244 (1926).

12. Armstrong, A. and J. Dunham, Armament Res. Est. Rep. No. 12/53 (1953).

13. Garabedian, P. R., Pacif. J. Math., 6, pp. 611-684 (1956) and Bull. Amer. Math. Soc., 62, pp. 219-243 (1956).

14. Kellog, O. D., Foundation of Potential Theory, Dover.

15. Zurmühl, R., Matrizen, 3, Aufl. Springer, Berlin (1961).

16. Gilbarg, D., Jets and Cavities, Handbuch der Physik, Vol. IX, pp. 311-445, Springer Berlin (1960).

17. Levinson, N., Ann. of Math., 47, pp. 704-730 (1946).

18. Zurmühl, R., Praktische Mathematik, 2, Aufl. Springer Berlin (1957).

19. Abramovitz, M., Handbook of Mathematical Functions: NBS, Appl. Math. Series, 55, M. Abramovitz, editor. Stegun (1964).

20. Rouse, H. and J. S. McNown, Studies in Engineering, State University of Iowa, Bullet. 32 (1946).

21. Carmody, T., Journal of Basic Engin., pp. 869-882, December 1964.

22. Eisenberg, P. and H. L. Pond, Navy Dep. TMB Rep. No. 668 (1948).

23. Schlichting, H., Boundary Layer Theory, Fourth Edition, McGraw-Hill, New York, 1960.

24. Hsu, E. Y. and B. Perry, Cal. Inst. of Tech., Hydrodyn. Lab., Rep. No. E-24.9 (1954).

25. Kiceniuk, T., Cal. Inst. of Tech., Hydrodyn. Lab., Rep. No. E-12.17 (1954).

26. Cox, R. N. and Maccoll, J. W., Proceedings of Symposium on Naval Hydrodyn., September 1956, F. S. Sherman, editor.

27. Fage, P., ARC rep. and memorand. No. 1766 (1937).

Additional Literature

Helmholtz., H., Monatsber. Akad. Wiss., Berlin, pp. 215-228 (1868). Wissenschaftl. Abh. 1, 154.

Kirchhoff, C., Journal reine angew. Mathem. 70, pp. 289-298 (1869). Ges. Abh. 416.

Birkhoff, G. and E. H. Zarantonello, "Jets, Wakes, Cavities," Academic Press, Inc., New York (1957).

Eppler, R., J. rat. Mech. and Analysis, 3, pp. 591-644 (1954).

Joukowsky, N., Coll. Works 2, No. 3, Rec., Math 25 (1890).

Roshko, A., NACA TN 3168 (1954).

Tulin, M. P., Journ. of Ship Res., pp. 16-37, January 1964.

Riabouchinsky, D. M., Recherches d'Hydrodynamique, Paris (1922).

Wu, T. Y., Journ. of Fluid Mech., 13, No. 2, pp. 161-181 (1962).

Reichard, H., Min. Aircraft Prod. Rep. and Transl. No. 766 (1946).

Fisher, J., Underwater Ballistics Res., Counc. Rep. No. 34 (1945).

APPENDIX A

THE EVALUATION OF THE ELLIPTIC INTEGRALS

In the evaluation of the surface integrals, we often encounter the integral expressions

$$F_n(k^2) = (-1)^n \int_0^{\pi/2} \frac{\cos\ (2n\varphi)}{[1-k^2\sin\ \varphi]^{1/2}}\, d\varphi, \tag{A.1}$$

$$G_n(k^2) = (-1)^n \int_0^{\pi/2} \frac{\cos\ (2n\varphi)}{[1-k^2\sin\ \varphi]^{3/2}}\, d\varphi. \tag{A.2}$$

For the nominator we choose the expansion

$$\cos\ (2n\varphi) = \cos^{2n}\varphi - \binom{2n}{2} \sin^2\varphi\ \cos^{2(n-1)}\varphi + \binom{2n}{4} \sin^4\varphi\ \cos^{2(n-2)}\varphi\ \ldots, \tag{A.3}$$

which, after integration, yields for the expression (A.1) the terms

$$F_o(k^2) = K(k^2) - G_o(k^2) - \frac{k^2}{2}\,[G_1(k^2) + G_o(k^2)] \tag{A.4}$$

and

$$F_1(k^2) = \left(\frac{2}{k^2} - 1\right) K(k^2) - \frac{2}{k^2}\, E(k^2) = -\, G_1(k^2) + \frac{k^2}{2}\,[G_1(k^2) + G_o(k^2)].$$

For the elliptic integral (A.2), we obtain for n = 0, 1, and 2, finally:

$$G_o(k^2) = E(k^2)/k'^2.$$

$$G_1(k^2) = \frac{1}{k^2}\left[\frac{1+k'^2}{k'^2}\, E(k^2) - 2K(k^2)\right]. \tag{A.5}$$

$$G_2(k^2) = \frac{1}{k^4}\left[\left\{1+k'^2+12+\frac{1+k'^2}{k'^2}\right\} E(k^2) - \left\{2k'^2+6(1+k'^2)+2\right\} K(k^2)\right]$$

where $k'^2 = 1 - k^2$.

APPENDIX B

The Asymptotic Development of the Integrals

In the vicinity of $s \to \sigma$, the modulus k^2 approaches unity, and the elliptic integrals have for $k'^2 \leq .5$ the series expansion

$$K(k^2) = -\frac{k'^2}{4} - \frac{63}{384}k'^4 - \frac{925}{7680}k'^6 - \ldots + \ln(4/k')\left[1 + \frac{k'^2}{4} + \frac{9}{64}k'^4 + \frac{25}{256}k'^6 + \ldots\right] \tag{B.1}$$

$$E(k^2) = 1 - \frac{k'^2}{4} - \frac{39}{192}k'^4 - \frac{90}{640}k'^6 - \ldots + \ln(4/k')\left[\frac{k'^2}{2} + \frac{3}{16}k'^2 + \frac{15}{128}k'^6 + \ldots\right],$$

where $k'^2 = 1 - k^2$.

We are able now to determine the first terms of $G_n(k^2)$ with this series expansion:

$$G_o(k^2) = \frac{1}{k'^2}\left[1 - \frac{1}{4}k'^2 - \frac{13}{64}k'^4 - \frac{81}{576}k'^6 \ldots + \ln(4/k')\left(\frac{1}{2}k'^2 + \frac{3}{16}k'^4 + \frac{15}{128}k'^6 + \ldots\right)\right.$$

$$G_1(k^2) = \frac{1}{k'^2}\left[1 + \frac{7}{4}k'^2 + \frac{115}{64}k'^4 + \frac{1026}{576}k'^6 + \ldots - \ln(4/k^2)\left(\frac{3}{2}k'^2 + \frac{21}{16}k'^4 + \frac{165}{128}k'^6 + \ldots\right)\right. \tag{B.2}$$

(equation (B.2) continued on next page)

$$G_2(k^2) = \frac{1}{k'^2}\left[1 + \frac{63}{4}k'^2 + \frac{1907}{64}k'^4 + \frac{25299}{576}k'^6 + \ldots\right.$$

$$\left. - \ln(4/k')\left(\frac{15}{2}k'^2 + \frac{285}{16}k'^4 + \frac{3585}{128}k'^6 + \ldots\right)\right.$$

In general, one can represent the elliptic integrals for $k'^2 \leqq .5$ by the summation formulas

$$K(k^2) = \ln(4/k')\sum_{\nu=1}^{\infty}\left(\frac{k'^{2\nu}}{\nu!\,\nu!}\prod_{\mu=0}^{(\nu-1)}(\tfrac{1}{2}+\mu)^2\right) - \sum_{\nu=1}^{\infty}\left(\frac{2}{1\cdot 2} + \frac{2}{3\cdot 4}\right.$$

$$\left. + \ldots \frac{2}{(2\nu-1)2\nu}\right)\prod_{\mu=0}^{(\nu-1)}(\tfrac{1}{2}+\mu)^2\,\frac{k'^{2\nu}}{\nu!\,\nu!}$$

and (B.3)

$$E(k^2) = \ln(4/k')\sum_{\nu=1}^{\infty}\left(\frac{k'^{2\nu}}{(\nu-1)!\,\nu!}\prod_{\mu=0}^{(\nu-1)}(-\tfrac{1}{2}+\mu)(\tfrac{1}{2}+\mu)\right) + 1 - \frac{1}{4}k'^2$$

$$- \sum_{\nu=2}^{\infty}\left(\frac{2}{1\cdot 2} + \frac{2}{3\cdot 4} + \ldots + \frac{2}{(2\nu-3)(2\nu-1)} + \frac{1}{(2\nu-1)2\nu}\right)$$

$$\cdot \frac{k'^2}{(\nu-1)!\,\nu!}\prod_{\mu=0}^{(\nu-1)}(-\tfrac{1}{2}+\mu)(\tfrac{1}{2}+\mu).$$

The previous equations are not suited for the region of very small k^2. The summation formulas for determining $K(k^2)$ and $E(k^2)$ are therefore different:

$$K(k^2) = \frac{\pi}{2}\left[1 + \sum_{\nu=1}^{\infty} \frac{k^{2\nu}}{\nu!\,\nu!} \prod_{\mu=0}^{(\nu-1)} (\tfrac{1}{2} + \mu)^2\right] = \frac{\pi}{2}\left[1 + C_1k^2 + C_2k^4 + \ldots\right]$$

and (B.4)

$$E(k^2) = \frac{\pi}{2}\left[1 + \sum_{\nu=1}^{\infty} \frac{k^{2\nu}}{\nu!\,\nu!} \prod_{\mu=0}^{(\nu-1)} (-\tfrac{1}{2} + \mu)(\tfrac{1}{2} + \mu)\right] = \frac{\pi}{2}\left[1+d_1k^2+d_2k^4+ \ldots\right] .$$

After the series have been determined, we insert the coefficients of $K(k^2)$ and $E(k^2)$ into the equation (A.5) and obtain for the region $k^2 \leqq .5$

$$k'^2(G_1(k^2) = \frac{\pi}{2}\left[(2[d_2-C_2] - [d_1-2C_1])k^2 + (2[d_3-C_3]-[d_2-2C_2])k^4 + \ldots\right].$$

(B.5)

$$k'^2G_2(k^2) = \frac{\pi}{2}\left[(16[d_4-C_4]-8[2d_3-3C_3] + d_2-8C_2)k^4 + (16[d_5-C_5]\right.$$

$$\left.-8[2d_4-3C_4] + d_3-8C_3)k^6 + \ldots\right] .$$

The Asymptotic Development of the Velocities for Small Cone Angles

For very small cone angles ($\beta \leqq 15°$), the series approximations derived in chapter IV.2, are not very well suited for the determination of the velocity components. For instance, the logarithmic terms of the velocity components become very large for small r(s); whereas, $f(s,\sigma)$ disappears rather rapidly with increasing σ. A special series approximation was therefore advisable for small cone angles.

We set again $\epsilon = \sigma - s$. For a cone, the following relations hold: $r = r's$, $\rho = r'\sigma$, and $x = x's$, $\xi = x'\sigma$.

The elliptic modulus k'^2 becomes now

$$k'^2 = \frac{(x-\xi)^2 + (r-\rho)^2}{(x-\xi)^2 + (r+\rho)^2} = \frac{\epsilon^2}{\epsilon^2+4r'^2 s(s+\epsilon)} , \qquad (B.6)$$

which is inserted into (B.1) and with (A.5), we obtain finally

$$G_o(k^2) \approx \frac{\epsilon^2+4r's(s+\epsilon)}{\epsilon^2} - \frac{1}{4} + \frac{1}{2} \ln \frac{8r's}{|\epsilon|} .$$

$$G_1(k^2) \approx \frac{\epsilon^2+4r's(s+\epsilon)}{\epsilon^2} + \frac{7}{4} - \frac{3}{2} \ln \frac{8r's}{|\epsilon|} .$$

$$G_2(k^2) \approx \frac{\epsilon^2+4r's(s+\epsilon)}{\epsilon^2} + \frac{63}{4} - \frac{15}{2} \ln \frac{8r's}{|\epsilon|} .$$

For simplicity, we retain the argument of the logarithmic terms.

We now introduce these expressions into the integrand of the u_n-velocity component and obtain the series

$$f(s,\sigma)_{u_n} = -q_n(s) \left[\frac{2r'x'}{\chi^{1/2}} + \frac{2r'x's}{\epsilon\chi^{1/2}} \right] + q_n'(s) \frac{2r'x's}{\chi^{1/2}} , \qquad (B.7)$$

where $\chi = \epsilon^2 + 4r'^2 s(s+\epsilon)$. In this expansion, all terms which were proportional to ϵ were dropped. The integral with the substitution

$$\chi_E = (s_E - s)^2 + 4r'^2 s s_E$$

finally becomes

$$\frac{1}{2\pi} \int_{-s}^{s_E-s} f(s,\sigma)_u \, d\sigma = - \frac{x'}{2\pi} \left\{ q_n(s) \left[2r' \ln \left| \frac{s_E - s + 2r'^2 s + \chi_E^{1/2}}{2r'^2 s} \right| \right. \right.$$

(equation (B.8) continued on next page)

$$+ \ln \left|\frac{r''(s_E+s)-\chi_E^{1/2}}{(s_E-s)(1-r')}\right| \Bigg] + q_n'(s)\ 2r's \ln \left|\frac{s_E-s+2r'^2 s+\chi_E^{1/2}}{2r'^2 s}\right| \Bigg] \Bigg\} . \qquad (B.8)$$

Next, we develop the v_n-component into a series

$$f(s,\sigma)_v = -2r'^2 \left\{ q_n(s) \left[\frac{s}{\epsilon \sqrt{\chi}} + \frac{1}{\sqrt{\chi}} + \frac{2s^2}{[\chi]^{3/2}} \left(1+2n-\ln \frac{8r's}{|\epsilon|} \right) \right] + \frac{q_n'(s)s}{\sqrt{\chi}} \right\} . \qquad (B.9)$$

The integration of this expression yields

$$\frac{1}{2\pi} \int_{-s}^{s_E-s} f(s,\sigma)_v \, d\sigma = \frac{1}{2\pi} \Bigg[q_n(s) \Bigg\{ r' \ln \left| \frac{r'(s_E-s)-\sqrt{\chi_E}}{(s_E-s)(1-r')} \right|$$

$$+ 2r'^2 \ln \left| \frac{s_E-s+2r'^2 s+\sqrt{\chi_E}}{2r'^2 s} \right| + \frac{1}{x'^2} \left[\frac{s_E-s+2r'^2 s}{\sqrt{\chi_E}} \left(1 + 2n-\ln \frac{8r's}{|s_E-s|} \right) \right.$$

$$\left. - (r'^2-x'^2) \left(1+2n-\ln \frac{8r's}{|s|} \right) \right] - \frac{1}{x'^2} \ln \left| \frac{s_E-s+2r'^2 s-\sqrt{\chi_E}}{2r'^2 s} \right|$$

$$- \frac{r'}{x'^2} \ln \left| \frac{r'(s_E+s)-\sqrt{\chi_E}}{(s_E-s)(1-r')} \right| \Bigg\} + q_n'(s)\ 2r'^2 s \ln \left| \frac{s_E-s+2r'^2 s+\sqrt{\chi_E}}{2r's} \right| \Bigg] . \qquad (B.10)$$

For the circumferential velocity component w_n, we obtain

$$f(s,\sigma)_w = n \left[q_n(s) \left\{ \frac{8r'^2 s^2}{[\chi]^{3/2}} \left(\ln \frac{8r's}{|\epsilon|} - 2 \right) \right\} \right] , \qquad (B.11)$$

and integrating this term, we can write

$$\frac{1}{2\pi}\int_{-s}^{s_E-s} f(s,\sigma)_w \, d\sigma = n\,\frac{q_n(s)}{2\pi}\left[\frac{2}{x'^2}\left\{\frac{s_E-s+2r'^2 s}{\sqrt{\chi_E}}\left(\ln\frac{8r's}{|s_E-s|}-2\right)\right.\right.$$

$$-(r'^2-x'^2)\left(\ln\frac{8r's}{|s|}-2\right)+\ln\left|\frac{s_E-s+2r's+\sqrt{\chi_E}}{2r'^2 s}\right|$$

$$\left.\left.+\,r'\ln\left|\frac{r'(s_E+s)-\sqrt{\chi_E}}{(s_E-s)(1-r')}\right|\right\}\right]. \qquad \text{(B.12)}$$

With the aid of the preceding expansion for the perturbation velocities, we obtain the normal component $V_N(s)$ as

$$f(s,\sigma)_{V_N} = 4q_n(s)r'^2x'^2s^2\left[\frac{1}{(\chi)^{3/2}}\left(\ln\frac{8r's}{|\epsilon|}-(1+2n)\right)\right]. \qquad \text{(B.13)}$$

The integral is

$$\frac{1}{2\pi}\int_{-s}^{s_E-s} f(s,\sigma)_{V_N}\,d\sigma = \frac{q_n(s)}{2\pi x'}\left[\frac{s_E-s+2r'^2 s}{\sqrt{\chi_E}}\left(\ln\frac{8r's}{|s_E-s|}-(1+2n)\right)\right.$$

$$-(r'^2-x'^2)\left(\ln\frac{8r's}{|s|}-(1+2n)\right)+\ln\left|\frac{s_E-s+2r'^2 s+\sqrt{\chi_E}}{2r's}\right|$$

$$\left.+\,r'\ln\left|\frac{r'(s_E-s)-\sqrt{\chi_E}}{(s_E-s)(1-r')}\right|\right]. \qquad \text{(B.14)}$$

Similar expressions for the tangential velocity $V_T(s)$ are

$$f(s,\sigma)_{V_T} = -2r'^2\left\{q_n(s)\left[\frac{s}{\epsilon\sqrt{\chi}} + \frac{1}{\sqrt{\chi}} + \frac{2r'^2s^2}{\chi^{3/2}}\left(1+2n-\ln\frac{8r's}{|\epsilon|}\right)\right] + \frac{q'(s)s}{\sqrt{\chi}}\right\},$$

$$\frac{1}{2\pi}\int_{-s}^{s_E-s} f(s,\sigma)_{V_T}\,d\sigma = -\frac{1}{2\pi}\left[q_n(s)\left\{2r'\ln\left|\frac{s_E-s+2r'^2s+\sqrt{\chi_E}}{2r's}\right|\right.\right.$$

$$+ \ln\left|\frac{r'(s_E+s)-\sqrt{\chi_E}}{(s_E-s)(1-r')}\right| + \frac{r'}{x'^2}\left[\frac{s_E-s+2r'^2s}{\sqrt{\chi_E}}\left(1+2n-\ln\frac{8r's}{|s_E-s|}\right)\right.$$

$$\left.\left. - (r'^2-x'^2)\left(1+2n-\ln\frac{8r's}{|s|}\right)\right] - \frac{r'}{x'^2}\ln\left|\frac{s_E-s+2r'^2s+\sqrt{\chi_E}}{2r'^2s}\right|\right.$$

$$\left. - \frac{r'^2}{x'^2}\ln\left|\frac{r'(s_E-s)-\sqrt{\chi_E}}{(s_E-s)(1-r')}\right|\right\} + 2r'sq_n'(s)\ln\left|\frac{s_E-s+2r'^2s+\sqrt{\chi_E}}{2r'^2s}\right|\Bigg].$$

(B.15)

After a closer inspection of these terms, we notice that they are not suited for determining the velocities around a blunt cone (disk), since $r' \to 1$ and $x' \to 0$.

APPENDIX C
THE COORDINATE TRANSFORMATION OF THE VELOCITIES

For the tangential and normal velocity components on a streamline, we find the following relations:

$$V_T = (1+u_o)x' - v_o r' \tag{C.1}$$

and

$$V_N = -(1+u_o)r' + v_o x'. \tag{C.2}$$

Certain relationships exist between the derivatives of the streamline and its curvature:

$$\kappa = x'r'' - r'x'' = r''/x' = -x''/r' \tag{C.3}$$

and

$$x'x'' + r'r'' = 0. \tag{C.4}$$

If we differentiate the normal velocity with respect to the arc length of a line on which V_N does not disappear, we obtain

$$\frac{dV_N}{ds} = -\frac{du_o}{ds} r' - (1+u_o)r'' + x' \frac{dv_o}{ds} + v_o x''. \tag{C.5}$$

With (C.3) and (C.4) the relation

$$(1+u_o)r'' = (1+u_o)x'\kappa; \quad v_o x'' = -v_o r'\kappa \tag{C.6}$$

is obtained. Inserting this relation into (C.5) and expressing the total differentials by the partial one,

$$\frac{du}{ds} = \frac{\partial u_o}{\partial x} x' + \frac{\partial u_o}{\partial r} r' \tag{C.7}$$

and

$$\frac{dv_o}{ds} = \frac{\partial v_o}{\partial x} x' + \frac{\partial v_o}{\partial r} r',$$

yields finally, with $\partial u_o/\partial r = \partial v_o/\partial x$,

$$\frac{dV_N}{ds} + V_T K = x'r' \left(\frac{\partial u_o}{\partial r} - \frac{\partial u_o}{\partial x} \right) + (x'^2 - r'^2) \frac{\partial u_o}{\partial r} . \tag{C.8}$$

Differentiating equation (C.1), we obtain, with the same relations, the change of the tangential equation along s:

$$\frac{dV_T}{ds} = x'^2 \frac{\partial u_o}{\partial x} + 2x'r' \frac{\partial u_o}{\partial r} + r' \frac{\partial v_o}{\partial r} . \tag{C.9}$$

Very simple relations are obtained after a coordinate transformation for equations (C.8) and (C.9). A rectangular coordinate system $\bar{\tau}$ and $\bar{\nu}$ has its origin at the separation point s_B. The $\bar{\tau}$-coordinate is orientated tangentially, and the $\bar{\nu}$-coordinate is normal to the free streamline. The normal $\bar{\nu}$ is positive if it points to the outside flow field (or to the left of the streamline).

The transformation equation is

$$(x-x_B) = x'\bar{\tau} - r'\bar{\nu}; \quad (r-r_B) = r'\bar{\tau} + x'\bar{\nu}. \tag{C.10}$$

The derivatives of the velocity potential $\varphi(x,r)$ with respect to the coordinates $\bar{\tau}$ and $\bar{\nu}$ are

$$\frac{\partial \varphi}{\partial \bar{\tau}} = \frac{\partial \varphi \partial x}{\partial x \partial \bar{\tau}} + \frac{\partial \varphi \partial r}{\partial r \partial \bar{\tau}}$$

and (C.11)

$$\frac{\partial \varphi}{\partial \bar{\nu}} = \frac{\partial \varphi \partial x}{\partial x \partial \bar{\nu}} + \frac{\partial \varphi \partial r}{\partial r \partial \bar{\nu}} .$$

If we replace in equation (C.11) the partial derivatives by the total derivatives of the streamline,

$$\frac{\partial x}{\partial \bar{\tau}} = x'; \quad \frac{\partial r}{\partial \bar{\tau}} = r'; \quad \frac{\partial x}{\partial \bar{\nu}} = -r'; \quad \frac{\partial r}{\partial \bar{\nu}} = x', \tag{C.12}$$

we will obtain the partial derivative of the potential with respect to the body coordinates x and r:

$$\frac{\partial \varphi}{\partial x} = \frac{\partial \varphi}{\partial \bar{\tau}} x' - \frac{\partial \varphi}{\partial \bar{\nu}} r' \tag{C.13}$$

and

$$\frac{\partial \varphi}{r} = \frac{\partial \varphi}{\partial \bar{\nu}} x' + \frac{\partial \varphi}{\partial \bar{\tau}} r'.$$

The next higher derivatives are

$$\frac{\partial^2 \varphi}{\partial x^2} = x'^2 \frac{\partial^2 \varphi}{\partial \bar{\tau}^2} - 2r'x' \frac{\partial^2 \varphi}{\partial \bar{\nu} \partial \bar{\tau}} + r'^2 \frac{\partial^2 \varphi}{\partial \bar{\nu}^2}$$

$$\frac{\partial^2 \varphi}{\partial x \partial r} = r'x' \left(\frac{\partial^2 \varphi}{\partial \bar{\tau}^2} - \frac{\partial^2 \varphi}{\partial \bar{\nu}} \right) + \frac{\partial^2 \varphi}{\partial \bar{\nu} \partial \bar{\tau}} (x' - r') \tag{C.14}$$

$$\frac{\partial^2 \varphi}{\partial r^2} = r'^2 \frac{\partial^2 \varphi}{\partial \bar{\tau}^2} + 2r'x' \frac{\partial^2 \varphi}{\partial \bar{\tau} \partial \bar{\nu}} + x'^2 \frac{\partial^2 \varphi}{\partial \bar{\nu}^2}.$$

The change of the normal velocity along the arc length is obtained by inserting these expressions into equations (C.8) and (C.9):

$$\frac{dV_N}{ds} + V_T K = \frac{\partial^2 \varphi}{\partial \bar{\nu} \partial \bar{\tau}}. \tag{C.15}$$

If the general line is a streamline, then the conditions $V_N = 0$ and $dV_N/ds = 0$ hold, and equation (C.15) becomes

$$V_T \kappa = \frac{\partial^2 \varphi}{\partial \bar{\nu} \partial \bar{\tau}} . \tag{C.16}$$

The change of the tangential velocity along s becomes an identity: $dV_T/ds = \partial^2\varphi/\partial s^2$.

We consider now the tangential and normal velocity of the body in normal flow. The tangential velocity is

$$V_{T_1} = u_1 x' + (\alpha + v_1) r', \tag{C.17}$$

and the normal velocity can be written as

$$V_{N_1} = -u_1 r' + (\alpha + v_1) x'. \tag{C.18}$$

The total derivative of the normal velocity with respect to s is with the relations mentioned above

$$\frac{dV_{N_1}}{ds} + V_{T_1} \kappa - \frac{d\alpha}{ds} x' = \frac{\partial^2 \varphi}{\partial n \partial t} . \tag{C.19}$$

The third term on the left side vanishes if the angle of attack α is constant along the body.

APPENDIX D

THE ERROR INTRODUCED BY NEGLECTING THE INFINITE WAKE

In all cases in which we employ models with an infinite wake and truncate the wake a finite distance downstream of the separation point at s_E we introduce an error. This error will definitely increase with decreasing distance of the end point s_E from the separation point s_B. However, since we specify the pressure distribution along the free streamline, the error will not influence the velocity distribution to any extent on the forebody and therefore the drag of the body; but it will influence the position of the free streamline, the source strength $q_n(s)$, the perturbation potential, and in the normal flow case, the angle of attack distribution.

The estimation of the magnitude of the error is our next goal. Some simplifying assumptions are made for this purpose:

(a) The wake downstream of the truncation point s_E is cylindrical,

$$\rho = r_E = \text{const.}$$

and therefore,

$$\sigma = \xi + \text{const.}$$

(b) The source strength along the truncated wake attenuates according to a simple law

$$q_n(x) = q_n(x_E)(x_E/x)^k \tag{D.1}$$

where k is not necessarily an integer.

The assumption (a) is exact for the dissipation model. For the Helmholtz model where $V_T(s) = 1$ on Γ_2, (a) is only an approximation. With respect to assumption (b), we should mention that Levinson determined in reference **17** the asymptotic shape of Γ_2 as

$$r = \frac{C^* \sqrt{x}}{(\ln x)^{1/4}} \left[1 - \frac{1}{8} \frac{\ln(\ln x)}{\ln x} + O(1/\ln x) \right], \tag{D.2}$$

where C^* represents a constant which can be brought into a relation with the drag of the body. For slender bodies, we can assume that

$$q_o(x) \approx \frac{dr}{dx} \approx \frac{C^*}{2\sqrt{x}} \frac{1}{(\ln x)^{1/4}} \left[1 - \frac{1}{2(\ln x)^{1/2}} + \ldots \right]. \qquad (D.3)$$

The source distribution $q_o(x)$ vanishes with about $1/\sqrt{x}$. On the other hand, we notice, after a close inspection of table 1, that the exponent for a cylindrical wake is $k \geq 8$.

In all cases, for the potential as well as for the velocity component, an integral of the form

$$\int_{x_E}^{\infty} q(\xi) k(x,\xi)\, d\xi$$

must be calculated. In order to carry out the integration along a finite distance, the integral boundaries have to be subjected to a transformation. We therefore set

$$\eta = \frac{1}{\xi}; \quad \frac{d\xi}{\xi^2} = -d\eta; \quad \xi^2 = \frac{1}{\eta^2}; \quad \eta_E = \frac{1}{x_E} \qquad (D.4)$$

and

$$\begin{aligned} a^2 &= (r+r_E)^2 + x^2, \\ \chi &= \eta^2 a^2 - 2x\eta + 1, \\ \chi_E &= \eta_E^2 a^2 - 2x\eta_E + 1. \end{aligned} \qquad (D.5)$$

With these substitutions, we obtain the expression

$$(\xi - x)^2 + (r+r_E)^2 = \frac{1}{\eta^2} [\eta^2 a^2 - 2x\eta + 1] - \frac{1}{\eta^2} \chi, \qquad (D.6)$$

and the elliptic modulus becomes

$$k^2 = \frac{4rr_E\eta^2}{\eta^2a^2 - 2x\eta + 1} = 4rr_E\eta^2/\chi. \tag{D.7}$$

We start with the evaluation of the potential. For the model with an infinite wake the perturbation potential is

$$\varphi_n(s) = -\frac{1}{2\pi}\int_0^{s_E} q_n(\sigma)\,\frac{2\rho\,F_n(k^2)d\sigma}{[(x-\xi)^2 + (r+\rho)^2]^{1/2}}$$

$$-\frac{r_E x_E^k\, q_n(x_E)}{\pi}\int_0^{\eta_E}\eta^{k-1}\,\frac{F_n(k^2)}{\chi^{1/2}}\,d\eta. \tag{D.8}$$

The corresponding expressions for the perturbation velocities are

$$u_n(s) = -\frac{q_n(s)r'}{2} + \frac{1}{2\pi}\int_0^{s_E} q_n(\sigma)\,\frac{2\rho(x-\xi)\,G_n(k^2)}{[(x-\xi)^2 + (r+\rho)^2]^{3/2}}\,d\sigma$$

$$+\frac{q_n(x_E)r_E x_E^k}{\pi}\int_0^{\eta_E}\frac{\eta^k(x\eta-1)\,G_n(k^2)}{\chi^{3/2}}\,d\eta. \tag{D.9}$$

$$v_n(s) = \frac{q_n(s)x'}{2} + \frac{1}{2\pi}\int_0^{s_E} q_n(\sigma)\,\frac{2\rho[rG_n(k^2)-\rho\{G_{n+1}(k^2)+G_{n-1}(k^2)\}/2]}{[(x-\xi)^2 + (r+\rho)^2]^{3/2}}\,d\sigma$$

$$+\frac{q_n(x_E)r_E x_E^k}{\pi}\int_0^{\pi_E}\frac{\eta^{k+1}(rG_n(k^2)-r_E\{G_{n+1}(k^2)+G_{n-1}(k^2)\}/2)}{\chi^{3/2}}\,d\eta. \tag{D.10}$$

$$w_n(s) = \frac{1}{2\pi}\int_0^{s_E} q_n(\sigma)\,\frac{\rho^2(G_{n-1}(k^2)-G_{n+1}(k^2))}{[(x-\xi)^2+(r+\rho)^2]^{3/2}}\,d\sigma$$

$$+\frac{q_n(x_E)r_E^2x_E^k}{\pi}\int_0^{\eta_E}\frac{\eta^{k+1}(G_{n-1}(k^2)-G_{n+1}(k^2))}{2\chi^{3/2}}\,d\eta. \qquad (D.11)$$

The additional tangential velocity component $\Delta V_T = \Delta u_n x' + \Delta v_n r'$ is

$$\Delta V_T(s) = \frac{q_n(x_E)r_E x_E^k}{\pi}\int_0^{\eta_E}$$

$$\cdot\,\frac{\eta^k(x\eta-1)x'G_n(k^2)+\eta^{k+1}r'[rG_n(k^2)-r_E(G_{n+1}(k^2)+G_{n-1}(k^2))/2]}{\chi^{3/2}}\,d\eta. \qquad (D.12)$$

The additional normal velocity component $\Delta V_N = -\Delta u_n r' + \Delta v_n x'$, which is induced by the neglected part of the wake, is given as

$$\Delta V_N(s) = \frac{q_n(x_E)r_E x_E^k}{\pi}\int_0^{\eta_E}$$

$$\cdot\,\frac{-\eta^k(x\eta-1)r'G_n(k^2)+\eta^{k+1}x'[rG_n(k^2)-r_E(G_{n+1}(k^2)+G_{n-1}(k^2))/2]}{\chi^{3/2}}\,d\eta. \qquad (D.13)$$

We replace the elliptical integrals in equations (D.8) through (D.13) by their respective series from appendix B and consider only the first few significant terms:

$$F_o(k^2) = \frac{\pi}{2}\left(1 + \frac{k^2}{4} + \ldots\right)$$

$$F_1(k^2) = \frac{\pi}{2}\left(\frac{k^2}{8} + \ldots\right)$$

$$G_o(k^2) = \frac{\pi}{2}\left(1 + \frac{3}{4}\,k^2 + \ldots\right) \qquad \text{(D.14)}$$

$$G_1(k^2) = \frac{\pi}{2}\left(\frac{3}{8}\,k^2 + \ldots\right)$$

$$G_2(k^2) = \frac{\pi}{2}\,(O(k^4) + \ldots).$$

If we assume that the expression for χ is only a little different than unity ($\chi \approx 1$), we can develop the expression for χ into a series. We obtain

$$\frac{1}{\chi^{1/2}} \approx 1 - \frac{1}{2}\,(a^2\eta^2) + x\eta + \ldots$$

$$\frac{1}{\chi^{3/2}} \approx 1 - \frac{3}{2}\,(a^2\eta^2) + 3x\eta + \ldots\,. \qquad \text{(D.15)}$$

We determine the additional normal velocity $\Delta V_N(s)$ on Γ_2 in the vicinity of the separation point by inserting the expansions (D.14) and (D.15) into (D.13). The most important term under the integral is then

$$\Delta V_N(s) \approx \frac{q_n(x_E)\,r_E\,x_E^k}{\pi} \int_o^{\eta_E} \frac{\pi}{2}\,\eta^k(r' + [x'r - r'x]\eta)(1 + 3x\eta)\,d\eta. \qquad \text{(D.16)}$$

The integration of this expression and inserting the proper integration boundaries yields the additional normal velocity

$$\Delta V_N(s) \approx \frac{q_n(x_E) r_E}{2} \left[\frac{r'}{k+1} \cdot \frac{1}{x_E} + \frac{x'r + 2r'x}{(k+1)\, x_E^2} + \ldots \right] . \qquad (D.17)$$

For very large x_E, we can also neglect the second term within the brackets.

$$\Delta V_N(s) \approx q_n(x_E) \frac{r_E}{2} \frac{r'}{k+1} \frac{1}{x_E} . \qquad (D.18)$$

The error is thus proportional to the source strength at x_E and inversely proportional to the distance x_E and the exponent k of the attenuation of the source strength.

NASA-Langley, 1970 —— 1

"The aeronautical and space activities of the United States shall be conducted so as to contribute . . . to the expansion of human knowledge of phenomena in the atmosphere and space. The Administration shall provide for the widest practicable and appropriate dissemination of information concerning its activities and the results thereof."

—NATIONAL AERONAUTICS AND SPACE ACT OF 1958

NASA SCIENTIFIC AND TECHNICAL PUBLICATIONS

TECHNICAL REPORTS: Scientific and technical information considered important, complete, and a lasting contribution to existing knowledge.

TECHNICAL NOTES: Information less broad in scope but nevertheless of importance as a contribution to existing knowledge.

TECHNICAL MEMORANDUMS: Information receiving limited distribution because of preliminary data, security classification, or other reasons.

CONTRACTOR REPORTS: Scientific and technical information generated under a NASA contract or grant and considered an important contribution to existing knowledge.

TECHNICAL TRANSLATIONS: Information published in a foreign language considered to merit NASA distribution in English.

SPECIAL PUBLICATIONS: Information derived from or of value to NASA activities. Publications include conference proceedings, monographs, data compilations, handbooks, sourcebooks, and special bibliographies.

TECHNOLOGY UTILIZATION PUBLICATIONS: Information on technology used by NASA that may be of particular interest in commercial and other non-aerospace applications. Publications include Tech Briefs, Technology Utilization Reports and Technology Surveys.

Details on the availability of these publications may be obtained from:

SCIENTIFIC AND TECHNICAL INFORMATION DIVISION

NATIONAL AERONAUTICS AND SPACE ADMINISTRATION

Washington, D.C. 20546